The Dissertation Committee for Martin Andreas Abel
certifies that this is the approved version of the following dissertation:

# Computation of Collision-Induced Absorption by Simple Molecular Complexes, for Astrophysical Applications

Committee:

_____

Michael Downer, Supervisor

_____

Lothar Frommhold, Supervisor

_____

Daniel Heinzen

_____

John Keto

_____

Manfred Fink

_____

Don Winget

# Computation of Collision-Induced Absorption by Simple Molecular Complexes, for Astrophysical Applications

by

## Martin Andreas Abel, M.A.

**DISSERTATION**

Presented to the Faculty of the Graduate School of

The University of Texas at Austin

in Partial Fulfillment

of the Requirements

for the Degree of

**DOCTOR OF PHILOSOPHY**

THE UNIVERSITY OF TEXAS AT AUSTIN

May 2012

Dedicated to my family.

# Acknowledgments

First of all I want to thank my supervisors, Drs. Lothar Frommhold and Michael Downer, for their kind support and encouragement throughout the whole time I worked together with them. Without them this work would not have been possible. It has been a true pleasure to work with you and I could learn a lot from you. Your experience is an invaluable merit. Discussions with you gave me a much deeper insight into the physics I would never have obtained otherwise.

Next I would like to thank Dr. Manfred Fink who was very engaged to make my exchange and my stay at the University of Texas possible. Furthermore, throughout the first year of my research he has kindly let me occupy space in his laboratory. This gave me the opportunity to get to know some of the collaborators and doctoral students of his group through daily interaction and learn about the exciting research his group is pursuing.

Thanks are also due to our astronomical advisors, Drs. Don Winget from the University of Texas at Austin Department of Astronomy and Didier Saumon from the Los Alamos National Laboratory. They gave us the motivation for the work and were always very helpful in pointing out what exactly is needed for applications and for writing grant proposals.

Furthermore, I would like to thank Drs. Hunt and Li from Michigan

# Computation of Collision-Induced Absorption by Simple Molecular Complexes, for Astrophysical Applications

Publication No. _____

Martin Andreas Abel, Ph.D.
The University of Texas at Austin, 2012

Supervisors:   Michael Downer
                Lothar Frommhold

The absorption due to pairs of $H_2$ molecules is an important opacity source in the atmospheres of various types of planets and cool stars, such as late stars, low mass main sequence stars, brown dwarf stars, cool white dwarf stars, the ambers of the smaller, burnt out main sequence stars, exoplanets, etc., and therefore of special astronomical interest. Astronomers are interested in the outer planets as they still contain primordal matter. Furthermore, recent observations by the Hubble space telescope (in operation since 1990) have revealed several thousand cool white dwarf stars with temperatures of several thousand Kelvin. It is surprising that none of them has temperatures lower than roughly 4000 K. This means that the white dwarf stars have not had enough time to cool down to the temperature of the cosmic background radiation. Astrophysicists believe that this information can be used for an alternative and more accurate method of cosmochronology. However, the emission

spectra of cool white dwarf stars differ significantly from the expected black-body spectra of their cores, largely due to collision-induced absorption by collisional complexes of residual hydrogen and helium in the stellar atmospheres. In order to model the radiative processes in these atmospheres, which have temperatures of several thousand kelvin, one needs accurate knowledge of the induced dipole and potential energy surfaces of the absorbing collisional complexes, such as $H_2$–$H_2$, $H_2$–He, and $H_2$–H. These come from quantum-chemical calculations, which, for the high temperatures and high photon energies under consideration in this work, need to take into account that the $H_2$ bonds can be stretched or compressed far from equilibrium length. Since no laboratory measurements for these high temperatures and photon energies exist, one has to undertake *ab initio* calculations which take into account the high vibrational and rotational excitation of the involved hydrogen molecules. However, before one attempts to proceed to higher temperatures and photon energies where no laboratory measurements exist it is good to check that the formalism is correct and reproduces the results at temperatures and photon energies where laboratory measurements exist, that is, at and below room temperature and for photon energies up to about 1.5 eV.

In this work a formalism is developed to compute the binary collision-induced absorption of simple molecular complexes up to temperatures of thousands of kelvin and photon energies up to 2.5 eV, properly taking into account vibrational and rotational dependencies of the induced dipole and potential energy surfaces. In order to make the computational effort feasible, the isotropic

potenial approximation is employed. The formalism is applied to collisional complexes of $H_2$–$H_2$, $D_2$–$D_2$, $H_2$–He, $D_2$–He, $T_2$–He, and $H_2$–H, and compared with existing laboratory measurements.

# Table of Contents

# List of Figures

xiv

xv

xvi

# Chapter 1

# Introduction

## 1.1 Collision-Induced Absorption

It is a well-known fact that noninteracting molecules with inversion symmetry do not possess a dipole moment. Hence, they do not interact with radiation fields of infrared frequencies. However, dense gases of nonpolar molecules, such as $H_2$, absorb infrared radiation. This absorption is continuous and ranges from the microwave and far infrared regions of the spectrum to the near infrared and visible, covering all frequencies in between. The reason for these absorption continua are collisionally interacting pairs of gas particles, which in contrast to the noninteracting gas particles in general possess transient dipole moments [34, 99] which are induced by the familiar van der Waals intermolecular forces.

## 1.2 Discovery of Collision-Induced Absorption

Collison-induced absorption (CIA) was first experimentally observed in the fundamental band of oxygen and nitrogen [100]. In 1949 Welch discovered and explained CIA [34]. Jansen's early discovery (late 19th century) in air is now understood to involve electronic CIA, discussed below, whereas Welsh and

1

associates' work represents rotovibrational CIA, but the underlying principles are the same. Later on, in 1954, Maryot *et al.* observed CIA in the microwave region, and Trafton found it in the infrared range in the outer planets in 1964. One of the early highlights was that Herzberg pointed out sizeable $H_2$ concentrations in the atmospheres of Uranus and Neptun for the first time [49]. This was rather spectacular, because, in general, nonpolar species such as $H_2$ and He are difficult to detect remotely in such cool environments using conventional spectroscopy. In the long history of CIA supermolecular signatures have been very important to reveal such gases. It is now understood that the early observations of absorption bands in compressed air and oxygen are of a supermolecular nature. Although CIA has lead to most significant advances in astronomy it is generally observed in virtually all dense matter, in the gaseous, liquid, as well as solid state. The earth's atmosphere is similarly affected by collision-induced signatures in all spectral bands. Any meaningful modeling of the atmospheres cannot ignore collision-induced absorption [90, 91].

## 1.3   Significance and current interest

The systematic expansion of the knowledge base of CIA has more recently lead astrophysicists to expect that a new, independent estimate of the age of the universe is possible, helped by collision-induced spectroscopy. For this endeavor, one requires accurate knowledge of collision-induced opacities of collisional complexes, which we view a kind of supermolecules, such as $H_2$–$H_2$ and $H_2$–He for absorption at temperatures up to 7000 K and photon ener-

2

gies up to 2.5 eV [61]. In particular, astrophysicists recently observed that the emission spectra of cool white dwarf stars differ significantly from the expected blackbody spectrum of their cores. They believe that the atmospheres of the cool white dwarf stars are so dense that the CIA of hydrogen and helium suppresses the infrared emission strongly [48, 54, 57, 73, 82, 83]. However, up to now detailed modeling of cool star atmospheres with proper accounting for the collision-induced opacities has been hampered by the highly incomplete or non-existent experimental as well as theoretical data on such opacities at temperatures of thousands of kelvin and photon energies up to 2.5 eV. Only calculations of the collision-induced absorption provide the necessary opacities at nearly arbitrary temperatures and photon energies.

Quantum-chemical calculations of the induced dipole surfaces of $H_2$–$H_2$ and other supermolecular complexes are well established [14, 15, 38, 68]. Molecular scattering calculations, based on such data and accounting for the interactions of the molecular complexes with a radiation field, have been undertaken. These have been compared to laboratory measurements at low temperatures, $T \leq 300$ K. Close agreement between theory and experiment has been observed [34]. However, at higher temperatures virtually no laboratory measurements of such opacities exist. With increasing temperature laboratory measurements of CIA become increasingly cumbersome, so that it seems unlikely that such measurements will become available in the near future. Since astrophysicists require such data at temperatures and photon energies, where laboratory measurements are not available, we decided to extend the quantum-

chemical calculations of the induced dipole (ID) and potential energy surfaces (PES) to account for the vibrational and rotational excitations as encountered at higher temperatures and higher photon energies [61].

## 1.4 Difficulties of laboratory measurements of CIA

Experimental studies of CIA spectra consist of laboratory absorption measurements in compressed gases and gas mixtures at different frequencies, densities, and temperatures. However, there are several obstacles that make laboratory measurements of CIA difficult and render their results uncertain. One problem is that CIA is generally much weaker than the absorption of infrared radiation by complexes of particles with a permanent dipole moment. It is a fact that weak absorption is more difficult to measure than strong absorption, which implies that experimentally CIA spectra can only be determined to a lesser accuracy than spectra of gases with a permanent dipole moment, and in particular the CIA absorption dips can only be observed with limited accuracy. To compensate for this weaker absorption, many experimentalists work with high gas densities, which may introduce ternary and higher order contributions that are likely to enter with increasing densities. Theoretically it is possible to separate these higher order contributions from the purely binary contributions by virial expansion techniques - described in detail in the theory section - but in practice this often introduces substantial uncertainties into the thus obtained binary absorption spectrum [18]. This is mainly a problem of laboratory measurements, because for most astrophysical applications higher

order contributions are usually insignificant, due to the low gas densities encountered there. Nevertheless, due to the long absorption path lengths CIA intensities have considerable values in planetary atmospheres. In contrast to that, laboratory path lengths seldom exceed several meters. However, we note that even in some astrophysical applications such as for cool white dwarf stars huge gas densities are encountered.

# Chapter 2

# Theory

As physical systems change their energetic state they can emit or absorb electromagentic radiation if an electric charge is accelerated in the process. There are different ways how this can happen. In atoms there occur quantum transitions, which typically have a relatively large spacing above their electronic ground state. The corresponding spectra are called Line spectra. These lines offer important information and were essential for the development of quantum mechanics. For astronomers line spectra have important information about the constituents of the universe. Since they are characteristic for the atoms or molecules involved in the transitions one can remotely determine the elements that exist on other planets and stars.

On the other hand, the rotovibrational energy structures of molecules have relatively small energy separations. Molecular spectra consist of a greater number of apart closely neighboring absorption lines which arise from the coupling of electrical oscillations and rotational excitations in the molecules, so that no separated energy differences are transfered but a whole spectrum of energy values. The thus generated spectra are referred to as Band spectra.

In a mixture of gases there usually occur broadening mechanisms such

as Doppler broadening and pressure broadening, so that individual lines become diffuse and some of them even overlap. Unresolved lines appear as continuous spectra. In addition, in a mixture of several different atoms and molecules at a given temperature T, for example in the sun, one can also observe continuous spectra. Under equilibrium conditions, at temperatures of several thousand kelvin the degree of ionization of rare gases is typically small [47]. Thus emission of light comes mainly from neutral-neutral collisions. At higher temperatures, when the degree of single ionization is still significantly smaller than unity, electron-neutral and electron-ion bremsstrahlung are among the principal sources for radiation. This bremsstrahlung is continuous radiation. The continuous spectrum of the sun is mainly due to bremsstralung. In addition, free-to-free radiative transitions of electron-ion pairs and free-to-free radiative transitions are continuous [47]. According to [47] negative ions, such as $H^-$ ([41, 43, 62, 92]) and $O^-$ ([24, 25, 33]), absorb light very effectively. The inverse reaction, radiative attachment, is therefore an important contributor to continuous emission spectra whenever negative ions may be formed [19, 20]. Continuous spectra may furthermore be due to collision-induced emission and absorption, which is investigated in this work. It generates continuous spectra in completely neutral environments [47].

In virtually any gas a certain, usually small fraction of atoms or molecules (monomers) exists as van der Waals molecules. These are systems of two or more monomers, bound together by the weak van der Waals intermolecular forces. This work is mainly concerned with complexes of two unbound

monomers which exist for the very short duration of a fly-by-encounter. Free and bound van der Waals systems have many properties in common. However, only the latter possess the relative stability of a molecule. Properties of bound and free van der Waals systems are referred to as supermolecular properties.

Collisional complexes in molecular gases have many more degrees of freedom than those of monatomic gases. Thus much richer collision-induced spectra are observed in a number of spectral bands. Any collisional pair possesses the degrees of freedom of the translational motion and an associated kinetic energy of relative motion. Furthermore, if molecular collisions are considered there are additional degrees of freedom and energies associated with the rotational and vibrational motion of one or more molecules of the complex. Correspondingly, photons may be absorbed and emitted over a much greater range of frequencies, in the vicinity of the various rotovibrational bands of the molecules, and at sums and differences of such rotovibrational frequencies, if two or more molecules interact.

For supermolecular spectra the following notation is common: in the Symbol $X_n(j)$, j = 0, 1, 2, ... corresponds to the rotational quantum number of the initial state. The subscript n = $\nu' - \nu$ is the difference of the vibrational quantum numbers of initial ($\nu$) and final ($\nu'$) vibrational state. X stands for one of the letters O, P, Q, R, S, ..., each specifying a different rotational transition: j' - j = ..., -2, -1, 0, 1, 2, ..., respectively. In literature the subscript n is often omitted if it is clear what vibrational band is referred to.

## 2.1 Supermolecular spectroscopy

It is observed that the spectra of dense gases differ from the spectra of the same gases at low densities. With from near zero increasing gas density first the familiar, allowed rotovibrational and electronic bands may appear in the appropriate frequency region (if there is such an allowed spectrum) [34]. Intensities of these spectra increase linearly with increasing gas density. As the gas density is further increased, at intermediate densities generally new absorption bands occur whose intensity increases in any case nonlinearly in gas density: quadratic, cubic, ... The origin of these new bands are van der Waals complexes of two or more molecules which may be free, *i.e.* weakly bound van der Waals molecules. Such absorption bands are generally found in the absorption spectra of all molecular gases, no matter whether the gases consist only of infrared-inactive molecules.

The $H_2$ molecule, like other diatomic molecules with inversion symmetry, is infrared inactive, because this symmetry is inconsistent with the existence of a dipole moment. Thus, at low gas densities no absorption of electromagnetic radiation by hydrogen molecules occurs. Nevertheless, in solid, liquid, and gaseous hydrogen at high enough densities absorption in the infrared part of the electromagnetic spectrum is observed. This absorption can be explained with the model of a supermolecular (collision-induced) process. Supermolecular spectra arise from interaction-induced dipole moments, *i.e.* dipole moments that do not exist in the non-interacting molecules.

Certain phenomena caused by collisions, such as pressure broadening

9

of spectral lines, have been known to spectroscopists for a long time. However, pressure broadened lines are normally not considered to be collision-induced. Pressure broadened means that existing line intensities are spread over a greater frequency band but no new intensity is created. In contrast to that collision-induced means that new intensities are created that do not have their origin in a single molecule but in the existence of supermolecules. The definition of interaction-induced absorption as it is used in this work implies the existence of a dipole moment that arises from the interaction of two or more atoms or molecules, leading at high enough gas density to discernable spectral line intensities in excess of the sum of the absorption of the atoms/ molecules of the complex.

Temperature control has been essential in much of the studies of collision-induced spectra. Temperature variation accesses different parts of the inter-molecular interaction potential. At low temperatures collision-induced lines are relatively sharp, so that induced lines may be resolved whose structures may be masked at higher temperatures. It is fair to expect laboratory measurements at room temperature to be more accurate than at other temperatures because for room temperature one does not have to deal with undesirable temperature gradients.

There is a small number of monographs, review articles, and other references such as the excellent book [34] that describe the general theory of collision-induced absorption. In this chapter a short overview, based on [45] will be given. Most of the presented equations are so general that they have

validity for a great variety of monatomic gas mixtures and pure or mixed diatomic gases. Throughout we employ the Born-Oppenheimer approximation, that is, the nuclear motions are assumed to be slow compared to the electronic motions, *i.e.* all potential energy and induced dipole surfaces are assumed to be independent of the velocity of the nuclei. All formulas are presented in cgs units. If one prefers SI units proper factors of $4\pi\epsilon_0$ have to be inserted in all formulas that contain electric fields. The necessary physical constants can be found in the appendix. Most pairs of atoms and molecules form bound composites, so called van der Waals molecules. These contribute to the CIA spectrum with relatively sharp features at low temperatures, *i.e.* in the order of hundred kelvin or less. This work only deals with higher temperatures and thus free-free transitions dominate the spectra. Therefore, van der Waals molecules can safely be ignored, since their effect at the temperatures considered is negligible. This is strictly only true for hydrogen and $H_2$–He mixtures. Other systems with heavier atoms or molecules form more strongly bound molecules, *e.g.* mercury-argon mixtures.

## 2.2 Virial expansions

The collsion-induced absorption intensitiy $I$ shows a strong dependence on the density $\rho$ of the considered species. Via a virial expansion binary, ternary, etc. contributions are distinguishable. In the low-pressure limit induced spectra may be described by a virial expansion [34],

$$I = A * \rho + B * \rho^2 + C * \rho^3 + ... \qquad (2.1)$$

with coefficients representing the dipole-allowed contributions, $A$, and the induced binary, $B$, ternary, $C$, ..., spectral components. For ordinary atoms or molecules, the intensity $I$ varies linearly with density $\rho$, whereas intensities of collision-induced spectra vary with the second and higher powers of density, in any case non-linearly. The virial expansion of the absorption coefficient in dense mono-molecular gases is according to [34] given by

$$\alpha(\omega) = \alpha_1(\omega) * \rho + \alpha_2(\omega) * \rho^2 + \alpha_3(\omega) * \rho^3 + ..., \qquad (2.2)$$

where $\alpha_1(\omega)$ is the allowed spectrum (if one exists at frequencies $\omega$ of interest), and $\alpha_j(\omega)$ $(j > 1)$ describes the binary, ternary, ..., collision-induced absorption. For infrared inactive gases the coefficient $\alpha_1(\omega)$ vanishes. At fixed frequency and temperature a virial expansion of the absorption coefficient is often possible. Note that the virial expansion is valid only when the magnitude of the detuning relative to a transition frequency is large compared to the reciprocal intercollisional time [72]. However, that condition is fullfilled for almost the entire spectra that will be considered in this work. The higher order coefficients with $j > 1$ are often separable in actual measurements. At low densities the second and higher order spectral virial terms are insignificant. However, they become important at sufficiently high density. At densities approaching liquid state density, many-body interactions may be expected to

dominate the optical properties. Under such conditions virial expansions become meaningless. One has to use other theories in these cases.

Due to virial expansions at intermediate gas densities one need not consider the complex many-body system consisting of all molecules of a collisional complex. Instead, the supermolecule may be described by a series of relatively simple two-, three-, ... body Hamilton operators [34]. At sufficiently small gas densities this series may be truncated after the first few leading terms to model the spectroscopic properties of the whole system accurately.

While in this work only binary complexes of molecules will be considered a few semi-quantitative data exist at present towards an understanding of ternary spectra which are much more complicated to treat theoretically. Nevertheles, there is experimental evidence of important spectral N-body contributions, with $N > 2$, even at densities that are much lower than condensed matter densities [36].

Most accessible and theoretically easy to understand are binary systems, from which the so-called pair spectra arise. However, experimentally it turns out to be difficult to distinguish binary contributions from those due to systems of three or more interacting molecules, which generally possess irreducible dipole components in addition to the pairwise additive components.

## 2.3 Intermolecular potentials

For non-interacting point particles the ideal gas law provides a valid description. It is also an often useful approximation for rarefied gases at high temperatures in that it is in close agreement with measurements of the pressure, density, and temperature. However, it obviously cannot describe important features of gaseous matter, such as condensation and incompressibility of liquids and solids.

As early as in 1873 van der Waals developed his famous equation of state [34] which was able to describe important features of gaseous matter. It was a significant improvement over the ideal gas law for the description of real gases. It assumes a repulsion like that of hard spheres at small separation and attraction at more distant range. However, to understand why repulsion occurs at close range the Pauli principle, discovered much later, was needed: when atoms or molecules approach each other closely enough so that their electronic clouds overlap, the potential energy increases because the Pauli principle forces electrons into higher states [34]. This causes repulsion according to the principle of energy minimization. Not only the electrons but also the Coulomb forces between the nuclei contribute to the repulsion at near range. However, the true nature of intermolecular forces could only be understood and described after the development of quantum mechanics in the 1920s and afterwards.

Up to the late 1960s most research on intermolecular forces was based on two assumptions. The first was that intermolecular potentials can be repre-

sented by simple functions such as the two-parameter Lennard-Jones potential. The second was that the intermolecular potential energy of a molecular complex is well represented by the sum of their pair interaction energies. However, it turned out that both assumptions are wrong and have obstructed significant progress in the field (Maitland *et al.*, 1981). With the advent of new accurate measurements of various bulk propterties since the 1970s this has changed significantly [34]. More recently also vastly improved *ab initio* calculations and direct inversions of measurements have been possible. These permit the construction of intermolecular potentials without any *ad hoc* assumption concerning the analytic form of the potential. As we know today the repulsive branch of the intermolecular energy of rare gas pairs has an exponential form, in contrast to the $R^{-12}$ dependence of the Lennard-Jones potential. Modern computational methods can now be used to compute accurate PESs [8, 61, 69].

### 2.3.1   The intermolecular potential of a supermolecular complex

According to [45], for an atom-diatom system the intermolecular potential can be expanded in Legendre polynomials as

$$V(\boldsymbol{r}, \boldsymbol{R}) = \sum_{\gamma} V_{\gamma}(r, R) P_{\gamma}(\hat{\boldsymbol{r}}, \hat{\boldsymbol{R}}) \tag{2.3}$$

where the subscripts $\gamma$ runs over even integers for a homonuclear diatom such as $H_2$–He, due to its inversion symmetry. For a diatom-diatom supermolecular complex a similar but more complex expansion is possible. According to [18] for two interacting diatoms it is appropriate to expand the potential energy in

angular basis functions as

$$
\begin{aligned}
V(\boldsymbol{r}_1, \boldsymbol{r}_2, \boldsymbol{R}) \;=\; & (4\pi)^{3/2} \sum_{\gamma_1 \gamma_2 \gamma} V_{\gamma_1 \gamma_2 \gamma}(r_1, r_2, R) \\
& \times \sum_{m_1 m_2 m} C(\gamma_1 \gamma_2 \gamma; m_1, m_2 m) Y_{\gamma_1 m_1}(\hat{\boldsymbol{r}}_1) \\
& \times Y_{\gamma_2 m_2}(\hat{\boldsymbol{r}}_2) Y^*_{\gamma m}(\hat{\boldsymbol{R}})
\end{aligned}
\tag{2.4}
$$

where the C are Clebsch-Gordan coefficients and the $Y$ are spherical harmonics.

### 2.3.2 The isotropic potential approximation (IPA)

In general, if molecules are involved, typical interaction potentials are anisotropic since angular dependencies reflecting the molecular symmetries have to be taken into account. For linear molecules, such as $H_2$ pairs, a minimum of five angular variables (and many more for bigger, nonlinear molecules) are needed for a complete description of the anisotropy. However, in many cases the isotropic potential approximation (IPA) can be used with sufficient accuracy [34].

Generally, molecules have internal degrees of freedom. They may vibrate or rotate, which modifies their interactions with other molecules. Vibrating molecules often appear bigger and more anisotropic. However, the vibrational dependence has only been carefully modelled for a few systems, and only a few molecular interaction potentials are well known.

16

## 2.4   Time scales

In the investigation of collisions, at not too high densities, one distinguishes three different times. They are the average time between collisions, the duration of a molecular fly-by, and the duration of the optical interaction.

The mean time between collisions $\tau_{12}$ is the reciprocal collision frequency [34]. It can be approximated by

$$\tau_{12} = n * \sigma * v_{12} = n * \sigma * \sqrt{\frac{\pi m_{12}}{8 \kappa T}} \tag{2.5}$$

where $\sigma$ is the cross section and $m_{12}$ is the reduced mass of the collisional pair,

$$m_{12} = \frac{m_1 * m_2}{m_1 + m_2} \tag{2.6}$$

with the masses $m_i$ of species $i$. $T$ is the temperature of the gas, $n$ is the gas density, and $\kappa$ is the Boltzmann constant.

The average relative speed of a collisional pair is of the order of the root-mean-square speed, which is approxmiately equal to the speed of sound and varies with temperature as $T^{-1/2}$. For hydrogen gas at standard temperature (273 K) and pressure (1 atmosphere) the mean time between elastic scattering collisions is roughly $0.07*10^{-9}$ s [34]. The mean time between collisions decreases inversely proportional with density $n$.

The duration of a fly-by encounter is according to [34] approximately given by

$$\Delta t \approx \frac{d}{v_{12}} \tag{2.7}$$

where $d = d_1 + d_2$ is the sum of the diameters of the interacting atoms (hard sphere approximation). It should, however, be kept in mind that in reality the size of atoms and molecules depends on the energy of the collisions and the atoms/ molecules themselves. This duration varies with temperature as $T^{-1/2}$, is density invariant, and for hydrogen gas at standard temperature amounts to roughly $1.6*10^{-13}$ s [34].

Near standard temperature and pressure, the time between collisions is about three orders of magnitude greater than the duration of collisions. Thus, a Maxwellian distribution of velocities is often a reasonable approximation, and, if interactions have a range not greater than the size of the atoms, the concept of binary collisions appears to be a good model [34]. However, at densities approaching liquid state density, *i.e.* several hundred amagats, the time between collisions and the duration of a collision become comparable and each particle is interacting with several partners at a time. Under such conditions the time scales considered above become meaningless.

Even though collisional complexes exist only for very short times, *i.e.* times in the order of $10^{-13}$ s, the duration of a molecular fly-by, they are a physical reality like van der Waals molecules. Whereas conventional spectroscopy emphasizes the concept of frequency and energy level measurement, collision-induced spectroscopy mainly aims for measurement of absorption intensity and line shape [34]. Collision-induced spectroscopy may be used to provide

18

information on the intermolecular interaction, *e.g.* multipole moments and range of forces, intermolecular dynamics, and optical bulk properties [40].

## 2.5  Bound and free states

It is a fact that in most gases bound dimers, called van der Waals molecules, exist. Infrared spectra of van der Waals molecules are well-known [66], including those of the $(H_2)_2$ dimer [34, 39, 65]. These spectra are due to the very same mechanisms that generate the CIA spectra: collisional pairs as well as bound pairs interact with electromagnetic radiation by means of the same interaction-induced dipole surface, which we consider here. The infrared spectra of van der Waals molecules are relatively sharp features, which appear against the background of the quasi-continuous CIA spectra.

In general collision-induced spectra consist of contributions arising from free-to-free, free-to-bound, bound-to-bound, and bound-to-free transitions. The kinetic energy of relative motion of a molecular pair is a continuum with width in the order of the thermal energy, $E_{free} \approx 3kT/2$ [34]. Radiative transitions between free states are relatively diffuse, in reflection of the short lifetime of the supermolecules. Van der Waals molecules such as $(H_2)_2$ have relatively few bound states. At not too low temperatures many more free pair states are populated than dimer states which results in smaller intensities of the dimer states. At temperatures much greater than the well depth of the intermolecular potential, the absorption is nearly fully due to free-to-free transitions, but individual dimer lines or bands may still be quite prominent unless pressure

broadening or perhaps ternary interactions have obliterated such structures. On the other hand, at low temperature, spectral components involving bound dimers become most prominent [34].

## 2.6 Two interacting particles

In the following I will attempt to describe the motion of two interacting particles, such as the electron and the proton in the hydrogen atom, in different frames. The physics is exactly the same in the two coordinate systems. However, in some coordinate frames the description is easier than in others.

### 2.6.1 Coordinate systems

There are two different coordinate systems useful in the description of a two-body system. In the lab frame we have the coordinates $\boldsymbol{r}_1 = \{x_1, y_1, z_1\}$ and $\boldsymbol{r}_2 = \{x_2, y_2, z_2\}$, in the relative to the center-of-mass coordinate system we have $\boldsymbol{R} = \{X, Y, Z\}$ and $\boldsymbol{r} = \{x, y, z\}$.

### 2.6.2 Two interacting particles in the center-of mass and relative coordinate systems

In the center-of-mass system we have to solve the following Schrödinger equation:

$$\mathcal{H}_{\text{cm}}U = \left[-\frac{\hbar^2}{2M}\boldsymbol{\nabla}^2_{\text{cm}}\right]U = T_{\text{cm}}U. \tag{2.8}$$
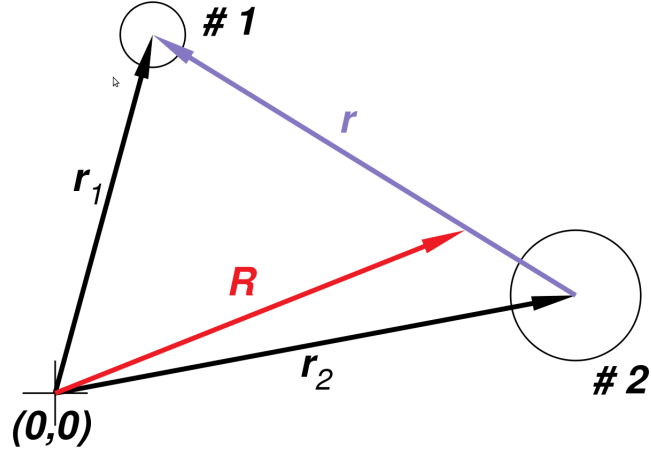
Figure 2.1: Coordinates for a twobody system.

That is, in the center-of-mass system the solution is trivial: we have a force-free motion with constant velocity.

For the relative motion we have the following Schrödinger equation:

$$\mathcal{H}_{\mathrm{rel}} u = \left[ -\frac{\hbar^2}{2m_{\mathrm{red}}} \boldsymbol{\nabla}_{\mathrm{rel}}^2 + V(r) \right] u = E_{\mathrm{rel}} u. \qquad (2.9)$$

This is the same equation as the one previously obtained, but with $m$ replaced by the reduced mass $m_{\mathrm{red}}$.

In the laboratory frame we have to solve the following Schrödinger equation:

$$\left\{ -\frac{\hbar^2}{2m_1} \boldsymbol{\nabla}_1^2 - \frac{\hbar^2}{2m_2} \boldsymbol{\nabla}_2^2 + V(|\boldsymbol{r}_1 - \boldsymbol{r}_2|) \right\} \psi(\boldsymbol{r}_1, \boldsymbol{r}_2) = E_{\mathrm{tot}} \psi(\boldsymbol{r}_1, \boldsymbol{r}_2). \qquad (2.10)$$

In relative coordinates we have to solve the following Schrödinger equation:

21

$$\left\{ -\frac{\hbar^2}{2m_{\text{red}}} \boldsymbol{\nabla}_{\text{rel}}^2 - \frac{\hbar^2}{2M_{\text{tot}}} \boldsymbol{\nabla}_{\text{cm}}^2 + V(r) \right\} \psi(\boldsymbol{r}, \boldsymbol{R}_{\text{cm}}) = E_{\text{tot}} \, \psi(\boldsymbol{r}, \boldsymbol{R}_{\text{cm}}). \quad (2.11)$$

The solution to this equation can be found wih a separation Ansatz:

$$\psi(\boldsymbol{r}, \boldsymbol{R}_{\text{cm}}) = u(\boldsymbol{r}) \cdot U(\boldsymbol{R}_{\text{cm}}) \quad (2.12)$$

with $E_{\text{tot}} = T_{\text{cm}} + E_{\text{rel}}$.

Just as in classical physics the variables transform as follows:

$$\frac{\partial}{\partial x_1} = \frac{\partial}{\partial x} \frac{\partial x}{\partial x_1} + \frac{\partial}{\partial X_{\text{cm}}} \frac{\partial X_{\text{cm}}}{\partial x_1} = \frac{\partial}{\partial x} + \frac{\partial}{\partial X_{\text{cm}}} \frac{m_1}{M}, \quad (2.13)$$

$$\frac{\partial}{\partial x_2} = \frac{\partial}{\partial x} \frac{\partial x}{\partial x_2} + \frac{\partial}{\partial X_{\text{cm}}} \frac{\partial X_{\text{cm}}}{\partial x_2} = -\frac{\partial}{\partial x} + \frac{\partial}{\partial X_{\text{cm}}} \frac{m_2}{M}, \quad (2.14)$$

$$\frac{\partial^2}{\partial x_1^2} = \frac{\partial^2}{\partial x^2} + 2 \frac{\partial^2}{\partial x \, \partial X_{\text{cm}}} \frac{m_1}{M} + \frac{\partial^2}{\partial X_{\text{cm}}^2} \frac{m_1^2}{M^2}, \quad (2.15)$$

$$\frac{\partial^2}{\partial x_2^2} = \frac{\partial^2}{\partial x^2} - 2 \frac{\partial^2}{\partial x \, \partial X_{\text{cm}}} \frac{m_2}{M} + \frac{\partial^2}{\partial X_{\text{cm}}^2} \frac{m_2^2}{M^2}. \quad (2.16)$$

Now consider any central force system, defined by a Hamiltonian given by

$$H = -\frac{\hbar^2}{2m_1} \boldsymbol{\nabla}_1^2 - \frac{\hbar^2}{2m_2} \boldsymbol{\nabla}_2^2 + V(r) \quad (2.17)$$

with $\boldsymbol{\nabla}_i^2 = \partial^2/\partial x_i^2 + \partial^2/\partial y_i^2 + \partial^2/\partial z_i^2$, $T_1 + T_2 = T_{\text{CM}} + T_{\text{rel}}$,

$$-\frac{\hbar^2}{2m_1}\,\boldsymbol{\nabla}_1^2 - \frac{\hbar^2}{2m_2}\,\boldsymbol{\nabla}_2^2 = -\frac{\hbar^2}{2M}\,\boldsymbol{\nabla}_{\text{CM}}^2 - \frac{\hbar^2}{2m_{\text{red}}}\,\boldsymbol{\nabla}_{\text{rel}}^2 \quad . \qquad (2.18)$$

The transformation of the separations and their time derivatives are given by

$$\boldsymbol{R}_{\text{cm}} = \boldsymbol{R} \;=\; \frac{1}{M}\,(m_1\boldsymbol{r}_1 + m_2\boldsymbol{r}_2) \quad\text{and}\quad \boldsymbol{r}_{\text{rel}} = \boldsymbol{r} = \boldsymbol{r}_1 - \boldsymbol{r}_2 \qquad (2.19)$$

$$\boldsymbol{V} \;=\; \frac{1}{M}\,(m_1\boldsymbol{v}_1 + m_2\boldsymbol{v}_2) \quad\text{and}\quad \boldsymbol{v} = \boldsymbol{v}_1 - \boldsymbol{v}_2. \qquad (2.20)$$

The inverse transformation is given as

$$\boldsymbol{r}_1 \;=\; \boldsymbol{R} + \frac{m_2}{M}\,\boldsymbol{r} \quad\text{and}\quad \boldsymbol{r}_2 = \boldsymbol{R} - \frac{m_1}{M}\,\boldsymbol{r} \qquad (2.21)$$

$$\boldsymbol{v}_1 \;=\; \boldsymbol{V} + \frac{m_2}{M}\,\boldsymbol{v} \quad\text{and}\quad \boldsymbol{v}_2 = \boldsymbol{V} - \frac{m_1}{M}\,\boldsymbol{v}. \qquad (2.22)$$

For the kinetic energy we have $\frac{1}{2}m_1\,v_1^2 + \frac{1}{2}m_2\,v_2^2 = \frac{1}{2}M\,V^2 + \frac{1}{2}m\,v^2$. This can be proved by substitution.

### 2.6.3 Scattering wave functions

A general solution of the Schrödinger equation is usually not an acceptable wave function unless

- $\Psi$ is finite everywhere,

- $\Psi$ is single valued everywhere,

- $\Psi$ and $\partial\Psi/\partial x$ are continuous everywhere, and

- $\Psi$ is square integrable.

### 2.6.4   Term schemes and radiative transitions

In a supermolecule that consists of a diatomic molecule and an atom, such as $H_2$–X, where X can for example be He, there can only occur radiative transitions in the molecule. The intermolecular potential curve corresponding to such a radiative transition is shown in figure 2.2. When infrared radiation of a suitable frequency is present, the collisional complex may undergo a radiative transition from the initial rotovibrational state to a final rotovibrational state. Such transitions involve a change of the rotovibrational states $E_{\nu j}$. The collisional partner X is implicit in the energy of relative motion, and of course the electric dipole moment without which no optical transition occurs.

In a diatom-diatom collisional complex, such as $H_2$–$H_2$ there can furthermore occur double transitions besides the single transitions. That is, one photon gets absorbed and both molecules simultaneously undergo a rotovibrational transition. The corresponding intermolecular potential curve is shown in figure 2.3. The single photon absorption is direct evidence that more than one molecule is involved.
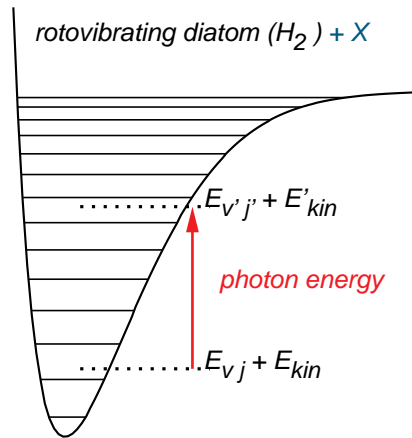
Figure 2.2: Intermolecular potential curve and radiative transition of the diatom-atom complex $H_2$–X, where X can for example represent He. The horizontal lines represent the vibrational energy levels of $H_2$. The energy spacing $\Delta E = E_f - E_i$ is the difference of the rotovibrational energy of initial and final states of the complex, $E_i = E_{\nu j} + E_{kin}$ and $E_f = E_{\nu' j'} + E'_{kin}$, respectively. A prime indicates the final state. Note that optical transitions $H_2^{(\nu j)} + X + \hbar\omega \rightarrow H_2^{(\nu' j')} + X$, corresponding to $E_{\nu j} + E_{kin} + \hbar\omega \rightarrow E_{\nu' j'} + E'_{kin}$ are dipole-forbidden in the non-interacting $H_2$ molecule.
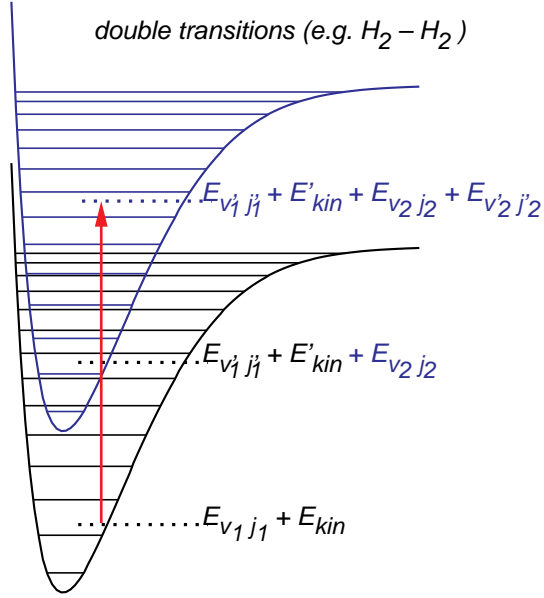
Figure 2.3: Intermolecular potential curves and radiative transitions of a diatom-diatom complex such as $H_2$–$H_2$. The horizontal lines represent the vibrational energy levels of $H_2$. The black curve is the same as above for a single transition, that is, for a transition in only one of the molecules. The blue curve corresponds to a double transition, that is, via absorption of a single photon both molecules undergo a rotovibrational transition. The energy spacing $\Delta E = E_f - E_i$ is the difference of the rotovibrational energy of initial and final states of the complex, $E_i = E_{\nu_1 j_1} + E_{\nu_2 j_2} + E_{kin}$ and $E_f = E_{\nu'_1 j'_1} + E_{\nu'_2 j'_2} + E'_{kin}$, respectively. A prime indicates the final state. Note that optical transitions $H_2^{(\nu_1 j_1)} + H_2^{(\nu_2 j_2)} + \hbar\omega \rightarrow H_2^{(\nu'_1 j'_1)} + H_2^{(\nu'_2 j'_2)}$, corresponding to $E_{\nu_1 j_1} + E_{\nu_2 j_2} + E_{kin} + \hbar\omega \rightarrow E_{\nu'_1 j'_1} + E_{\nu'_2 j'_2} + E'_{kin}$ are dipole-forbidden in the non-interacting $H_2$ molecules.

## 2.7 Electric dipole moments induced by interactions

In classical electrodynamics, an accelerated electric charge emits radiation. In quantum mechanics, radiation is emitted or absorbed in quanta of energy by a charged particle. In most cases of practical significance here dipole transitions (as opposed to monopole transitions) are considered the main sources of emission and absorption where these are "dipole allowed". If in a molecule the centers of positive and negative charge do not coincide these molecules have a permanent dipole moment. Such dipole moments can also be induced by external fields (polarization) or momentarily by collisional interactions. Absorption and emission of rotating or vibrating electric dipoles generally occur at the frequencies of rotation and vibration. In contrast to that translationally accelerated charges (dipoles) emit continuous radiation. Even if no permanent dipole moment exists, molecules can emit in transitions between electronic states, but these transitions typically require more energy than rotovibrational ones, a higher photon energy for absorption and a higher excitation energy, such as provided by higher temperature, for emission. Common homo-nuclear diatomic molecules, such as hydrogen and nitrogen, do not undergo electronic transitions at frequencies in the infrared at room temperature. Because the inversion symmetry is inconsistent with the existence of a dipole moment no absorption is observed. In contrast to that, supermolecular systems usually possess a transient dipole moment during their short existence.

So far collision-induced absorption by pure monatomic gases has never been observed. This is easy to understand, since collisional pairs of like atoms
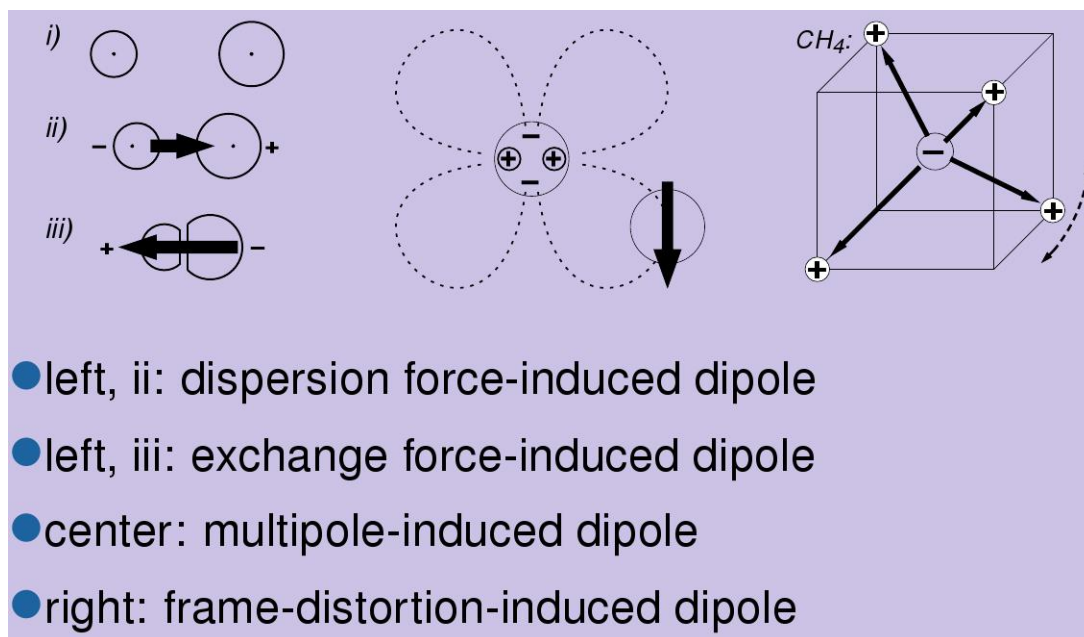
Figure 2.4: The mechanisms that can generate a dipole moment.

cannot develop a collision-induced dipole due to their inversion symmetry which is inconsistent with the existence of a dipole moment [34]. Nevertheless, theoretically triatomic and higher order complexes of like atoms could absorb infrared radiation, but the fact that no absorption has been observed suggests that these absorption coefficients are rather small [36]. Only a very small upper limit of the infrared absorption coefficient could be established for a few rare gases in liquefied form. Pure monatomic gases are probably the only gases that do not show significant collision-induced absorption at any frequency well below x-ray frequencies.

In the following I will discuss some of the forces that can generate dipole moments in supermolecules. Induced dipole moments (see figure 2.4)

28

are generated by the same processes which cause intermolecular repulsion at near range and attraction at long range. Dispersion and exchange forces are both quantum mechanical in nature. The former may be described in semi-classical terms of fluctuating dipole induced dipole interactions and the latter arise from the exchange symmetry of the electronic wave functions imposed by the Pauli principle [34]. If at least one of the interacting particles is a molecule further induction mechanisms arise.

On a scale of the order of atomic size, molecular multipole fields vary strongly with orientation and separation. Thus, there can generally be found induced dipole components arising from field gradients of first and higher order which interact with the so-called dipole-multipole polarizability tensor components [40].

Not all of these induced dipole types exist in any given system. The components that exist generally couple in different ways to the translational, rotational, vibrational, etc. states of the complex and usually are associated with different selection rules, thus generating different parts of the collision-induced spectra.

Supermolecules usually possess an electric dipole moment even if its individual constituent molecules are nonpolar. From the studies of intermolecular forces there are four different universal mechanisms known that can generate these dipoles in supermolecules, which are familiar from the studies of the intermolecular forces [40]:

29

(1) Dispersion force-induced dipoles:

Dispersion forces control the attractive part of the intermolecular interactions. The electronic charge clouds of the constituent molecules may be slightly displaced by intermolecular dispersion forces during intermolecular interactions, generating an electric dipole moment of the supermolecule. Over moderately wide separations, atoms or molecules interact through dispersion forces that arise from electronic intercorrelation. For dissimilar pairs, these are associated with a dipole moment whose asymptotic strength is to leading order in the expansion in terms of 1/R proportional to the inverse seventh power of the intermolecular separation R [40]. The dispersion force-induced dipole is usually weaker than multipole-induced and overlap-induced dipoles, but generally discernible in discriminating analyses.

(2) Exchange force-induced dipoles:

In a collision at near range, when the electronic charge clouds of the collisional partners overlap, according to the Pauli exclusion principle a momentary redistribution of electric charge occurs that is caused by electron exchange. A slight displacement of the electronic charge clouds relative to their nuclei may be caused by intermolecular exchange forces. In general, this will generate a net dipole moment in the supermolecule [40]. Exchange forces control the repulsive part of the intermolecular interactions. Because dispersion forces are attractive and caused by an enhancement of electronic charge in the space between the molecules the polarity of that induced dipole is the opposite of the dispersion force-induced dipole. On the other hand, exchange forces are

repulsive and cause a depletion of electric charge in the region between the interacting constituent molecules. This mechanism is usually the dominant one when dissimilar particles collide. Exchange force-induced dipoles in molecules can also have a certain anisotropy of quadrupolar or higher symmetry.

(3) Multipole-induced dipoles:

In general molecules are surrounded by an electric field which may be described, as is well known from classical electrodynamics, by a multipole expansion, *i.e.* by a superposition of dipole, quadrupole, octopole, ... fields. While molecules are electrically neutral, the electric field surrounding each molecule is set up by the internal electronic and nuclear structure of the molecule. In the field of the permanent multipoles the interacting atoms or molecules will be polarized [40]. For all neutral homo-nuclear diatomic molecules the monopole and dipole terms are zero, so that the lowest order multipole is a quadrupole. When two such molecules interact, the collisional partners are polarized and thus for the duration of the collision possess dipole moments that interact with electromagnetic radiation.

For the case of pure compressed hydrogen gas quadrupolar induction is responsible for nearly 90 percent of the total induced absorption [40]. Because the quadrupole field rotates with the molecule, the collision-induced rotational S lines are quite prominent in the spectra of compressed hydrogen.

(4) Collisional frame distortion-induced dipoles:

Many molecules of a high degree of geometric symmetry possess strong

31

internal dipoles which are arranged that way that the net dipole moment is zero in the unperturbed frame. For example the H–C branches in the $CH_4$ molecule possess four very strong dipole moments. Owing to the tetrahedral symmetry these add up to zero in the unperturbed $CH_4$ molecule. However, during a collision a proton may temporarily be displaced and thus a transient, sizable supermolecular dipole moment may be generated [40].

At large separations, a collisional complex such as He–Ar will be non-polar. However, at intermediate separations dispersion forces may induce a dipole moment in any dissimilar pair and at near range exchange forces induce a dipole moment of opposite polarity.

In general some or all of the mechanisms mentioned above will induce electric dipole moments whenever molecules or dissimilar atoms interact, no matter what kind of particles is considered or how many particles actually interact at any given time, or whether the particles are bound (van der Waals molecules) or free (in collisional interaction). They cause collision-induced absorption, as well as the absorption of bound van der Waals systems. Like intermolecular forces, supermolecular dipoles are omnipresent.

In the vibrational band of pure, *i.e.* unmixed hydrogen, two major induction processes occur, namely overlap- and quadrupole-induction shape the spectra. Consequently, two types of spectral profiles are expected. The isotropic overlap induction generates most of the Q line intensity and quadrupole induction shapes the S lines, and also a small component of the Q branch related to the orientational magnetic transitions is discernable [34]. Thus,

32

the Q branch is a superposition of at least two different profiles. A total of eleven components must be expected for the fundamental band of hydrogen [34]. Specifically, the eleven profiles include the obvious single transitions in just one of the two colliding $H_2$ molecules. These are the $S_1(0)$, $S_1(1)$, and $Q_1(1)$ transitions in one of the two interacting molecules. There also take place double transitions in both collisional partners, such as the simultaneous transitions $Q_1(1)+S_0(0)$, which occur near the $S_1(0)$ transition frequency and $Q_1(1)+S_0(1)$ near $S_1(1)$. With their superposition the measurements can be reproduced closely [34].

Accurate interaction induced dipole surfaces can be obtained from elaborate quantum-chemical calculations [67]. For several binary systems *ab initio* dipoles and empirical ones are available in literature. Even though the subject of this work is not to compute collision-induced dipole surfaces, in the following physical mechanisms will be discussed that can cause an induced dipole moment. This work is mainly concerned with binary complexes of $H_2$. These pairs have inversion symmetry so that no dipole moment can be produced. This is clear in all cases of two identical atoms, but also in the case of two identical molecules with all quantum numbers equal. As an example one may consider two hydrogen molecules, with both vibrational and rotational quantum numbers equal to zero. Since $j$ being zero also implies that $m_j$ is equal to zero they do not possess a collision-induced dipole moment [45]. The van der Waals force of two nonpolar particles can be divided into two components [79]. There is a short range exchange term which has its origin in the Pauli

exclusion principle and prohibits extensive overlap of the electronic charge distributions, and there is a long range dispersion term which has its origin in charge fluctuations causing dipole-dipole interaction.

In the case when at least one particle is a molecule another mechanism, called multipole-induction appears. The hydrogen molecule naturally carries a permanent quadrupole moment. If another particle, for example an atom, is in its proximity, this particle will be polarized in the quadrupole field of the hydrogen molecule. This mechanism is apparently more long range than the van der Waals interaction [89].

If molecular gases are considered the infrared spectra are richer than those in the rare gases. Even if the molecules are non-polar, besides the translational spectra various rotational and rotovibrational spectral components may be expected. Furthermore, other than overlap other induction mechanisms may become important. Dipole components may be thought of as being modulated by the vibration and rotation of the interacting molecules so that induced supermolecular bands appear at the rotovibrational frequencies of the interacting molecules. Lines at sums and differences of these frequencies also occur [34].

The electronic charge distribution of $H_2$ is inversion symmetric and thus the $H_2$ molecule is necessarily non-polar. $H_2$–$H_2$ pairs, just like pairs of virtually all other molecules possess an induced dipole moment, except for certain molecular orientations of high symmetry. However, the hydrogen molecule differs from most other neutral molecules by its large rotational constant, $B_0$

$= 59$ cm$^{-1}$, compared to rotational constants of $N_2$ and $O_2$ of just a few wavenumbers [34]. Therefore collision-induced spectra of systems containing $H_2$ generally show well separated $H_2$ rotational lines, unless temperatures are so high that lines begin to merge.

The lowest order multipole consistent with the symmetry of $H_2$ is the electric quadrupole moment. The $H_2$ $S_0$ lines basically arise from quadrupolar induction; a small overlap component is nearly negligible [68]. A rotation of the $H_2$ molecule through 180 degrees creates an identical electric field. This means that for every full rotation of a $H_2$ molecule the dipole induced in the collisional partner oscillates twice through the full cycle. Thus, quadrupole induced lines occur at twice the classical rotation frequencies, or with selection rules J$\to \pm 2$ like rotational Raman lines of linear molecules. Orientational transitions (J = constant, $\Delta M$ not equal to zero) occur at zero frequency and make up the translational band [34]. For $H_2$–$H_2$, molecule 1 induces a dipole in molecule 2 and vice versa, thereby doubling intensities.

In quantum-chemical calculations the Cartesian components of the dipole moment are obtained, $\boldsymbol{\mu}_x$, $\boldsymbol{\mu}_y$, and $\boldsymbol{\mu}_z$. An example can be found in table 1 in [37]. Because of the induction of the dipole, in scattering calculations it is convenient to perform the transformation into spherical coordinates. According to [76] one has

$$\boldsymbol{\mu}_0 = \boldsymbol{\mu}_z, \tag{2.23}$$

35

$$\boldsymbol{\mu}_\pm = -\frac{1}{\sqrt{2}}(\pm\boldsymbol{\mu}_x + i\boldsymbol{\mu}_y). \tag{2.24}$$

The dipole spherical-tensor coefficients $A_{\lambda_1\lambda_2\Lambda L}$ are according to [6] computed by fitting the spherical dipole components to the expansion

$$\mu_n = \sum_{\lambda_1\lambda_2\Lambda L} A_{\lambda_1\lambda_2\Lambda L}(r_1, r_2, R) Y^{1n}_{\lambda_1\lambda_2\Lambda L}(\Omega_1, \Omega_2, \Omega). \tag{2.25}$$

The vector coupling functions are given by [102]

$$
\begin{aligned}
Y^{1n}_{\lambda_1\lambda_2\Lambda L}(\Omega_1, \Omega_2, \Omega) &= \frac{4\pi}{\sqrt{3}} \sum_{MM_1M_2M_\Lambda} C(\lambda_1\lambda_2\Lambda; M_1M_2M_\Lambda) \\
&\times C(\Lambda L1; M_\Lambda Mn) Y^{M_1}_{\lambda_1}(\Omega_1) Y^{M_2}_{\lambda_2}(\Omega_2) Y^M_L(\Omega)
\end{aligned} \tag{2.26}
$$

where $\Omega_1$ and $\Omega_2$ are the orientation angles of molecules 1 and 2; $\Omega$ denotes the orientation angles of the intermolecular vector; the $Y^m_l$ are spherical harmonics; and the C are Clebsch-Gordan coefficients. Thirty-one A coefficients were actually computed, but only fifteen were found to be significant for collision-induced absorption: $\lambda_1\lambda_2\Lambda L = 0001, 0221, 0223, 2021, 2023, 2211, 2233, 0443, 0445, 4043, 4045, 2465, 2467, 4265, 4267$.

The most important dipole components are the $A_{0223}$, which describe basically the dipole induced *via* the trace of the polarizability tensor of molecule 1 by the electric field of the quadrupole moment of molecule 2, and $A_{2023}$ where molecules 1 and 2 are exchanged. Figure 2.5 shows as an example the former at the fixed intermolecular separation of R = 4 bohr.

36
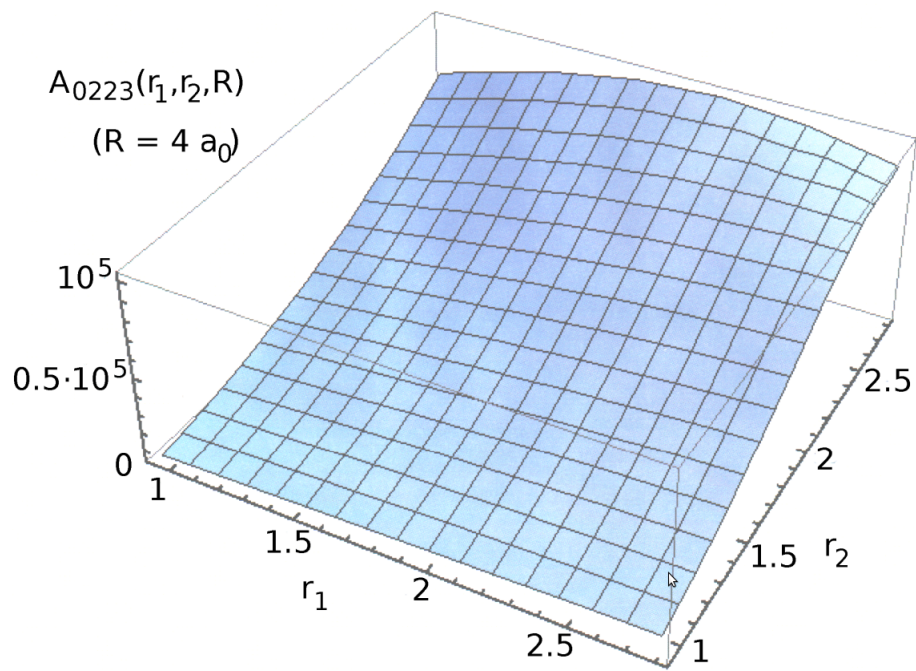
Figure 2.5: The $H_2$–$H_2$ dipole tensor component $A_{0223}(r_1, r_2, R)$ at R = 4 bohr.
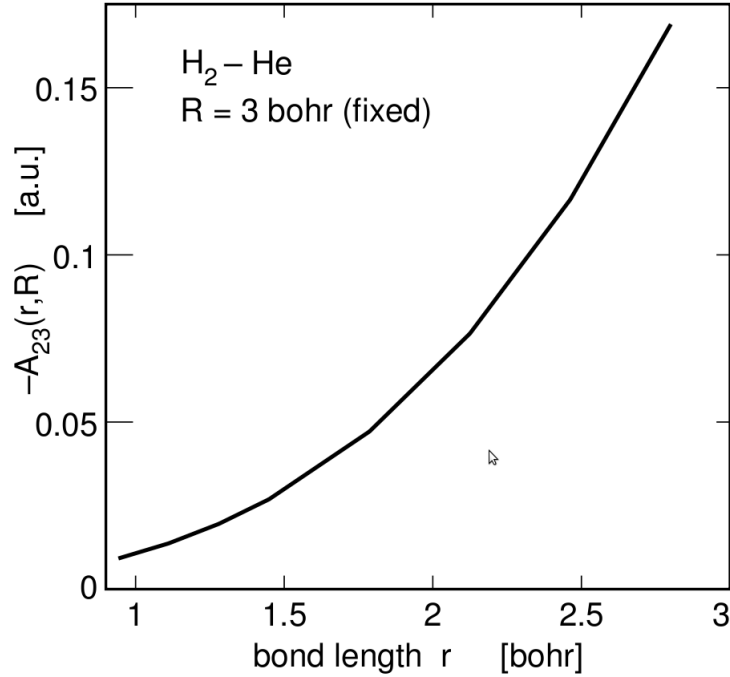
Figure 2.6: The $H_2$–He dipole tensor component $A_{23}$ *versus* the $H_2$ bond length r, at the fixed intermolecular separation of R = 3 bohr.

An expression similar to equation (2.25) may be written down for the spherical dipole tensor components $A_{\Lambda L}$ (r, R) of $H_2$–He collisional systems [34]. An example of the IDS obtained at fixed separation R = 3 bohr is shown in figure 2.6. One of the strongest induced dipole components is the one with the expansion parameters $\Lambda L = 23$, which arises mainly by polarization of the He atom in the electric quadrupole field of the $H_2$ molecule. Together with the isotropic $A_{01}$ component these are the strongest induced dipole components of the $H_2$–He complex.

According to [34], in order to calculate the collision-induced absorption

spectra one needs the vibrational matrix elements of the tensor components $A_{\lambda_1 \lambda_2 \Lambda L}$,

$$B_{\lambda_1 \lambda_2 \Lambda L}^{\nu_1 j_1 \nu_2 j_2 \nu_1' j_1' \nu_2' j_2'}(R) = \langle \nu_1' j_1' \nu_2' j_2' | A_{\lambda_1 \lambda_2 \Lambda L} | \nu_1 j_1 \nu_2 j_2 \rangle \qquad (2.27)$$

for the lines arising from the transition $\nu_1 j_1 \nu_2 j_2 \rightarrow \nu_1' j_1' \nu_2' j_2'$. Note that only the radial part of the $H_2$ rotovibrational wave functions enters the right-hand side of equation 2.27; the angular parts defining the selection rules can be obtained in closed form and are included later in the equation for the absorption coefficient.

For the actual computations of spectral profiles the potential energy surface $V_{000}(r_1, r_2, R)$ must be known, along with the dipole tensor coefficients $A_{\lambda_1 \lambda_2 \Lambda L}(r_1, r_2, R)$. The dipole tensor coefficients are obtained from the induced dipole surface $\boldsymbol{\mu}(\boldsymbol{r_1}, \boldsymbol{r_2}, \boldsymbol{R})$. At the temperatures characteristic for cool white-dwarf atmospheres, the CIA spectra depend on transition dipole matrix elements with vibrational quantum numbers up to $\nu \approx 7$ [61]. To evaluate these matrix elements the induced-dipole and interaction energies of pairs of hydrogen molecules are needed with bond lengths ranging from 0.942 a.u. to 2.801 a.u. (1 a.u. $= 5.29177249^*10^{-11}$ m). For comparison, the vibrationally averaged internuclear separation in $H_2$ is 1.449 a.u., in the ground vibrational state. The PES and the pair induced dipole for $H_2$–$H_2$ have been calculated using MOLPRO 2000 [101] by finite-field methods, at coupled-cluster single and double excitation level, with triple excitations treated perturbatively [CCSD(T)] [61]. MOLPRO's aug-cc-pV5Z(spdf) basis has been employed, consisting of

(9s 5p 4d 3f) primitive Gaussians contracted to [6s 5p 4d 3f]; this gave 124 contracted basis functions for each of the $H_2$ molecules. This basis gives accurate energies and properties [58]; yet it is sufficiently compact to permit calculations on $H_2$ pairs with 28 different combinations of $H_2$ bond lengths, at seven different intermolecular separations, in 17 different relative orientations, and at a minimum of six different applied field strengths for each geometrical configuration [61]. A similar set was used for $H_2$–He complexes, which however also included g functions. For $H_2$–$H_2$ complexes 28 bondlength combinations $r_1$, $r_2$ were chosen from the set {0.942, 1.111, 1.280, 1.449, 1.787, 2.125, 2.463, 2.801 bohr}. 17 independent geometries $\theta_1$, $\theta_2$, $\phi_2$ with $\phi_1 = 0$ were computed, see figure 2.7. Supermolecular properties, such as the potential energy surface of $H_2$–$H_2$ complexes and the induced dipole surface, are obtained at separations R = 3.4, 3.6, 3.8, 4.0, 4.5, 4.0, 6.0, 7.0, 8.0, 9.0, 10.0 bohr. Previous calculations of the $H_2$–$H_2$ induced dipole surface exist [14, 15, 38]. Agreement with the present results is excellent where a comparison is possible [61]. The present work evaluates a greater set of dipole coefficients $A_{\lambda_1 \lambda_2 \Lambda L}(r_1, r_2, R)$ over a greater set of bond distances $r_1$, $r_2$, as necessary for work at elevated temperatures and high frequencies (*e.g.* near the higher $H_2$ overtones). The interested reader can find more detailed information about the *ab initio* calculations in [61].

Highly developed intermolecular potentials exist for many systems, including $H_2$–$H_2$ and $H_2$–He complexes [79, 88]. For the present purposes these are, however, not well suited, because of the common neglect of the rotovi-
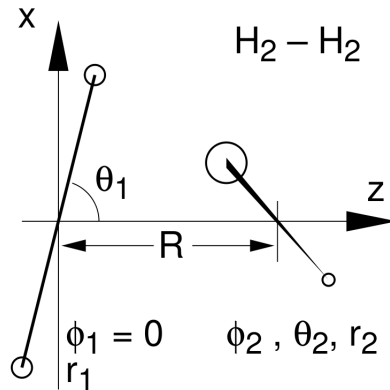
Figure 2.7: Quantum-chemical calculations of two $H_2$ molecules. The $\phi$ and $\theta$ are azimuthal and polar angles of molecule 1 (to the left) and 2 (right); R is the center-to-center separation; bond distances $r_1$ and $r_2$ over a range from 0.942 to 2.801 bohr are chosen.

bratinal state dependence of the molecules involved. "Effective" potentials have been proposed that are said to account for "average" rotovibrational excitations under certain experimental conditions; see for example Ref. [80] for $H_2$–$H_2$. For state to state scattering calculations, effective potentials used on a trial basis were not very successful and we decided to use an *ab initio* potential energy surface which was obtained using quantum chemical computations. The best computational potential models tend to give very accurate repulsive cores, but typically have some uncertainties in the well region, where empirical data are used to improve theoretical potential models when substantial rotovibrational excitations do not occur, at low temperatures, say 300 K or so. Our present interest is CIA at high temperatures, up to thousands of kelvin. Under such conditions the well and long-range regions of the intermolecular

41

potentials of $H_2$–$H_2$ and $H_2$–He do not really matter, as test calculations at 300 K have shown.

Several anisotropic components of the new PES for $H_2$–$H_2$ and $H_2$–He are actually available, but for most calculations we used the isotropic parts only. The accounting for the anisotropy for the scattering process is possible, but complicates the computational effort immensly.

The isotropic parts $V_{000}(r_1, r_2, R)$ and $V_{00}(r, R)$, of the potential energy surfaces $V$ of $H_2$–$H_2$ and $H_2$–He at fixed intermolecular separations $R$ are shown in figures 2.8 and 2.9, respectively. Potential energies change significantly with changes of the bond distances $r$. This fact suggests that the rotovibrational states, and changes of such states, affect the molecular interactions quite noticeably as was observed previously for even small vibrational excitations [86].

The energy levels for a rotovibratinal state corresponding to the vibrational and rotational quantum numbers $\nu$ and $j$ are labelled $E_{\nu j}$. They are considered to be unperturbed during collisions, which is another way to express the assumption that the colliding partners have strong internal interaction while they interact weakly with each other.

The Hamilton operator describing the interaction between two hydrogen molecules with rotating and vibrating degrees of freedom in the presence of a radiation field is according to [45] given by
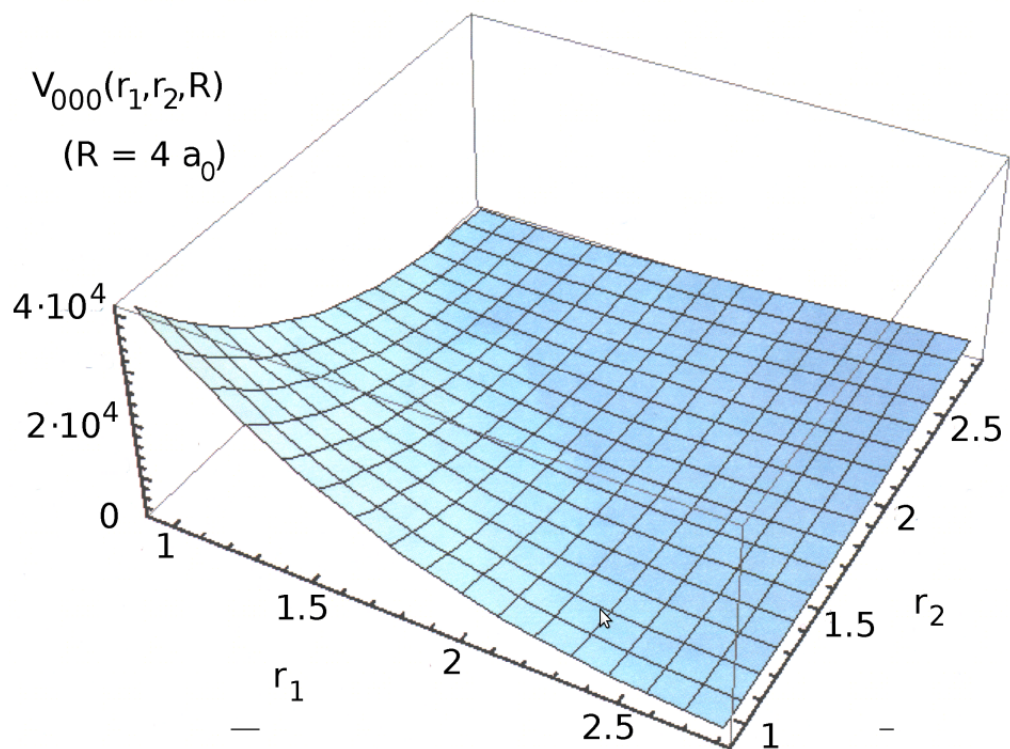
Figure 2.8: The isotropic part $V_{000}(r_1, r_2, R)$ of the $H_2$–$H_2$ potential energy surface at the intermolecular separation of R = 4 bohr.
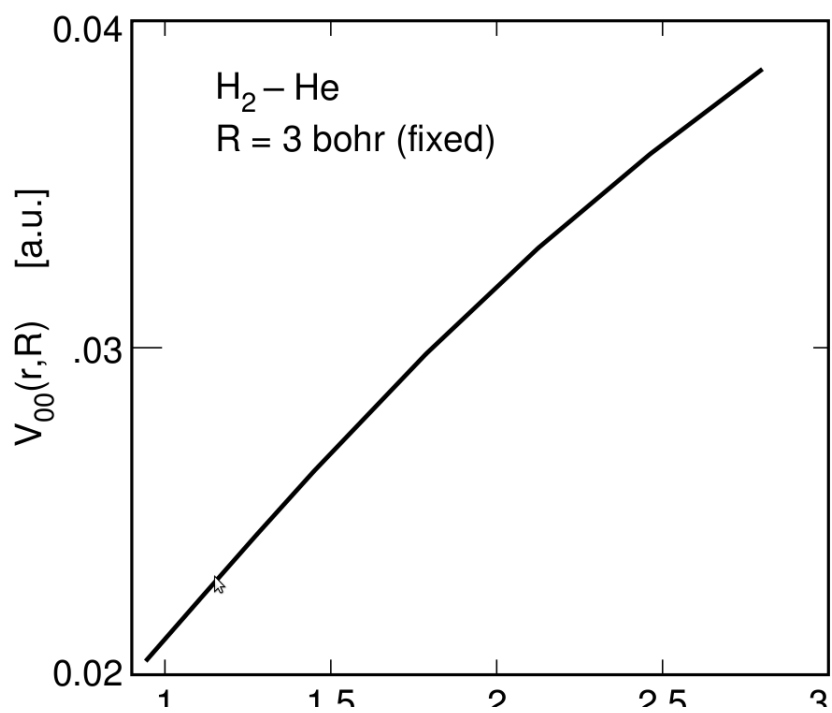
Figure 2.9: The isotropic part $V_0(r, R)$ of the $H_2$–He potential energy surface at the fixed intermolecular separation of R = 3 bohr.

$$H(\mathbf{r}_1, \mathbf{r}_2, \mathbf{R}) = H_1^{H-H}(\mathbf{r}_1) + H_2^{H-H}(\mathbf{r}_2) - \frac{\hbar^2}{2m}\nabla_{\mathbf{R}}^2 + V(\mathbf{r}, \mathbf{R}) + V^{rad}(\mathbf{r}, \mathbf{R}) + H^{rad},$$
$$(2.28)$$

where $V$ is the intermolecular potential of the $H_2$–$H_2$ complex and $m$ is the reduced mass. Above the Hamilton operator for the isolated $H_2$ molecule, $H^{H-H}$, is given. The inter-atomic potential is included in $H^{H-H}$ and not in $V$. The reduced mass is the two particle mass,

$$m = \frac{m_1 + m_2}{m_1 \times m_2}. \tag{2.29}$$

The radiative coupling $V^{rad}$ and the Hamilton operator for the isolated photon field $H^{rad}$ are the ones discussed above. The total wave function can be factorized as the product of the scattering wave function and the photon state [45],

$$\Psi_\alpha(\boldsymbol{r}_1, \boldsymbol{r}_2, \boldsymbol{R}; E) \otimes |n\rangle = \sum_{\alpha' n'} \frac{v_{\nu_1 j_1 \nu_1' j_1'}(r_1)}{r_1} \frac{v_{\nu_2 j_2 \nu_2' j_2'}(r_2)}{r_2} \frac{1}{R} F_{\alpha'\alpha}^{n'n}(R; E) Y_{j'l'}^{J'M'}(\hat{\boldsymbol{r}_1}, \hat{\boldsymbol{r}_2}, \hat{\boldsymbol{R}}) \otimes |n'\rangle,$$
$$(2.30)$$

where $\alpha = (\nu_1, j_1, \nu_2, j_2, l, J, M)^T$ and $Y_{j'l'}^{J'M'}(\hat{\boldsymbol{r}_1}, \hat{\boldsymbol{r}_2}, \hat{\boldsymbol{R}})$ is the vector coupling function, corresponding to $\mathbf{J} = \mathbf{j} + \mathbf{l}$, i.e. the total angular momentum is the sum of rotational and translational angular momentum. Now the Schroedinger equation reads

$$(H - E \times \boldsymbol{I}) \Psi_\alpha \otimes |n\rangle = 0. \tag{2.31}$$

45

Operating from the left with

$$\langle n'' | \otimes \int r v^{\star}_{\nu 1'' j 1'' \nu 2'' j 2''}(r) \, dr \int Y^{J'' M'' \star}_{j'' l''}(\hat{\boldsymbol{r}}_1, \hat{\boldsymbol{r}}_2, \hat{\boldsymbol{R}}) \, d\hat{\boldsymbol{r}}_1 \, d\hat{\boldsymbol{r}}_2 \, d\hat{\boldsymbol{R}} \qquad (2.32)$$

integrates out five of the six spatial variables [45], where the integral $\int d\hat{\boldsymbol{r}}_1 \, d\hat{\boldsymbol{r}}_2 \, d\hat{\boldsymbol{R}}$ denotes the integral over the solid angles of the vectors $\boldsymbol{r}_1$, $\boldsymbol{r}_2$, and $\boldsymbol{R}$, respectively. Evaluation yields the radial equation

$$\left( E_{\nu_1'' j_1'' \nu_2'' j_2''} - \frac{\hbar^2}{2m} \frac{d^2}{dR^2} + \frac{\hbar^2 l'' (l'' + 1)}{2mR^2} s + n'' \hbar \omega - E \right) F^{n'' n}_{\alpha'' \alpha}(R; E) \qquad (2.33)$$

$$+ \sum_{\alpha' n'} \left[ V_{\alpha'' \alpha'}(R) \, \delta_{n'' n'} + W_{\alpha'' \alpha'}(R) \, \delta_{n'' \pm 1, n'} \right] F^{n'' n}_{\alpha'' \alpha}(R; E) \; = \; 0,$$

which is a coupled differential equation in the intermolecular spacing $R$.

## 2.7.1 Ternary systems

Spectroscopic signatures arising from more than just two interacting atoms or molecules have also been discovered in the studies of collision-induced absorption [36]. These involve a variation with density of the normalized profiles, $\alpha(\omega)/\rho^2$, which are density invariant only in the low-density limit. In early years after the discovery of ternary dipoles in supermolecular systems models were proposed that treat the ternary dipoles in terms of pairwise-additive dipole components [34]. These attempts were not very successful. More recently, evidence, experimental as well as theoretical, has emerged that substantial irreducible ternary dipole components exist [34], at least for some

46

systems. For all systems for which reliable pair dipoles are known, pairwise-additive ternary dipole components were reported. Significant shortfall of the calculated spectral moments compared with measurements of the ternary spectral moments of the absorption spectra of numerous gases and mixtures has been observed. This has been interpreted as an indicator that irreducible ternary dipole components exist in most - if not all - systems considered, certainly in unbound systems consisting of three $H_2$ molecules.

With increasing temperature the significance of these irreducible dipole contributions increases rapidly [34]. This suggests that the ternary dipole components result from close encounters, *i.e.* from triple collisions with more or less overlapping electron clouds. Generally, the interaction-induced dipoles resulting from three interacting molecules consist of the vector sum of the pairwise additive dipole components, in addition to an irreducible ternary surface. Several studies suggest that the principal irreducible dipole component is of the exchange quadrupole-induced dipole (EQID) type, but more work is needed for a better understanding of the irreducible ternary dipole surfaces [34]. Momentarily, during a binary collision, at near range exchange forces displace the electronic molecular clouds relative to the nuclei to the far sides of the binary complex. This generates momentarily a strong quadrupole moment. In the electric field of the exchange force-induced quadrupole the third molecule is then polarized.

EQID is a quantal mechanism. In early years it was proposed that the irreducible dipole could be the classical permanent quadrupole-induced dipole-

induced dipole. It was found that this dipole is not nearly as strong as EQID
in the three interacting $H_2$ molecules [34].

In dense systems such as in liquids and solids, the three-body and
probably higher order cancellations due to destructive interference are very
important. Two components of translational spectra are distinguished, one
due to the diffusive and the other due to the oscillatory ("rattling") motions
of the molecules in a liquid. The latter is analog to the intercollisional spectrum
and consists of a dip to very low intensities near zero frequency. In contrast to
the good understanding of translational spectra of mono-atomic liquids, very
little is known about those of molecular liquids. The understanding of ternary
and higher order spectra is in its beginnings.

Although some attempts exist to model ternary systems, exact quan-
tum treatments of collision-induced spectra are presently only known for bi-
nary systems. In moderately dense media this binary contribution dominates
the spectra.

### 2.7.2   Intercollisional dips

Correlations of interaction-induced dipoles can lead to destructive in-
terference in subsequent collisions. This is the reason for the experimentally
observed quite striking absorption dips of isotropic induced dipole components,
typically at zero frequency shift, *e.g.* Q- branches. These so called intercoll-
sional absorption dips may be considered many body effects. When the time
t between collisions is much larger than the mean duration $\Delta t$ of a collision,

these dips are sharp features. At such frequencies virial expansions of the line shape are not possible, in other words, it is impossible to separate contributions at frequencies where absorption dips occur. If one considers small enough frequency shifts the absorption dips may be considered true many-body effects [34]. In the past the shapes of absorption dips have often been modelled by inverted Lorentzian profiles [34].

Theoretical studies of the intercollisional dip [34] of rare gas mixtures have shown that without the assumption of an irreducible ternary dipole component in rare gas triples the experimentally observed spectra could not be reproduced theoretically. Furthermore, in 1995 Reddy and associates found a spectral feature in the interaction-induced second overtone band of $H_2$ that corresponds to a simultaneous transition in three molecules, three $H_2$ molecules in collisional interaction, underwent a simultaneous vibrational transition in the presence of a single photon. These simultaneous triple transitions with absorption of a single photon have long been predicted by theorists [40]. They are believed to be due to the irreducible dipole components.

Remarkably, a single, semi-quantitative dipole model explains the three independent observations (third virial coefficient, intercollisional dip, triple transitions) which support the existence of irreducible dipole components.

### 2.7.3   The absorption coefficient

The absorption coeficient $\alpha(\omega, T)$ is not only a function of frequency $\omega$ but also of temperature $T$, density, and, of course, the nature, composition,

and state of matter (gaseous, liquid, solid) of the sample.

We approximate the intermolecular potential with an isotropic form,

$$V(\boldsymbol{r_1}, \boldsymbol{r_2}, \boldsymbol{R}) \approx V_{000}(r_1, r_2, R) \tag{2.34}$$

which makes the extensive molecular scattering computations manageable. We are interested in weak radiation fields (*i.e.*, single photon absorption) so that the standard perturbation treatment of the $-\mu \times \boldsymbol{E}$ term is sufficient. After applying the usual separation of variables procedures to the Schroedinger equation above, the numerical work begins with the integration of the radial Schroedinger equations of initial and final state for a given optical transition. Radial scattering wave functions $\Psi_{k,l}^{\nu_1 j_1 \nu_2 j_2 \nu_1' j_1' \nu_2' j_2'}(R)$ are obtained using Cooley's method [26, 31] of integration. The radial wave functions are energy-density normalized [14, 34],

$$\int_0^\infty \Psi_{k'',l}^{\nu_1 j_1 \nu_2 j_2 \nu_1' j_1' \nu_2' j_2' *}(R) \Psi_{k,l}^{\nu_1 j_1 \nu_2 j_2 \nu_1' j_1' \nu_2' j_2'}(R) dR = \delta(E_{k''} - E_k) \tag{2.35}$$

where $\delta(x)$ is Dirac's $\delta$ function. $k$ and $k'$ are the wave vectors of the initial and final states; $k''$ is the wave vector of an arbitrary energy. The intermolecular potential is given by the radial rotovibrational matrix element of the potential energy surface (PES),

$$V_{000}^{\nu_1 j_1 \nu_2 j_2} = \langle \nu_1 j_1 \nu_2 j_2 | V_{000}(r_1, r_2, R) | \nu_1 j_1 \nu_2 j_2 \rangle. \tag{2.36}$$

50

Once the radial scattering wave functions $\Psi^{\nu_1 j_1 \nu_2 j_2}_{k,l}(R)$ and $\Psi^{\nu_1' j_1' \nu_2' j_2'}_{k',l'}(R)$ are computed, the profiles of individual spectral lines may be obtained according to [34],

$$
\begin{aligned}
VG^{\nu_1' j_1' \nu_2' j_2' \nu_1 j_1 \nu_2 j_2}_s(\bar{\omega}, T) &= \lambda_0^3 \hbar \sum_{l,l'} (2l+1) C(lLl'; 000)^2 \times \\
&\times \int_0^\infty e^{-E_t/kT} \\
&|\langle \Psi^{\nu_1' j_1' \nu_2' j_2'}_{k',l'}(R) | B^{\nu_1 j_1 \nu_2 j_2 \nu_1' j_1' \nu_2' j_2'}_s(R) | \Psi^{\nu_1 j_1 \nu_2 j_2}_{k,l}(R) \rangle|^2 dE_t.
\end{aligned}
\tag{2.37}
$$

The label $s$ stands for one of the sets of dipole expansion parameters $\lambda_1 \lambda_2 \Lambda L$ and $\bar{\omega}$ is $2\pi$ times the frequency shift relative to the line center $\omega_{ctr}$,

$$
\hbar \omega_{ctr} = (E_{\nu_1' j_1'} - E_{\nu_1 j_1}) + (E_{\nu_2' j_2'} - E_{\nu_2 j_2}).
\tag{2.38}
$$

The partial wave angular momentum quantum number is called $l$ and $\lambda_0$ is the thermal de Broglie wavelength [34]. The factor $V$ of $G$ to the left of the equation is typical of all second virial coefficients [72]; it is the volume.

If van der Waals molecules exist, one must account for bound-state to bound-state, and for bound-to-free and free-to-bound transitions, in addition to the free-to-free transitions. The procedures are the same as explained above. The spectral density then becomes

51

$$VG_s^{\nu_1'j_1'\nu_2'j_2'\nu_1j_1\nu_2j_2}(\bar{\omega},T) = \lambda_0^3\hbar\sum_{l,l'}(2l+1)C(lLl';000)^2 \times \qquad (2.39)$$

$$\times\,(\int_0^\infty e^{-E_t/kT}$$

$$|\langle\Psi_{k',l'}^{\nu_1'j_1'\nu_2'j_2'}(R)|B_s^{\nu_1j_1\nu_2j_2\nu_1'j_1'\nu_2'j_2'}(R)|\Psi_{k,l}^{\nu_1j_1\nu_2j_2}(R)\rangle|^2dE_t$$

$$+\sum_{\nu_i,\nu_f}e^{-E\nu_il_i/kT}$$

$$\langle E_{\nu_fl_f}l_f|B_s^{\nu_1j_1\nu_2j_2\nu_1'j_1'\nu_2'j_2'}(R)|E_{\nu_il_i}l_i\rangle|^2\delta(E_{\nu_fl_f}-E_{\nu_il_i}-\hbar\omega)$$

$$+\sum_{\nu_i}e^{-E\nu_il_i/kT}$$

$$\langle E_{\nu_il_i}+\hbar\omega,l_f|B_s^{\nu_1j_1\nu_2j_2\nu_1'j_1'\nu_2'j_2'}(R)|E_{\nu_il_i}l_i\rangle|^2$$

$$+\sum_{\nu_f}e^{-(E_{\nu_fl_f}-\hbar\omega)/kT}$$

$$\langle E_{\nu_fl_f}l_f|B_s^{\nu_1j_1\nu_2j_2\nu_1'j_1'\nu_2'j_2'}(R)|E_{\nu_fl_f}-\hbar\omega,l_i\rangle|^2)$$

with $l_f = l_i \pm 1$.

The first term will in general give the most substantial contribution which is from free-to-free transitions. The radial wave functions $\Psi_{k,l}^{\nu_1j_1\nu_2j_2}(R)$ correspond to free states, that is states of positive energy. This first term gives a relatively unstructured, diffuse spectral 'line'.

The second term describes the bound-to-bound contributions, that is the rotovibrational bands of the van der Waals dimer. If the system does not form dimers, this term and the following two terms all vanish. For practical use, the $\delta$ function in this term should be replaced by an instrumental slit function, or perhaps with some Lorentzian if pressure broadening affects the

52

individual lines (as will often be the case). In any case, the $\delta$ function is symbolic for the relatively sharp dimer lines that must be contrasted with the very diffuse free-to-free contribution of the first term.

The third and fourth terms give the bound-to-free and free-to-bound contributions, respectively. These are diffuse continua, more or less structured if scattering resonances are important.

The resulting absorption spectrum is the superposition of the profiles of all lines $(\nu_1' j_1' \nu_2' j_2' \nu_1 j_1 \nu_2 j_2)$ and dipole components $(s)$,

$$\alpha(\omega, T) = \frac{2\pi^2 N_a^2}{3\hbar c}\rho^2\omega(1 - e^{-\hbar\omega/kT})Vg(\omega, T). \tag{2.40}$$

$N_a = 2.67 \times 10^{18} cm^{-3}$ is Loschmidt's number, and [34]

$$\begin{aligned} Vg(\omega, T) &= \sum_s \sum_{\nu_1' j_1' \nu_2' j_2' \nu_1 j_1 \nu_2 j_2} (2j_1 + 1)P_1(T)C(j_1\lambda_1 j_1'; 000)^2 \quad (2.41) \\ &\times (2j_2 + 1)P_2(T)C(j_2\lambda_2 j_2'; 000)^2 \\ &\times VG_s^{\nu_1' j_1' \nu_2' j_2' \nu_1 j_1 \nu_2 j_2}(\omega - \omega_{\nu_1' j_1' \nu_2' j_2' \nu_1 j_1 \nu_2 j_2}, T). \end{aligned}$$

The $P_i(T)$ are population probabilities of the initial rotovibrational states of molecules $i = 1, 2$. The Clebsch-Gordan coefficients imply the selection rules $|j_i' - j_i| \leq \lambda_i$ for $i = 1, 2$.

## 2.8 Spectral moments

For a detailed study of collision-induced spectra and the comparison of measurements with theory, certain integrals of the spectra, the spectral moments, are of interest. The nth spectral moment is defined as an integral of the line profile according to [34] as

$$M_n = \int_{-\infty}^{\infty} \nu^n V g(\nu) d\nu, \tag{2.42}$$

where $g(\nu)$ is the spectral density function and the order number $n$ is a non-negative integer. These integrals converge due to the nearly exponential fall-off of typical spectral functions. Rather than reflecting the specific shape of the absorption profile the zeroth order moment represents the total intensity and is related by theory to familiar sum formula. The first order moment corresponds to the mean width. For nearly classical systems, that means massive pairs at high temperature and not too high frequencies, the first moment is relatively small and drops to zero in the classical limit. The ratio of second and zeroth moment defines some average frequency squared that may be considered a mean spectral width squared.

Theoretically, a complete set of spectral moments may be considered equivalent to the knowledge of the spectral line shape [34]. However, practically speaking, moments higher than the second have rarely been determined, presumably because of experimental difficulties related to the exponential intensity fall-off of the profiles. Nevertheless, knowledge of only the lowest three

moments, and a good choice of a model profile are sufficient to obtain surprisingly good representations of many spectra of practical significance [34]. Up to now only the zeroth, first, and second spectral moments have been computed with semi-classical expressions. For higher order moments one has to take into account quantum mechanics. For the spectral moments also virial expansions exist.

## 2.9   Theoretical importance of CIA

Collision-induced absorption of electromagnetic radiation is important in any cool, *i.e.* cool enough that molecules still exist in sufficient numbers and are not mainly dissociated, and dense environment, *i.e.* dense enough so that binary collisional pairs provide discernable induced intensities. Since the discovery of CIA many absorption bands by binary complexes of molecules have been investigated both theoretically and experimentally. Rotovibrational and electronic bands are found even in regions which are forbidden in the non-interacting molecules. There also occur new bands at sums and differences of rotovibrational frequencies. Supermolecular absorption is due to interaction-induced dipole moments of two or more molecules [40]. A complex of two or more molecules may be considered another molecule, with new properties and spectra, besides those of its constituents. Their origin causes the super-molecules to have new interaction-induced and interaction-modified properties besides the sum of the properties of the unperturbed, *i.e.* non-interacting or well separated, constituent molecules. Such a complex is called a super-

molecule, even if its lifetime is rather short. The term molecule will be reserved for the constituents that make up a supermolecule. Changed properties include multipole moments and polarizabilities, and the associated rotovibrational, electronic, and Raman spectra, especially in (dipole-) forbidden bands [40]. Furthermore, via single photon emission/ absorption there can occur simultaneous double, triple, ... transitions, at sums and differences of molecular transition frequencies and these transitions can even take place at (dipole-) forbidden frequencies of the single constituents.

Collision-induced absorption is generally observed in gases, liquids, solids, and even in plasmas [34]. However, since induced dipole moments are usually weaker than most familiar permanent dipoles, for measurements high collision-rates are necessary. This may lead to the assumption that the denser the medium the stronger the absorption. This suggests that liquids and solids should be better suited for measurements than dilute gases. However, due to the inversion symmetry a perfectly isotropic liquid prohibits any interaction-induced dipole moments. In real liquids there are particle fluctuations around the isotropic configuration, so that nevertheless interaction-induced dipoles come about, but the CIA in liquids is generally weaker than expected from their high particle density.

### 2.9.1 Comparison between regular rotovibrational and interaction-induced spectra

There are a number of differences between regular rotovibrational molecular and interaction-induced spectra. Spectral intensities are proportional to the square of the dipole moment from which they arise. Thus, (dipole-) allowed rotovibrational lines of a polar molecule may be stronger than an induced one by several orders of magnitude. However, at intermediate gas densities many more pairs, triplets, ... exist than monomers, and for dense systems induced spectra may actually be quite strong because of large numbers of supermolecules. Due to the generally great differences in intensity between dipole-allowed lines or bands and interaction-induced lines the latter are discernable without ambiguity. In general the dipole strengths of supermolecules are several orders of magnitude weaker than those of the constituents, who usually possess a dipole moment in the order of 1 debeye. Accordingly, line intensities of supermolecular spectra are typically insignificant at low densities, but they may be quite striking as gas densities are increased. Moreover, interaction-induced lines usually possess dimer features near the line centers. It should also be mentioned that supermolecular dipole strengths fall of rapidly with increasing separation. This is one of the reasons why it took so long to discover supermolecular spectra.
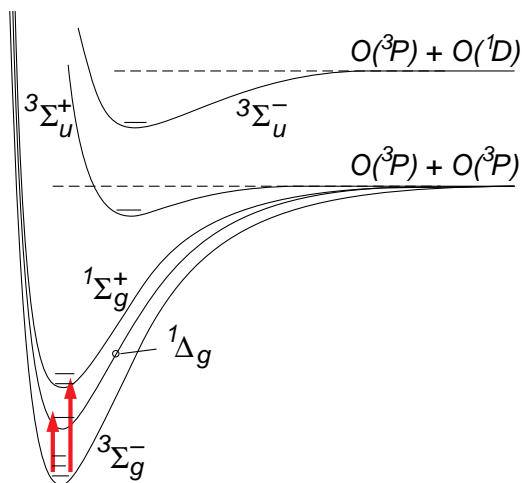
Figure 2.10: The low-lying electronic states of the $O_2$ molecule. The lowest vibrational levels are also indicated.

## 2.10   Electronic collision-induced spectra

All spectra this work is concerned with arise from supermolecular transitions that leave the electronic states of the collisional partners unchanged. If photon energies are sufficiently small, the possibility of changing electronic states is finite. Typically collision-induced electronic spectra occur at higher photon energies than those considered here [34]. However, some of the common molecules possess electronic states with excitation energies so low that electronic collision-induced spectra in the infrared, visible, and near ultraviolet region can occur. As an example one may consider the $O_2$–$N_2$ and $O_2$–$O_2$ spectra in the visible [34]. In figure 2.10 an example of the electronic transitions for $O_2$ is shown.

## 2.11  Van der Waals molecules

Compared to chemical forces that bind the common molecules van der Waals forces are weak, so weak that most dimer-monomer collisions will dissociate the dimer. Typically, this destruction is balanced out by a certain rate of formation, so that the bound dimer concentrations are kept at a low level [34]. In many cases the average lifetime of bound dimers corresponds to a free mean time between monomer collisions, which is roughly in the order of $10^{-9}$ s in air at standard temperature and pressure, and decreases correspondingly with increasing density and temperature [36]. For comparison, a collisional complex may be thought to exist for the time of the duration of a fly-by encounter which is three orders of magnitude shorter. Van der Waals dimer bands are known to be highly susceptible to pressure broadening, which is one reason why it took so long to actually record dimer bands. Moreover, for spectroscopical resolution of dimer bands high spectral resolution has to be employed.

## 2.12  Collision-induced emission

While this work only deals with collision-induced absorption it should be noted that any gas that absorbs electromagnetic radiation will also emit. Supermolecular absorption and emission are inseparable [40]. Cold gases emit in the infrared, which often goes unnoticed. Striking supermolecular emission occurs in hot and dense environments, such as in shock waves and cold stars.

# Chapter 3

# Various Considerations of CIA Spectra

## 3.1 Why *ab initio* calculations of CIA spectra are required

The theory of collision-induced absorption developed by van Kranendonk and coworkers [94] and other authors ([21],[29], [28], [70], [71]) has emphasized spectral moments (sum formulas) of low order. These are given in closed form by relatively simple expressions and can be obtained from spectroscopic measurements by integration over the profile as discussed in the last chapter. Two different kinds of spectral moments are widely used: one kind characterizes an individual line profile, say of a quadrupole-induced (or overlap-induced) line profile. In this case typically three numbers are given, $M_0$, $M_1$, and $M_2$, which describe line intensity ($M_0$), mean line width ($M_1/M_0$), and mean line width squared ($M_2/M_0$). It should be noted that occasionally even third and higher order moments are given. A line profile would be defined if the infinitely many moments $M_i$ were known. These moments are usually preferred in theoretical considerations.

The other kind of spectral moments gives certain integrated intensities of a whole band, *e.g.* of the $H_2$ fundamental band. In that case typically two numbers are given, the total band intensity $\gamma_0$, and the integral of intensity

over frequency, $\gamma_1$. These quantities are typically specified in experimental (spectroscopic) work, but they can also be expressed in terms of the $M$ moments, if all significant induction mechanisms are known.

The spectral moments characterize spectral profiles in important ways. However, it is clear that some information is lost if a spectroscopic measurement is reduced to just one or two numbers. Furthermore, even if large parts of the spectra are known accurately, for the determination of experimental spectral moments substantial extrapolations of the measured spectra to low and high frequencies are usually necessary [34]. Thus, for detailed analyses of measured spectra line shape calculations are indispensible, especially where the complete absorption spectra cannot be measured. Moments are integrals, *i.e.* averages, of the spectral function and are thus generally less discriminating than line shape calculations to the subtle differences of dipole model and interaction potential, if only a small number of moments is known.

Early attempts to calculate the induced dipole moments of $H_2$–$H_2$ from first principles are described in [14]. It took some time until substantial problems of those computations could be controlled and precise data be generated by SCF and CI calculations, so that the basis set superposition errors were small and the CI excitation level adequate for the long-range effects. Details of these computations can be found in [14] and [38]. The SCF-CI quantum chemical methods are clearly the methods of choice for the computation of induced dipole surfaces where practicable. However, the computational requirements are high and approximations with much less stringent demand are

61

of considerable interest.

Some applications require supermolecular absorption spectra at temperatures, for which no laboratory measurements exist or when laboratory measurements had to be taken at much higher densities than atmospheric densities. In these cases calculations of spectral profiles and intensities of supermolecular spectra are necessary [34]. Given that one has reliable intermolecular potential and induced dipole functions available using a quantum formalism the spectra of interacting pairs of molecules may be modeled. Since for many applications the anisotropy of the interaction potential may be neglected the isotropic potential approximation can be used [34]. This simplifies the computational procedures enormously and makes it possible to do complete line shape calculations on personal computers within a few days. As a first step such calculations involve the determination of the rotovibrational energies of the bound dimer. It is already possible to compute reliable free-to-free, free-to-bound, bound-to-free and bound-to-bound transition dipole matrix elements so that complete spectra can be composed for comparison with measurements and for various applications in planetary and earth science. In the past close agreement between these calculated spectra and the measured ones has been observed [34].

However, calculations accounting for the anisotropy of the intermolecular potential may be done but are very computation intensive [18]. They may be marginally feasible for the massive molecular systems one is concerned with in studies of the earth's atmosphere. Thus, it is interesting to compare the

results of these calculations that take into account the anisotropy of the intermolecular potential with simplified quantum calculations that can be done in minutes even on personal computers, whereas close coupled computations may take months of computer time.

It should be mentioned that due to the smallness of interaction-induced dipoles measurements of supermolecular absorption spectra are quite demanding [34]. To make up for that deficiency in laboratory measurements one may be tempted to use high gas densities. However, one has to be careful to avoid ternary and higher-order contributions that may not be present, to such an extent, in atmospheric research, where gas densities are generally lower. Furthermore, measurements of the so-called enhancement spectra of gas mixtures usually possess a somewhat greater uncertainty than measurements of pure gases [40]. This is a result of the fact that in gas mixtures such as of helium and hydrogen one has to subtract the $H_2$–$H_2$ contributions from the sum of absorptions due to the $H_2$–$H_2$ and $H_2$–He pairs. Since the spectra are fairly similar subtraction of comparable intensities renders the end result more uncertain.

Some calculations exist that account for the anisotropy of the intermolecular interactions, based on the close coupled (CC) scheme ([18], [45]). Their computational procedures are substantially more complicated and such calculations are very time consuming.

Rotovibrational combination lines are usually very diffuse and overlap, so much that individual lines cannot be resolved. However, in the isotropic

potential approximation their contribution to the opacity must be calculated individually and afterwards summed over all dipole-allowed and significant lines.

## 3.2 Line shape calculations

As mentioned above measurements of binary collision-induced absorption spectra and their intensities are difficult and only a limited number of accurate measurements for certain species and temperatures exist so far. However, for astrophysical applications, in particular for the modeling of planetary and stellar atmospheres, one needs absorption spectra at arbitrary temperatures. For this, extrapolations of the measured absorption coefficients to temperatures and frequencies of interest are needed, but these are often not purely binary and frequently quite noisy and thus not always sufficient for serious modeling. Alternatively, one can rely on accurate computed absorption profiles. These profiles can be computed with high precission and made available for applications for arbitrary temperatures.

For the computation of the binary collision-induced absorption the intermolecular potential, or potential energy surface is needed, in order to determine the dynamics of the collision [34]. In addition, one needs the interaction-induced dipole surface to obtain the radiative transition probabilities [18]. For the interaction-induced dipole surfaces the best data are almost exclusively obtained from quantum-chemical *ab initio* calculations. However, the most reliable values for the potential of the weakly interacting van der Waals com-

plexes are typically semi-empirical [34]. It is generally possible with *ab initio* calculations to obtain the long-range attractive part and the short range repulsive part with good precision, but for the intermediate region, better results are obtained from measurements of scattering cross sections [34].

Given these intermolecular potentials and interaction-induced dipoles one can compute CIA line shapes to provide astrophysicists and other specialists with the data they need. Since its discovery the understanding of collision-induced absorption by binary systems has made huge progress and quantum calculations of CIA line shapes are in good agreement with laboratory measurements [36]. For the calculation of collision-induced absorption spectra for this work Fortran program codes and the Intel Fortran compiler were used.

### 3.2.1  Opacity calculations

For comparisons of measured spectra of diatomic molecules with quantum calculations the isotropic potential approximation (IPA) [34] has been applied. In this approximation one neglects the dependence of the intermolecular potential on the orientation of the diatomic molecule, which simplifies the calculations enormously (and makes extended calculations possible at the elevated temperatures envisioned).

### 3.2.2 About collision-induced spectral "lines"

The collision-induced absorption (CIA) pair spectra consist of a great number of spectral "lines" at the rotovibrational transition frequencies,

$$\hbar\omega_{\nu_1 j_1 \nu_1' j_1' \nu_2 j_2 \nu_2' j_2'} = E(\nu_1' j_1') - E(\nu_1 j_1) + E(\nu_2' j_2') - E(\nu_2 j_2) , \qquad (3.1)$$

which are their center frequencies. The $E(\nu_i j_i)$ are the well-known rotovibrational levels of the $H_2$ molecule. $\nu$ and $j$ are vibrational and rotational quantum numbers, respectively. i labels the molecule (i = 1 or 2). Unprimed quantum numbers represent the initial rotovibrational state and a prime indicates the final such state of the two interacting molecules considered. It should be remarked that ternary and higher-order collisional complexes require different treatment [34] and are not considered in this work. The rotovibrational combination "lines" are actually quasi-continuous, *i.e.* they are very broad (a spectroscopist would say "diffuse") and usually overlap, so much that individual lines cannot be resolved. Typical atomic lines in the visible have a natural width in the order of about $10^{-3}$ cm$^{-1}$, independent of temperature. CIA "lines," on the other hand, are rougly 100,000 times broader, amounting in dense hydrogen gas to about 100 cm$^{-1}$ at 300 K, because of the short duration of a (binary) collision: $\Delta t \approx 10^{-13}$ s, compared to the lifetime of atomic states in the order of $10^{-8}$s: $\Delta t \times \Delta\omega \geq \frac{1}{2}$, Heisenberg's uncertainty relation. Nevertheless, in the IPA, their contribution to the opacity has to be calculated individually and must be summed over all significant (dipole-)

allowed supermolecular lines in the end.

The angular frequency $\omega = 2\pi f = 2\pi ck$ in equation (3.1), and the associated frequencies $f$ and $k$, are "absolute" frequencies and always non negative. These are to be distinguished from the frequency shifts, relative to the line centers,

$$\omega_{\text{sh}} = \omega - \omega_{\nu_1 j_1 \nu_1' j_1' \nu_2 j_2 \nu_2' j_2'} \,. \tag{3.2}$$

Frequency shifts are considered when the wings of the individual lines are concerned. They may be positive or negative and will be distinguished by a subscript, $\omega_{\text{sh}}$, $f_{\text{sh}}$, and $k_{\text{sh}}$, respectively, and describe the wings of the induced lines relative to their line centers.

### 3.2.3 About the ID and PE surfaces

The CIA spectra are quasi-continua in the infrared and extend at high enough temperatures into the visible part of the electromagnetic spectrum [34]. The absorption profiles and -intensities can be calculated if

i) the induced dipole (ID) and

ii) the intermolecular potential energy (PE) surfaces

are known (IDS, PES). These must come from quantum-chemical computations that are refined to the point where the weak (!) van-der-Waals interactions are accounted for with sufficient accuracy. Drs. K.L.C. Hunt and X. Li at Michigan State University [61] have provided such data for pairs of

highly rotovibrating hydrogen molecules. These have been cast in spherical tensor form, *i.e.* the direct results of the quantum-chemical calculations, which are obtained in cartesian tensor form, $\boldsymbol{B}(\boldsymbol{r}_1, \boldsymbol{r}_2, \boldsymbol{R})$ with $\boldsymbol{B} = (B_x, B_y, B_z)^T$, and $V(\boldsymbol{r}_1, \boldsymbol{r}_2, \boldsymbol{R})$ are converted to spherical tensor form $B_{\lambda_1 \lambda_2 \Lambda L}(\boldsymbol{r}_1, \boldsymbol{r}_2, \boldsymbol{R})$ and $V_{\lambda_1 \lambda_2 L}(\boldsymbol{r}_1, \boldsymbol{r}_2, \boldsymbol{R})$, of which only the leading component $V_{000}(r_1, r_2, R)$ is used in the isotropic potential approximation [34]. $\boldsymbol{r}_1$ and $\boldsymbol{r}_2$ are the separation vectors of the nuclei of each molecule, and $\boldsymbol{R}$ is the center-to-center separation of the molecules, also in vector form. The $\lambda_1$, $\lambda_2$, $\Lambda$, and $L$ are the expansion parameters [34]. The dipole $\boldsymbol{B}$ is a rank 1 tensor and the potential energy $V$ is of rank 0. The spherical tensor components of the IDS and PES of $H_2$–$H_2$ complexes were made available in table form.

## 3.3 Calculation of collision-induced absorption spectra from first principles

The collision-induced absorption spectra are functions of angular frequency $\omega$ and temperature $T$ and are calculated according to

$$\alpha(\omega, T) = \frac{2\pi}{3\hbar c} \frac{1}{2} N_a^2 \rho^2 \, \omega \left( 1 - \exp\left[ -\frac{\hbar\omega}{k_B T} \right] \right) \, V g(\omega, T), \qquad (3.3)$$

where $N_a$ is Avogadro's number, $\rho$ is the number density of the gas in amagat units, $k_B$ is Boltzmann's constant, $V$ is the volume, and $g(\omega, T)$ is the spectral function [34],

$$V g(\omega, T) = \sum_{s,s'} P_s \sum_{t,t'} V P_t \frac{1}{4\pi\epsilon_0} \left| \langle t \,|\, \boldsymbol{B}_{s,s'}(R) \,|\, t' \rangle \right|^2 \, \delta(\omega_{s,s'} + \omega_{t,t'} - \omega) \ . \quad (3.4)$$

Here, $s = \{\nu_1 j_1 \nu_2 j_2\}$ labels the initial rotovibrational states of molecules 1 and 2. A prime indicates the final state. $P_s$ and $P_t$ are the (temperature-dependent) population probabilities of the molecular and the translational states [34]. $t = \{E_t \ell\}$ labels the translational state of the collisional pair. Dirac's $\delta$ distribution conserves energy, with $\omega_{s,s'}$ given by equation (3.1). The spectral function may be rewritten according to [34], as

$$g(\omega, T) \qquad\qquad\qquad\qquad\qquad\qquad\qquad\qquad\qquad (3.5)$$
$$= \sum_{\lambda_1 \lambda_2 \Lambda L} \sum_{s,s'} (2j_1 + 1) P_1 \, C(j_1 \lambda_1 j_1'; 000)^2 \, (2j_2 + 1) P_2 \, C(j_2 \lambda_2 j_2'; 000)^2$$
$$G_{\lambda_1 \lambda_2 \Lambda L}(\omega - \omega_{s,s'}, T).$$

The $G$ functions are the individual "line profiles", [34], and $\omega_{\mathrm{sh}} = \omega - \omega_{s,s'}$ is the frequency shift relative to the line center. Energy conservation may be written as

$$E(\nu_1 j_1) + E(\nu_2 j_2) + \hbar\omega + E_t = E(\nu_1' j_1') + E(\nu_2' j_2') + E_{t'} \ , \qquad (3.6)$$

or simply $\hbar\omega_{\mathrm{sh}} = E_{t'} - E_t$.

### 3.3.1 ID and PE matrix elements

The induced dipole and potential energy surfaces of a pair of hydrogen molecules were obtained by Hunt and Li by highly refined quantum-chemical methods, which account for the weak van-der-Waals interactions of collisional pairs of molecules. Induced dipoles and intermolecular interaction potentials depend on the rotovibrational states of the two molecules involved, which at the temperatures of interest is of quite significant importance. These quantities were obtained for a set of separations ($3.4 \leq R \leq 10$ bohr) and bond distances ($0.942 \leq r_1, r_2 \leq 2.801$ bohr) [61]. The cartesian tensor components of rank 1 and 0 were then converted to spherical tensor components, $B_{\lambda_1 \lambda_2 \Lambda L}(r_1, r_2, R)$ and $V_{000}(r_1, r_2, R)$, the anisotropic components $V_{\lambda_1 \lambda_2 \Lambda}(r_1, r_2, R)$ are ignored in the isotropic potential approximation. Up to 31 dipole components with different labels $\lambda_1 \lambda_2 \Lambda L$ are known, but only about half of them are significant for opacity calculations. These $B$ and $V_{000}$ coefficients were made available in the form of numerical tables, in atomic units.

The supermolecular dipole transition elements are calculated from these tables, according to

$$B_{\lambda_1 \lambda_2 \Lambda L}^{s,s'}(R) = \langle \nu_1 j_1 \nu_2 j_2 | B_{\lambda_1 \lambda_2 \Lambda L}(x_1, x_2, R) | \nu_1' j_1' \nu_2' j_2' \rangle. \qquad (3.7)$$

The $B_{\lambda_1 \lambda_2 \Lambda L}(x_1, x_2, R)$ are analytical functions, obtained by a *least-mean-squares* fit of each complete table by two-dimensional polynomials of 3rd order, with $x_i = r_i - \langle r \rangle$ for i = 1, 2, with $\langle r \rangle = 1.449$ bohr. It should be remarked here that the preferrable product ansatz of two polynomials, e.g. $P_1(x_1) \times P_2(x_2)$,

70

did not give the desired accuracy at the more highly excited rotovibrational states and was abandoned. The $|\nu_1 j_1 \nu_2 j_2\rangle$ are the *radial* rotovibrational matrix elements of the molecular pair, ignoring at this point the translational state of relative motion of the pair. The matrix elements $B_{\lambda_1 \lambda_2 \Lambda L}^{s,s'}(R)$ are made available in the so-called $b$- or $\beta$-functions, for example b0223.for, b0445.for, etc., etc., where the four numerals stand for $\lambda_1$, $\lambda_2$, $\Lambda$, $L$, and the ending .for is the typical Fortran extension. These thirty-one $\beta$ functions are labeled with the expansion parameters just mentioned, but will implicitly reflect the molecular states $s$, $s'$ as well: Prior to any call to these $\beta$ functions, there must be a call to betacom, an entry used but once in these Fortran functions, which prepares these functions for the various molecular states as required. It should be noted that the Clebsch-Gordan coefficients in equation (3.5) eliminate all but a few of the final rotational states:

$$j_1 - \lambda_1 \leq j_1' \leq j_1 + \lambda_1 \quad \text{and} \quad j_2 - \lambda_2 \leq j_2' \leq j_2 + \lambda_2 \qquad (3.8)$$

corresponding to the selection rules from the triangular inequalities of the Clebsch-Gordan coefficients, with $j_1 \geq 0$ and $j_2 \geq 0$. For a given set of initial rotovibrational quantum numbers $s$, all other $j'$ values give zero contributions to the opacity. However, no selection rules exist for the vibrational molecular states $\nu_1$, $\nu_2$. In other words, many overtones and combination overtones exist in the CIA profiles.

71

### 3.3.2 Translational ID matrix elements

The radial translational dipole matrix elements are obtained from equation (3.7) by calculating the translational wave functions of relative motion of the pair $|t\rangle = |E_t, \ell\rangle$ by integrating the radial Schroedinger equation. Since a great variety of initial and final states is required, the intermolecular potential energy surface — the state-sensitive intermolecular potential — must be set up such that initial and final states are appropriately reflected. This is done by calling the entry vacumon once prior to calling the V000rvib.for function, with the appropriate bimolecular states $s$ and $s'$. This is done automatically when running cirme.for. (This is similar to running betacom in order to set up the $\beta$ functions, also done automatically when starting cirme.for.)

The fortran program cirme.for computes the translational dipole matrix elements,

$$\left\langle E_t\ell \left| B^{s,s'}_{\lambda_1\lambda_2\Lambda L}(R) \right| E_{t'}\ell' \right\rangle, \tag{3.9}$$

required in the individual line profiles. Cirme stands for "collision-induced radial matrix elements." The program requires carefully selected input ("cirme.in") and produces many MB of output ("_X.RME") to store the significant $10^6$ or so matrix elements and labels, equation (3.9). A follow-up fortran program aline.for (for "absorption line") then computes the individual line profile and outputs files of these profiles on a frequency and temperature grid. These must be then summed over all significant line profiles, for use by the astronomers.

## 3.4 The Computer programs (overview)

### 3.4.1 Supermolecular levels and transitions (LINES)

First of all one has to choose a certain mean temperature $\langle T \rangle$, a frequency range one is interested in and a cut-off value for the population probabilities one wants to account for in the calculations. This is input for the program lines.for. This Fortran program gets furthermore as input the potential energy levels of the atomic species under consideration. While running lines.for an output file, lines.out, is produced, which lists the quantum numbers of the transitions that have a higher probability than the previously described probability cut-off and are important for the temperature and frequency range chosen. These quantum numbers become input for the Fortran program cirme.for, to be discussed in the next section.

### 3.4.2 Translational transition probability matrix elements (CIRME)

The collision-induced translational radial dipole matrix elements, equation (3.9), are computed by running CIRME.FOR for the many "lines" that contribute to the absorption at the frequencies of concern. cirme.for must be compiled and linked with a beta function, the appropriate intermolecular potential function (V000rvib.for or vaoo.for), and several mathematical subroutines as needed. After that, a suitable input file cirme.in must be written. Reasonable choices must be made for a number of very important quantities, such as:

- a suitable range of partial waves with quantum numbers $0 \leq \ell \leq \ell_{max}$

- one of many "lines" of interest must be chosen: $\nu_1 j_1 \nu_2 j_2 \rightarrow \nu_1' j_1' \nu_2' j_2'$, depending on the frequency range considered, and corresponding to the lines output

- an array (called a range) of frequency shifts $\omega_{sh}$ must be chosen, units are $cm^{-1}$

- an array (called again a range) of free-state kinetic energies, $E_{CI}$, of relative motion must be chosen, for the chosen "mean temperature", units are also $cm^{-1}$

- a few other choices may be made to shorten the extensive calculations.

There are plenty of choices one has to make and many of them can go wrong, but no internal warnings are issued — one just gets bad numbers. It is therefore of the utmost significance to check the calculations carefully every step along the way: convergence of sum over partial waves, suitably dense range of frequency shifts and kinetic energies, sum formulas, etc.. (Most of these checks can be made only after running aline.for, to be discussed in the next section). If anyone of the checks does not look 100% solid, it is often possible to obtain a clue as to the likely cause of the inaccuracy, unless there were too many bad choices.

Before one can compute the translational dipole matrix elements, equation (3.9), one needs the operator $B^{s,s'}_{\lambda_1 \lambda_2 \Lambda L}(R)$ of these matrix elements. This is done automatically: prior to every call of the beta function, the ENTRY

74

BETACOM is called where for the given "line" the necessary operations are done. Similarly, for each new "line" a different intermolecular potential function is needed, which is set up automatically by calling VACOM prior to any call to VA. It should be mentioned that the results of executing cirme.for are stored in the file _X.RME, which usually has a size between 10 and 50 MB. Since there will in the end be very many of these, it is best to immediately run aline.for after cirme.for and let the file _X.RME be overwritten by executing another cirme.for run. However, the results of aline.for are to be archived carefully — which is all that is needed for the calculations of opacities, and their names are carefully designed so that overwriting does not happen (except the aline.out files will go away, which is o.k. once all the checks were made).

When choosing a "line", selection rules must be obeyed. First $\lambda_1$ and $\lambda_2$ are selected by choosing a b$\lambda_1\lambda_2\Lambda L$.for function, and then $j_1$ and $j_2$, to obtain the possible upper rotational states (regardless of the $\nu_1$, $\nu_2$ values),

$$j_1 - \lambda_1 \leq j_1' \leq j_1 + \lambda_1, \tag{3.10}$$

$$j_2 - \lambda_2 \leq j_2' \leq j_2 + \lambda_2,$$

with the additional requirements, $j \geq 0$ and "even $j \to$ even $j$" and "odd $j \to$ odd $j$" for each $H_2$ molecule.

The chosen "mean temperature" $\langle T \rangle$ or "mean energy" $\langle E_{ci} \rangle = \langle k_B T \rangle$ defines a meaningful range of kinetic energies, $E_{ci}$, of relative motion. In previous work in the group, it was found necessary to choose a range of free state energies from roughly $\frac{1}{20}\langle k_B T \rangle$ to $20\langle k_B T \rangle$; a geometric progression is desir-

75

able, which, however, limits the increments to approximately $k_B\mathrm{T}$ or less for the lowest temperatures of about $\frac{1}{2}\langle k_B T\rangle$ anticipated. It should be remarked that such a choice of a mean temperature permits usually opacity calculations for temperatures $T$ from $\frac{1}{2}\langle T\rangle$ to $2\langle T\rangle$, if the $E_{ci}$ array is properly chosen.

The array of frequency shifts $\omega_{sh}$ must go from large negative values to large positive values, so that the lowest wing intensities are small enough for the range of opacities anticipated. For instance, if the peak of the opacity is, for example, $10^{-5}$ cm$^{-1}$ amagat$^{-2}$, and one wants the smallest meaningful opacities to be around $1/1000$ or $1/10000$ of the peak, for each line opacities must be computed down to well below that desired value. The red wing falls off faster than the blue wing and requires smaller negative shifts than the blue wing. At shifts near the line center a dense grid is desirable (to get the spectral integrals with good accuracy), but the nearly exponential fall-off of the far wings usually permits much larger shifts (and permits reasonable inter- and even extrapolations).

### 3.4.3 "Line" profiles (ALINE)

To run aline.for, it must be compiled and linked with several mathematical functions as usual. The input, aline.in, is straight-forward; a range of temperatures should be specified such that its output can directly be included in the opacity tables to be discussed in the next subsection. The name of the output tape is a series of twelve one-digit numbers,

$$\lambda_1\lambda_2\Lambda L\nu_1 j_1\nu_2 j_2\nu_1' j_1'\nu_2' j_2'. \tag{3.11}$$

76

For example, the file with the name 022301010103 represents one of the main quadrupole-induced components of the important (collision-induced) rotational $S_0(1)$ line of $H_2$: specifically, molecule 1 remains in the groundstate and molecule 2 undergoes the $S_0(1)$ transition (which is (dipole-) forbidden in non-interacting $H_2$ molecules). Each number has just one digit - the name is 4+8 single digit numbers long. Since rotational quantum numbers greater than 9 will eventually arise, A is used for 10, B for $11, \cdots$, Z for 36. It should be repeated here once more that these files (3.11) must be carefully archived, if one does not want to repeat the corresponding line calculations over and over. Aline.out is not needed once all the necessary testing is done, described in the previous subsection - which must precede the archiving of the above files.

It should be mentioned here that many lines have an identical twin. Whenever $\lambda_1 \neq \lambda_2$,

$$\lambda_1 \lambda_2 \Lambda L \nu_1 j_1 \nu_2 j_2 \nu_1' j_1' \nu_2' j_2' \quad \text{and} \quad \lambda_2 \lambda_1 \Lambda L \nu_2 j_2 \nu_1 j_1 \nu_2' j_2' \nu_1' j_1' \tag{3.12}$$

are identical (exchange of molecules!). If one wants to save computer time one should not compute identical results (although it would be perfectly alright): lengthy cirme calculations need not be duplicated. Rather, one must set up a procedure that generates identical files.

### 3.4.4 Spectral profiles (OPACITY)

Finally, after the contributions from all significant lines have been computed in the way described above the absorption intensities from the different

dipole components and lines have to be sumed up. This is done by running the Fortran program opacity.for. This program gets as input a selected temperature within the range of $\frac{1}{20}\langle k_B T\rangle$ to 20 $\langle k_B T\rangle$ and the lines that were computed with lines.for. It produces as output a table that lists the absorption coefficient $\alpha$ as a function of frequency $\omega$, in the form of a table, in increments of 20 cm$^{-1}$.

### 3.4.5  The data base (HITRAN)

The astronomers, who have great need for the opacity data, want the results in the form of a big (!) table.

- Temperatures from 1000 to 7000 K as a minimum, in steps of 250 K. (For brown dwarfs, temperatures down to 50 K are of interest)

- Opacities at absolute frequencies from 667 through 20,000 cm$^{-1}$ are needed, in steps of 20 cm$^{-1}$.

Such tables are readily compiled by summing the various tapes directly — a trivial task. However, it is of great importance that these tapes are good.

## 3.5  The calculations

For most calculations in this work the isotropic potential approximation (IPA) was used, which simplified the calculations enormously. An example of an anisotropic potential CIA calculation can be found in [18]. It is easy to generate some numbers with a computer, but the important part of the work

was to make sure that these numbers are correct and meaningful. To ensure the reliability of the generated numbers several checks were performed:

### 3.5.1 Convergence of partial wave expansion

The expansion of partial waves is in general infinte. However, since one has only finite computer time available and the higher order waves have less and less contribution, one has to truncate the partial wave expansion at a certain cut-off angular momentum. However, one has to make sure that one does not truncate the partial wave expansion too soon and takes into account all physically relevant features. The programs were run with different numbers of included partial waves and the results of these runs were compared with each other to ensure convergence. It should be noted that the higher the highest energy $E_{ci}$ and temperature, the more partial waves are needed. Here as above $E_{ci}$ denotes the initial kinetic energy of relative motion of the colliding pair of molecules. It should furthermore be pointed out that exchange force-induced dipole components may require more partial waves than multipole-induced ones so that it was necessary to compare the complete spectra for each number of partial waves. Nevertheless, agreement between all calculations for different numbers of included partial waves to better than 0.2 % was observed.

### 3.5.2 Properly selected array of frequency shifts $\omega_{sh}$

Since the collision-induced lines are very asymmetric with respect to their line centers, negative frequency shifts as well as positive ones have to be

considered. It should be pointed out that the blue wing is much wider than the red wing so that much larger positive frequency shifts (the blue wing) had to be chosen than negative ones. In general, a very dense spacing was chosen near zero frequency shifts to ensure that the zeroth moments along with the strongest contributions of the lines were obtained accurately. Farther out into the wings, where nearly exponential fall-off sets in, monotonically increasing larger spacings were used, in order to ensure that spline interpolation was still accurate. The lowest and highest frequency shifts were chosen generous.

Again to ensure numerical accuracy the programs were run with a chosen array of frequency shifts $\omega_{sh}$ and afterwards the same calculations were repeated with an array of frequency shifts with the double step size. The two results were compared and a relative deviation of a maximum of 0.5% was observed. It was furthermore ensured that the line wings were computed down to small enough opacities, both in the red and in the blue wing. For the strongest lines, the ratio between line center intensity to wing intensities was larger than $10^7$. For the weak lines, the calculated extreme wing intensities where comparable to the cut-off values chosen for the strong lines. If this were not the case, it would be possible to find steps in the final opacity spectrum, which of course would be an undesirable artifact. In this work the focus is on single-photon absorption processes and the broad free-free features of collision-induced spectra. These allow for a rather sparse frequency grid, so that the computer times were accepable.

### 3.5.3 Properly selected array of free state energies $E_{ci}$

The initial kinetic energies of the relative motion of the colliding pair of molecules, $E_{ci}$, depend on the temperatures considered. The calculated radial matrix elements have to be averaged over the free state energies of the Maxwell distribution of velocities. The processes relevant for collision-induced absorption take place in an energy intervall from roughly $\frac{1}{20}k_B T$ to $20 k_B T$. For the averaging procedure spline integration was chosen, based on an energy grid $E_{ci}$, properly chosen for the temperatures under consideration. Similar to the array of frequency shifts the calculations were performed with a selected array of free state energies $E_{ci}$ and afterwards the same computation was repeated with an array of free state energies with twice the step size. Again the two results were compared and the relative deviation was seen to be less than 0.5%.

### 3.5.4 Accounting for all relevant lines

After a certain frequency range was chosen as input for lines.for and the calculations were performed a wider frequency range was chosen to make sure that all contributing transitions are included in the calculation. The results of the two computations were compared and agreement was observed.

Since there were many choices to be made repeated calculations were performed in order to ensure that the produced numbers are reliable. For each change of data set a new calculation was run. As a further test of these line shape calculations, the zeroth, first and second spectral moments have been computed in two different independent ways: by integration of the spectral

functions with respect to frequency and also from the well known quantum sum formulas. The two results were compared and agreement to better than 1.5% was observed.

As input for the calculation of absorption profiles and -intensities the induced dipole (ID) and the intermolecular potential energy (PE) surfaces have to be known. As mentioned above these come from quantum-chemical computations which are refined to the point where the weak van der Waals interaction is accounted for with sufficient accuracy. Such data of highly rotovibrating hydrogen molecules were provided for this work from Drs. K.L.C. Hunt and X. Li at Michigan State University [61]. The direct results of the quantum-chemical calculations which have been obtained in cartesian tensor form were cast in spherical tensor form. For the isotropic potential approximation only the leading component is used. The isotropic interaction potential [64] supports just one vibrational dimer level, the ground state $n = 0$. For the computation of the collision-induced spectra the radial Schroedinger equation was integrated numerically. For supermolecules with a limited number of electrons, such as $H_2$–$H_2$, $H_2$–He, ..., very accurate quantum-chemical calculations of the dipole surfaces exist. Such *ab initio* results show clearly the various dipole components: exchange force-induced dipoles show an exponential decrease with increasing separation R between the interacting molecules. Dispersion force-induced dipoles fall of to leading order in the expansion in terms of $1/R$ as $R^{-7}$, and multipole-induced dipoles have their characteristic long-range behavior of exactly $R^{-N}$, with $N = 3$ for dipolar induction, $N = 4$

for quadrupolar induction, etc. It is important to mention that quantum-chemical studies of this kind can provide some guidance for the development of empirical models for bigger systems that cannot be treated by the demanding quantum-chemical methods.

For binary multi-electron supermolecules, such as the ones found in the Earth's atmosphere ($N_2$–$N_2$, $N_2$–$O_2$, ...) or the $H_2$–$H_2$ supermolecules considered in this work, the dipole surfaces may often be represented by the (semi-) classical multipole-induced dipole approximation, which neglects or else models empirically the quantum effects of the exchange forces. Generally applicable expressions have been given by Poll and Tipping.

The multipole-induced dipole components are typically much stronger than the overlap and exchange contributions if one or both of the interacting molecules are highly polarizable [34]. Thus, the former may be neglected or perhaps represented by small and relatively inexact, empirical corrections. Then the induced dipole components may be computed by use of classical electrodynamics from the knowledge of molecular multipole strengths and polarizabilities. Tensor calculations by Hunt and collaborators also account for the non-uniformity of the local electric field, the gradient of the field, the dispersion dipole, and the hyperpolarizabilities. It should be mentioned that the electronic supermolecular spectra arise similarly by multipolar induction, but in this case the electronic multipoles are due to electronic configurations.

### 3.5.5 Symmetry considerations

For $H_2$–$H_2$ the two interacting hydrogen molecules can be considered to be chemically distinguishable at the kinetic energies considered in this work [45]. Thus, exchange of one proton belonging to molecule 1 with one of molecule 2 and similar with 1 and 2 interchanged does not have to be considered. This proton exchange only has to be taken into account when the two interacting molecules have the same total nuclear spin. Therefore, p-$H_2$ and o-$H_2$ are distinguishable from one another, whereas two p-$H_2$ molecules as well as two o-$H_2$ molecules have to be considered identical particles and their wave functions must be symmetrized correctly. Since for ground state hydrogen both electrons are in s orbitals the electronic wave functions are unaffected from this operation.

p-$H_2$ has zero nuclear spin so that the weights for symmetric, $\omega^+$, and antisymmetric, $\omega^-$, respectively, are [18]

$$w^+_{pp} = 1 \qquad (3.13)$$

and

$$w^-_{pp} = 0. \qquad (3.14)$$

Therefore, the only allowed solutions for the coupled equations involving p-$H_2$ are symmetric. In the case of o-$H_2$ molecules (nuclear spin one), the normalized nuclear weights are

84

$$w_{oo}^+ = 2/3 \qquad\qquad (3.15)$$

and

$$w_{oo}^- = 1/3. \qquad\qquad (3.16)$$

As long as no magnetic material is present in reality the probability for spin flips is extremely small. Thus, in the present model no interaction is involved that can flip spin, so that the $\pm$ symmetry is conserved in the calculations.

### 3.5.6 Comparison with measurements

From the measured intensities $I$ the absorption coefficient $\alpha(\nu)$ may be obtained via

$$\alpha(\nu) = -Log[I(\nu)/I_0(\nu)]/L, \qquad\qquad (3.17)$$

where $I$ denotes the transmitted intensity and $I_0$ is the incident intensity, either measured, when the cell is evacuated or filled with helium gas. The optical path length is denoted by $L$. The absorption coefficient is generally a function of frequency $\nu$, temperature $T$, and gas density $\rho$. The binary absorption coefficient is defined according to

$$\alpha_0(\nu) = \alpha(\nu)/\rho^2. \qquad\qquad (3.18)$$

It gives, to good approximation, the total absorption due to supermolecules, if ternary and higher order contributions are negligible. Since even in the best measurements ternary and possibly higher order contributions to the absorption may be present, the binary absorption coefficient is best obtained via extrapolation to the limit of zero density of the values $\alpha_0(\nu)$, at fixed frequencies $\nu$.

# Chapter 4

# Results and analysis

Translational spectra involve transitions between states of relative motion of the collisional pair, without changing the rotovibrational or electronic states of the interacting molecules themselves. They occur at zero frequency but due to their considerable widths, their wings generally extend well into the microwave and far infrared regions of the electromagnetic spectrum.

Translational transitions of an unbound pair correspond to vibrational transitions of a bound pair. Since no restoring force is present, the center frequency is zero in atom-atom collisions (*e.g.* He–Ar), or if no rotovibrational transitions occur if molecules are involved.

## 4.1 Results for $H_2$–$H_2$

### 4.1.1 The Rototranslational spectrum of hydrogen

The research described in this section is published in [2, 6, 61]. Previously [18] a comparison of a measurement of the collision-induced absorption by hydrogen in the rototranslational band with calculations of binary collision-induced absorption was undertaken to test the binary nature of the measurement, but certain inconsistencies were observed in the blue wing of the spectrum. At that time no definite conclusion could be drawn wether the measurement was affected by three-body and higher-order interactions or the earlier calculations were not sufficiently converged to the high-order spherical dipole tensor coefficients [18]. For example, theory could have truncated the expansion of the spherical tensor components of the induced dipole surface too soon, when including more dipole components was no option at that time. On the other hand, measurements of the far wing of the translational spectrum are difficult because of the weak absorption, so that fairly high gas densities have to be employed for recording of low-noise signals. However, as pointed out above, with increasing gas densities ternary and perhaps higher order contributions do usually appear which may be difficult to separate from the desired purely binary ones. Thus, it could have been possible that the measurement was affected by ternary and possibly higher order contributions, to an unknown extent. Theory is capable of calculating the binary spectra. Calculations of ternary spectra have not yet been attempted. The measurement ([18], [22]) was undertaken in the expressed desire to provide accurate

knowledge of absorption data of dense hydrogen gas at wavelengths around 5 $\mu$m where traces of other contributions could possibly be discovered in an analysis of the Voyager spectra ([30], [63]). However, at that time no definite conclusion could be drawn whether the measurement was deficient or the theory.

In the meantime, new quantum-chemical calculations of the dipole surfaces have been made with a greater selection of spherical tensor components [61]. It is therefore interesting to reconsider the comparison of the latest theory and the existing measurements. In the previous calculation [18] only the $\lambda_1\lambda_2\Lambda L = 0001, 0221, 0223, 2021, 2023, 2211, 2233$ dipole components were used, along with the lumped together 0443+0445 and 4043+4045 components, as described in [38]. In the present calculation the latter dipole components are now appropriately separated. Besides, components where one of the $\lambda_1$, $\lambda_2$ equals 2 and the other 4 are now also available [61].

In figure 4.1 the rototranslational collision-induced absorption spectrum at 300 K is shown. The spectrum is given in a semi-logarithmic plot so that regions of high and low absorption are rendered with constant relative precession. In this figure an *ab initio* calculation (solid curve), based on the new dipole and potential energy surfaces, is compared with two measurements ([18], [22]). Over the whole range of frequencies shown the measured and the calculated spectrum agree very well with each other. The quadrupole-induced dipole components, $\lambda_1\lambda_2\Lambda L = 0223, 2023$ are the most important components of the spectrum. Near the rotational lines these give the dominating contribu-
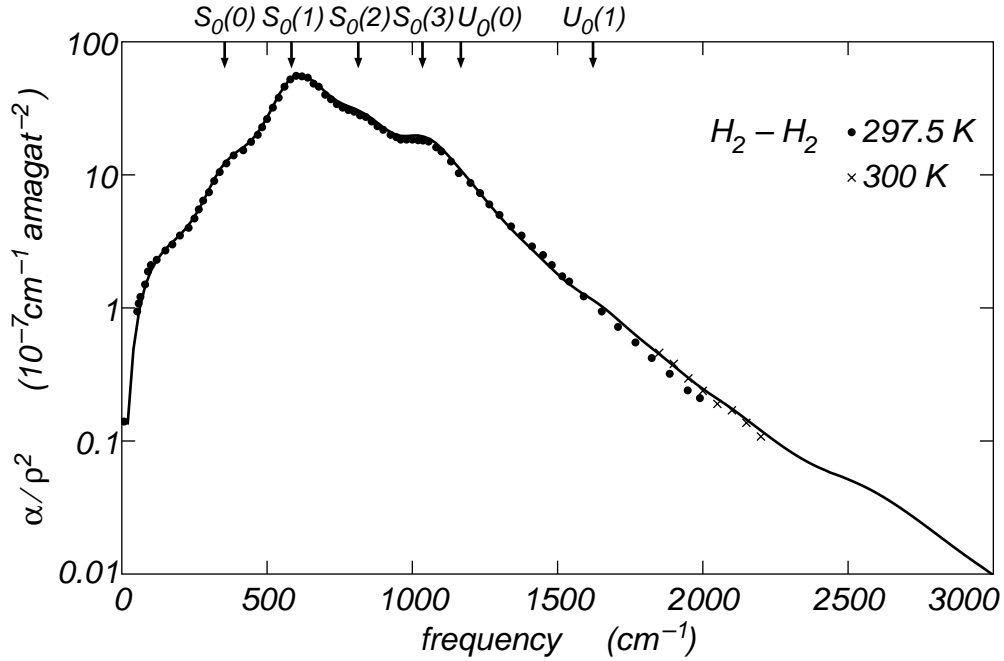
Figure 4.1: The $H_2$–$H_2$ absorption spectrum at temperatures around 300 K in the rototranslational band. Measurements: dots: [27], crosses: [22]; calculation: solid curve.

tions. Near the $S_0(0)$ and $S_0(1)$ lines, these quadrupole-induced intensities are nearly identical with the total intensity and differ from it only at high frequencies, where the quadrupole interacting with the anisotropy of the polarizability ($\lambda_1\lambda_2\Lambda L = 2233$) and some other components ($\lambda_1\lambda_2\Lambda L = 0221$, 2021, 0443, 4043, 0445, 4045) add significantly to the total absorption. The structures are numerous because many rotational states are populated.

In contrast to the earlier calculation [18] the calculation based on the new dipole surface reproduces the measurements in the far blue wing closely, whereas the comparison of the earlier calculation with the measurements yielded that the calculation gave too much intensity in the far blue wing
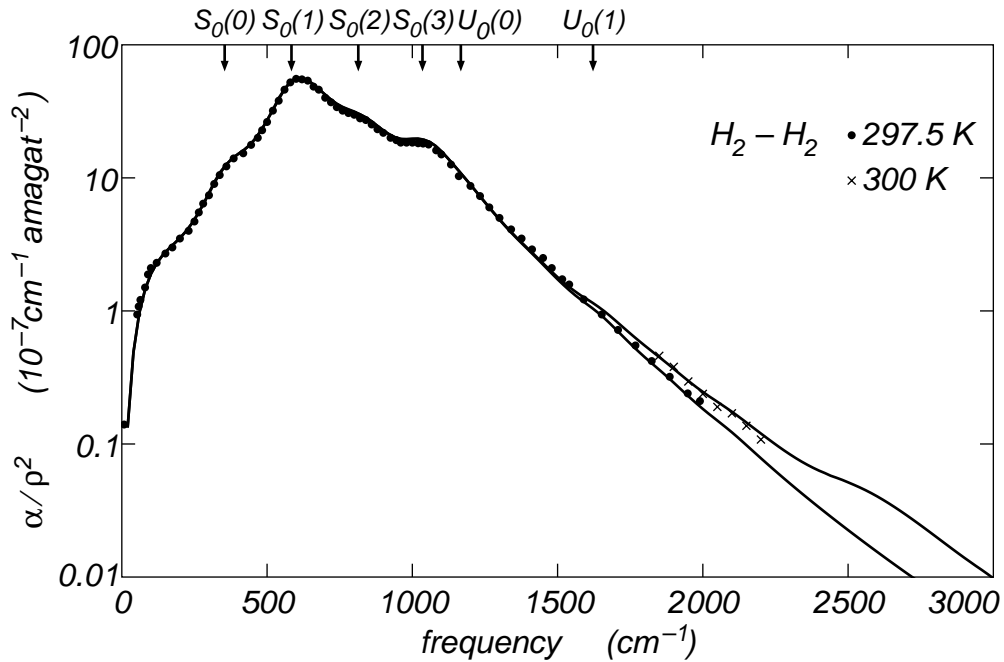
Figure 4.2: The H$_2$–H$_2$ absorption spectrum at 300 K (upper curve). The lower curve corresponds to a calculation in which the $\lambda_1\lambda_2\Lambda L = 0443$, 0445, 4043 and 4045 dipole components were omited.

[18]. In the far blue wing several of the small dipole components contribute significantly to the absorption. The $\lambda_1\lambda_2\Lambda L = 0443$, 0445, 4043 and 4045 dipole components are nearly insignificant near the centers of the diffuse S lines but in the far wing they contribute substantially to the absorption. This is obvious in figure 4.2 which shows the calculation of the same spectrum but without these dipole components (lower curve). For comparison the calculation from figure 4.1 (upper curve) is also shown. At the lower frequencies the two curves are nearly identical. However, in the far blue wing there is a substantial difference.

91

It should be remarked here that in previous calculations in the group it was found that the spectra based on those new dipole components that were also available in the earlier calculations, *i.e.* the $\lambda_1 \lambda_2 \Lambda L = 0001$, $0221$, $0223$, $2021$, $2023$, $2233$ dipole components, were nearly identical with the ones based on the old dipole surface. However, in the present calculation the $\lambda_1 \lambda_2 \Lambda L = 0443+0445$ and $4043+4045$ dipole components are now appropriately separated. The new dipole surface can explain the measured spectra of the roto-translational spectrum of $H_2$–$H_2$ at the temperature of 300 K.

It should be mentioned here that the other nineteen dipole components have negligible contribution to the calculated spectrum. Also the $\lambda_1 \lambda_2 \Lambda L = 0001$ dipole component has negligible contribution to the rototranslational spectrum at the temperature of 300 K. If one calculates the spectrum based only on the $\lambda_1 \lambda_2 \Lambda L = 0221$, $0223$, $2021$, $2023$, $2233$, $0443$, $0445$, $4043$ and $4045$ dipole components and compares it with the calculation in which all dipole components are included the relative difference amounts to less than 1%, which is remarkable.

The far wing is also noticeably shaped by the repulsive part of the potential energy. The isotropic potential approximation was applied since close-coupled calculations require prohibitive computer time. As the figure shows, the isotropic potential approximation is in quite good agreement with the measurement at that temperature and in the frequency range considered here. *Ab initio* calculations that account for the anisotropy of the intermolecular potential where not yet undertaken at the temperature of 300 K for $H_2$–$H_2$.

92

In [18] a close-coupled calculation at the temperature of 77 K was undertaken and quite striking differences were observed between the isotropic and the anisotropic calculation. However, since in calculations that take into account the anisotropy the Hamilton operator is not diagonalizable these calculations require much more computer time. The close-coupled calculation [18] required several months of computer time. Since at the temperature of 300 K many more excited states have a significant population probability many more transitions can take place which makes the computations even more time consuming. The good agreement between the calculation based on the isotropic potential approximation and the measurements suggests that the anisotropy does not have much influence on the spectra at higher temperatures. Nevertheless it would be desirable to compare IPA calculations with calculations that take into account the anisotropy of the intermolecular potential at higher temperatures, but for this one will probably have to wait until more computer power is available.

In figure 4.3 we compare measurements in the 5 $\mu m$ band of the CIA spectrum with the fundamental theory. In the 5 $\mu m$ band, the far wing of the induced rotational S lines, absorption is relatively weak and reliable measurements became available only recently [18]. Moreover, certain dipole components are important in that band that are quite unimportant in regions of stronger absorption, near the peaks of the induced S lines of $H_2$. In other words, both theory and measurements are challenging in the 5 $\mu m$ band. For applications in planetary science, the opacity in the 5 $\mu m$ band is, however, of

a special interest. Accurate knowledge of the $H_2$–$H_2$ absorption is necessary so that the opacities observed in the Voyager fly-by missions may be corrected for the known contributions to separate and study suspected unknown contributions to the opacity.

Figure 4.3 compares theory and measurement at the temperature of 77.5 K. The lower solid curve shows the new calculations based on the IPA. The absorption is increasingly lower than the measurement with increasing frequencies. The upper solid curve is the CC calculation, which accounts for the anisotropy of the intermolecular interactions. That result nearly agrees with the measurement, which fact demonstrates that - contrary to earlier observations at different frequencies [34] - the anisotropy of the intermolecular interactions cannot be ignored in certain spectral bands (where CIA is weak).

The comparison, figure 4.3, does not show perfect agreement but certainly agreement within the combined error limits of measurement and calculation actually exists. On an absolute scale, the uncertainties of the measurement are probably slightly larger than indicated by the error bars, which merely represent statistical uncertainties ($3\sigma$).

As mentioned above, as the frequencies approach zero, absorption falls off to zero for several reasons. One of them is stimulated emission. The rapid increase of absorption with frequency increasing from zero and the first broad peak correspond to translational absorption. The next two peaks near 354 and 585 cm$^{-1}$ are the collision-induced $S_0(0)$ and $S_0(1)$ lines of $H_2$. The remaining two broad peaks are double rotational transitions of the type S(0)+S(1) and
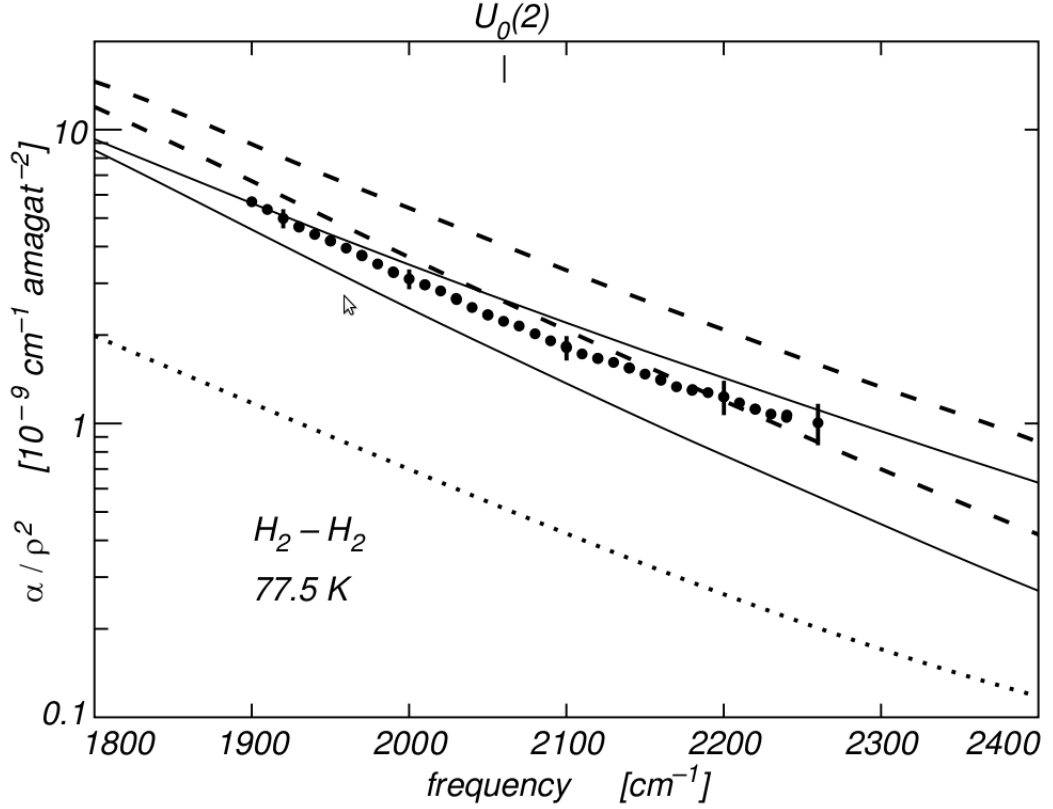
94

Figure 4.3: The absorption coefficient $\alpha$ of $H_2$–$H_2$ collisional complexes as a function of frequency, normalized by the square of density $\rho$, near wavelengths of 5 $\mu m$, at a temperature of 77.5 K. Lower solid curve: calculation based on the IPA and the new IDS. Upper solid curve: calculation based on the new IDS and close-coupled scattering theory, which accounts for the anisotropy of the interaction potential. Lower dashed curve: IPA calculation with previous IDS. Upper dashed curve: CC calculation with previous IDS (from [18]). Dotted curve: same as lower solid curve, except that the 0443+0445 and 4043+4045 dipole components are suppressed to demonstrate the significance of those dipole components, which were previously not well enough determined [18]. Dots: measurements from [18].

95

S(1)+S(1), combined with a change of the translational state of the pair by absorption of a single photon, truly a supermolecular feature.

### 4.1.2 Dependence of the calculated spectrum on the intermolecular potential energy surface

In order to model the radiative processes in the atmospheres of cool-white dwarf stars, for which collision-induced absorption by supermolecular complexes of hydrogen up to temperatures of at least 7000 K is important, besides knowledge of the dipole surface one needs accurate knowledge of the potential energy surface of $H_2$–$H_2$. These surfaces come from quantum-chemical calculations with the $H_2$ bonds stretched or compressed far from equilibrium length. Since no measurements of the collision-induced absorption for these high temperatures exist, one has to undertake *ab initio* calculations which take into account the high rotovibrational excitation of $H_2$. Up to now no potential was available that accounts for these high rotovibrational levels, since for the lower temperatures considered in previous *ab initio* calculations they could be ignored, due to their low population probability. They also do not have much influence at the temperature of 300 K. However, for the temperatures envisioned they have to be taken into account. For these purposes Drs. K.L.C. Hunt and X. Li at Michigan State University [61] have provided such data of pairs of highly rotovibrating hydrogen molecules. Nevertheless, before one proceeds to higher temperatures it is important to test the new intermolecular potential energy surface. Therefore the rototranslational spectrum of $H_2$–$H_2$ at the temperature of 300 K was calculated with two different potential energy

96

surfaces, and the two results where compared (see figure 4.4). The Schaefer-Koehler potential, which does not take into account the vibration of the $H_2$ molecules, *i.e.* corresponds to the rigid rotor approximation, is further described in [1], and is only applicable for the ground state of $H_2$–$H_2$. It is used by linking cirme.for with the potential function vaoo.for. On the other hand, the isotropic potential provided by Li and Hunt [61] is used by linking cirme.for with the Fortran program V000rvib.FOR. Besides the vibrational ground state it is furthermore applicable for highly vibrating $H_2$–$H_2$ supermolecules such as those encountered at temperatures of several thousand kelvin. Nevertheless, at low temperatures the two potential energy surfaces should give similar results since nearly no vibrations occur at these temperatures.

As the comparison between the two differently calculated spectra (figure 4.4) shows the agreement is quite good over the complete range of frequencies considered. The solid curve corresponds to the calculation with the potential accounting for the vibrational excitation, the dashed one to the calculation for which the Schaefer-Koehler potential was used. The two curves are nearly indistinguishable from one another. The difference between the two curves is less than what can be distinguished with the accuracy of the plot. This is remarkable, since all previous *ab initio* calculations of collision-induced absorption by dense hydrogen gas were based on the Schaefer-Koehler potential. It shows furthermore that as theory suggests the vibrational excitation can be neglected even at the temperature of 300 K. What is even more this comparison shows that the new potential energy surface is capable of reproducing the
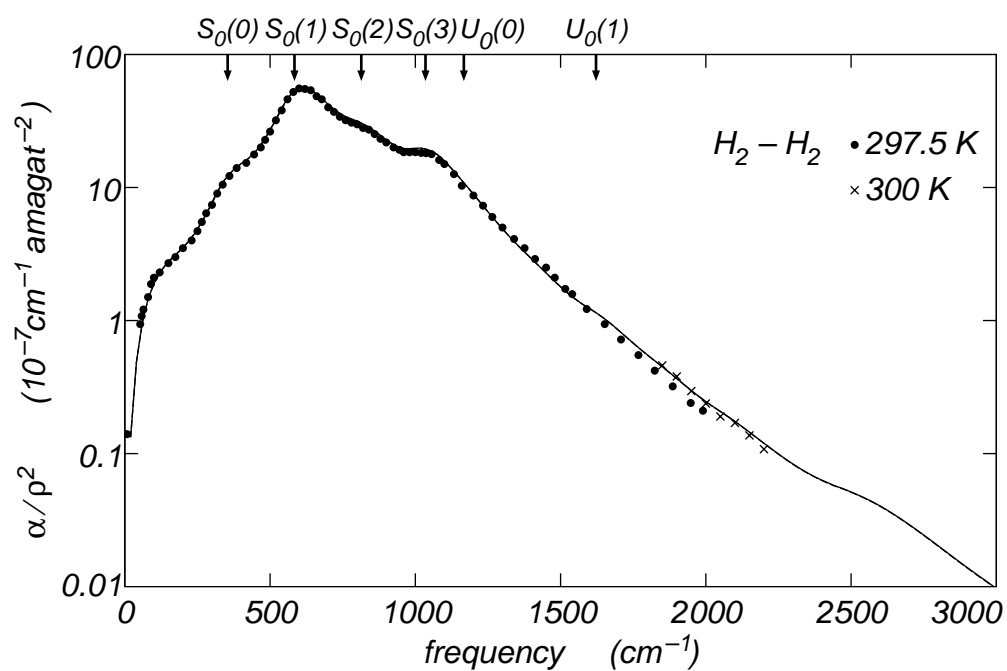
Figure 4.4: The H$_2$–H$_2$ absorption spectrum at 300 K, calculated using the Hunt potential (solid curve), and using the Schaefer-Koehler potential (dashed curve)

existing measurements. Thus it can be considered tested and one can safely proceed to the higher temperatures which are of great interest for astrophysical applications.

### 4.1.3   Temperature dependence of the calculated spectrum

It should be pointed out at this point that as mentioned above collision-induced absorption spectra show a strong dependence on temperature. To further demonstrate this dependence the rototranslational spectrum of $H_2$–$H_2$ has been calculated at the temperatures of 275 K and 325 K and was compared to the calculation at 300 K (see figure 4.5). At frequencies below about 600 cm$^{-1}$ the calculations for the three temperatures give quite similar results. This can easy be understood by consideration of the Boltzmann factor in the equation for the absorption coefficient. At low frequencies the temperature dependence of the argument of the exponential function is negligible since it is small due to the small frequencies. However, as excitation energies $h\nu$ become comparable to the thermal energy $k_B T$ the temperature dependence becomes quite striking. At the higher frequencies it can be seen that the collision-induced absorption intensities become greater with increasing temperature (see figure 4.5) which again can be understood by consideration of the Boltzmann factor.

While at temperatures around 300 K temperature control should not be too difficult in measurements, since these temperatures are fairly close to room temperature, it is fair to expect measurements at different temperatures
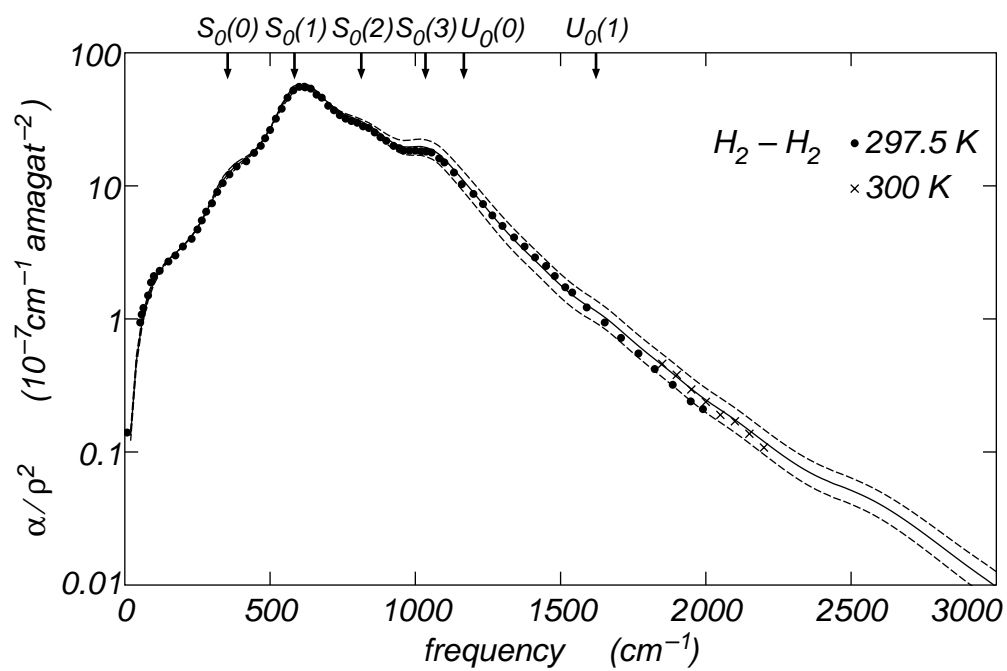
99

Figure 4.5: The calculated $H_2$–$H_2$ absorption spectrum at 300 K (solid curve), at 275 K (lower dashed curve) and at 325 K (upper dashed curve).

to be likely to be affected by temperature gradients. As can be seen in figure 4.5 the temperature has a great influence on the absorption intensities. This is a point one should keep in mind when attempting to do measurements of collision-induced absorption at temperatures far from room temperature.

### 4.1.4 The fundamental band of hydrogen

As a further test of the new method the collision-induced absorption of dense hydrogen gas was investigated in the fundamental band. *Ab initio* calculations of the absorption were compared with measurements at the temperature of 300 K (see figure 4.6). As for the rototranslational band the agreement between fundamental theory and experiment is remarkable.

For the rototranslational band of $H_2$–$H_2$ it was seen that the collision-induced absorption spectrum is essentially composed of a number of dipole components labeled $\lambda_1\lambda_2\Lambda L = 0221, 2021, 0223, 2023, 2233, 0443, 4043, 0445$ and 4045. For the fundamental band also the $\lambda_1\lambda_2\Lambda L = 0001$ component, completely negligible in the rototranslational spectrum, has significant contribution to the absorption, arising from overlap induction. It occurs because a vibrating $H_2$ molecule differs from a non-vibrating one.

Astrophysicists want to determine the species which are present in planetary atmospheres as accurately as possible. Since in general one has to do this remotely an important way of determining the abundant species is to subtract the calculated absorption of the known species, hydrogen and helium, from the measured absorption. The remaining absorption intensity corresponds to
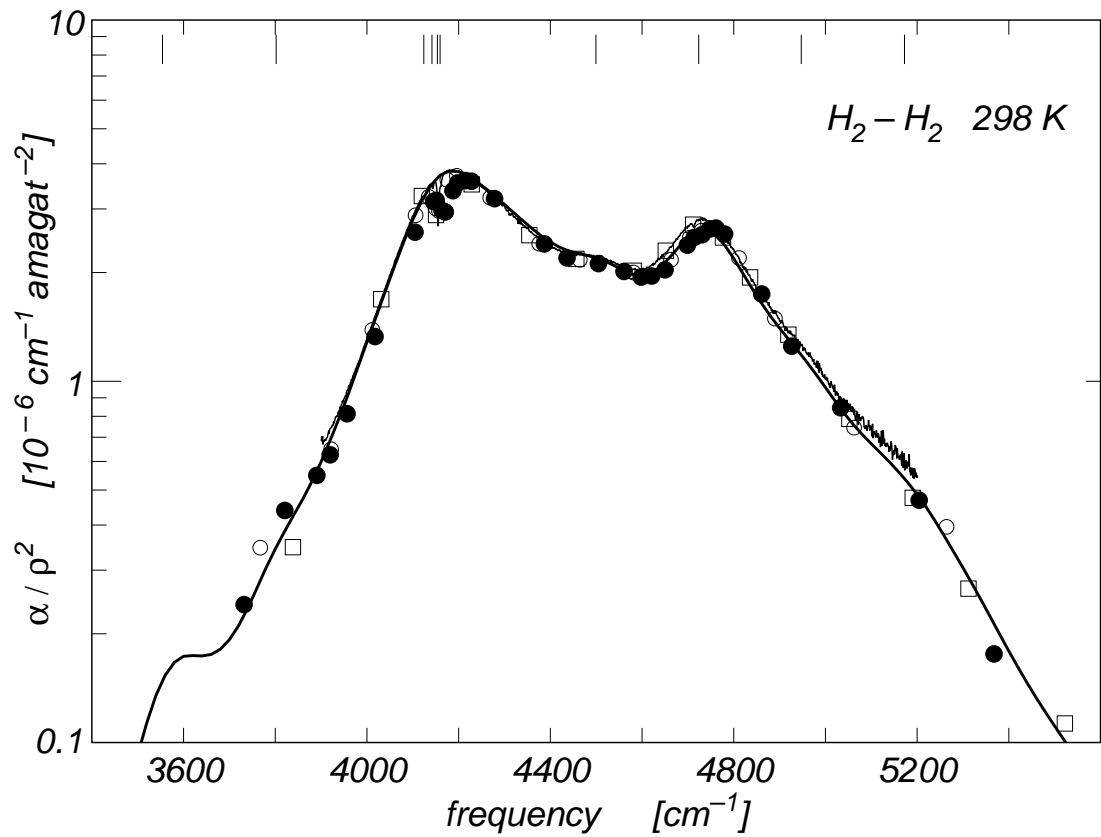
101

Figure 4.6: Comparison between the calculated (heavy solid curve) $H_2$ absorption spectrum at 300 K in the region of the fundamental band and the measured spectrum (squares: [97], big dots: [51], circles: [95], slightly noisy trace: [23]).
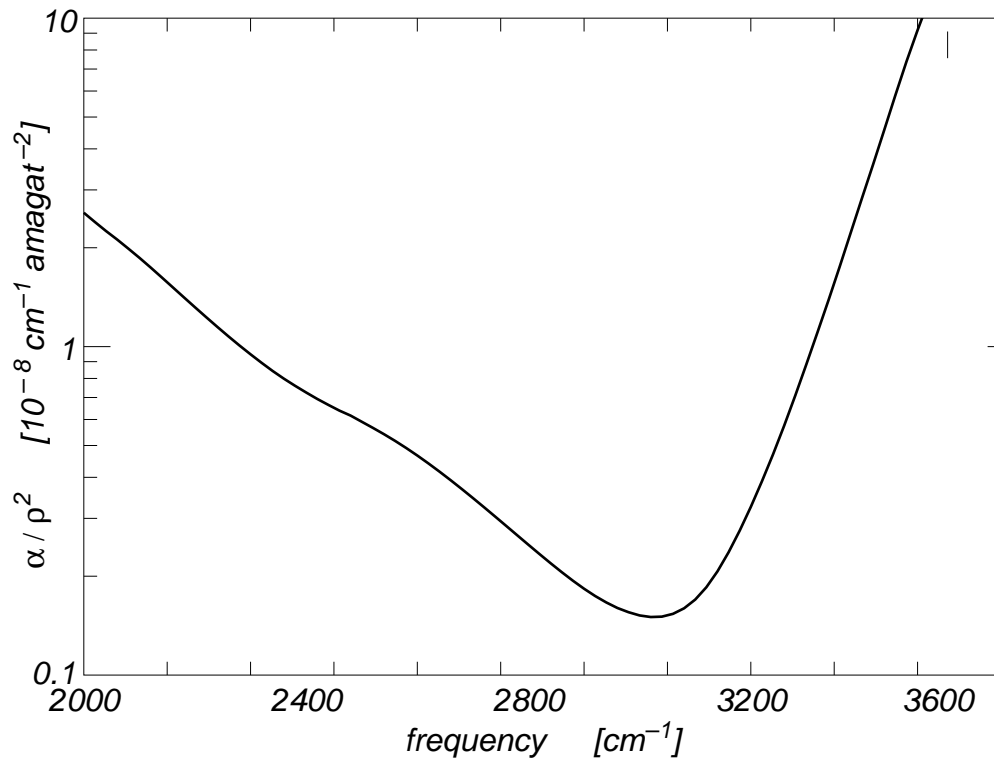
Figure 4.7: The calculated absorption in the region between the rototranslational and fundamental band of dense hydrogen gas at the temperature of 300 K.

other species and gives one a hint of the amount of other species present in planetary atmospheres. Whereas regions of great absorption of molecular hydrogen have been known accurately for quite a while the same cannot be said about regions of weak absorption. Therefore, the region of weak absorption by collisional hydrogen complexes in between the rototranslational and fundamental band was further investigated. In figure 4.7 the calculated absorption of this region is magnified so that astrophysicists and other specialists may find information about this important absorption region.

103

### 4.1.5 The first and second overtone band of hydrogen

At the temperature of 300 K there are furthermore measurements reported of the collision-induced absorption by $H_2$ in the first and second overtone region. As a further test of the new method *ab initio* calculations of the absorption were undertaken for these absorption regions and compared with the measurements (see figures 4.8, 4.9). Again close agreement between calculated and measured spectra is observed (see figures 4.8, 4.9), which demonstrates that the new method is capable of reproducing the existing measurements closely.

Summarizing this section, agreement of the fundamental theory and existing laboratory measurements is observed, as the figures above demonstrate. Because of the agreement, reliable predictions of the opacity of hydrogen pairs at higher frequencies and temperatures appear to be quite reasonable.

### 4.1.6 Intermolecular Potential

It has long been known that for the calculations of CIA spectra reliable intermolecular potentials must be used [34]. Advanced methods have been used to compute the intermolecular forces accurately, especially the repulsive wall region and a number of dispersion coefficients. If the well region of an intermolecular potential needs to be known accurately, empirical information has often been added, such as the rotovibrational spectra of van der Waals dimers, if known [79]. For our work with elevated temperatures, most $H_2$ molecules are initially rotovibrationally excited. After the absorption of a
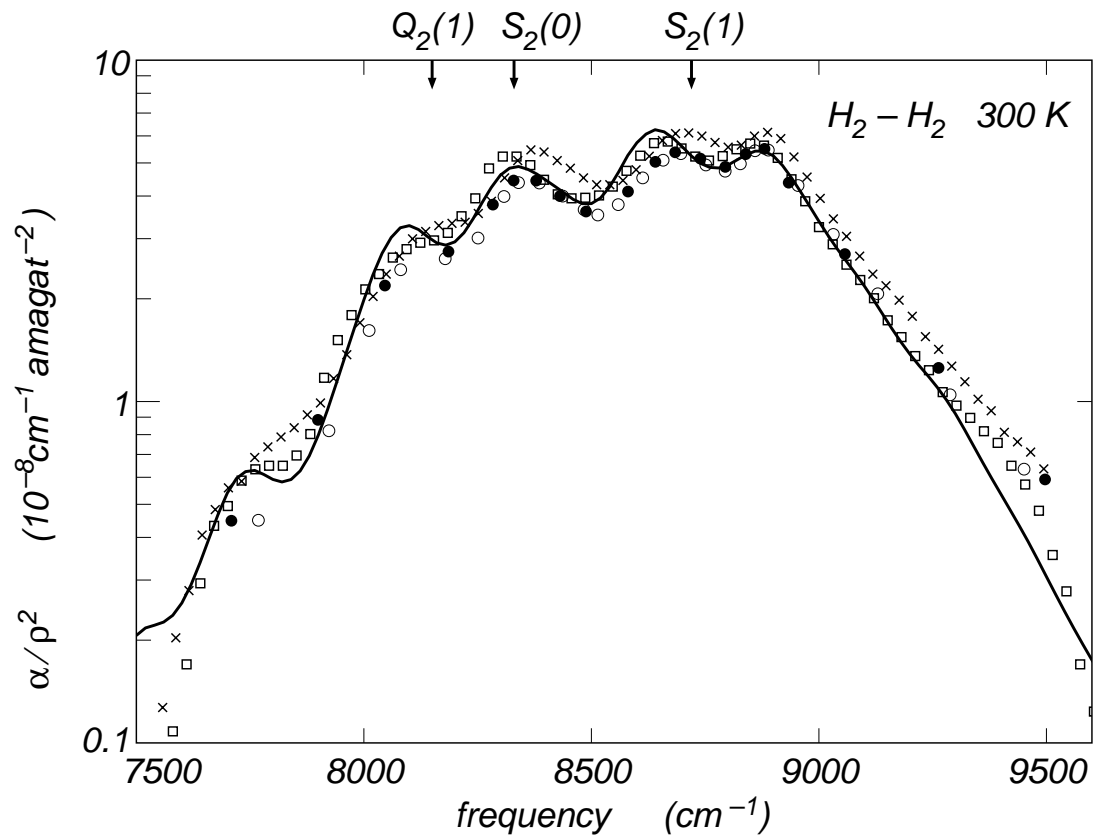
Figure 4.8: Comparison between the calculated (heavy solid curve) $H_2$ absorption spectrum at 300 K in the region of the first overtone and the measured spectrum (squares: [32]), crosses: [98], dots: [53]).
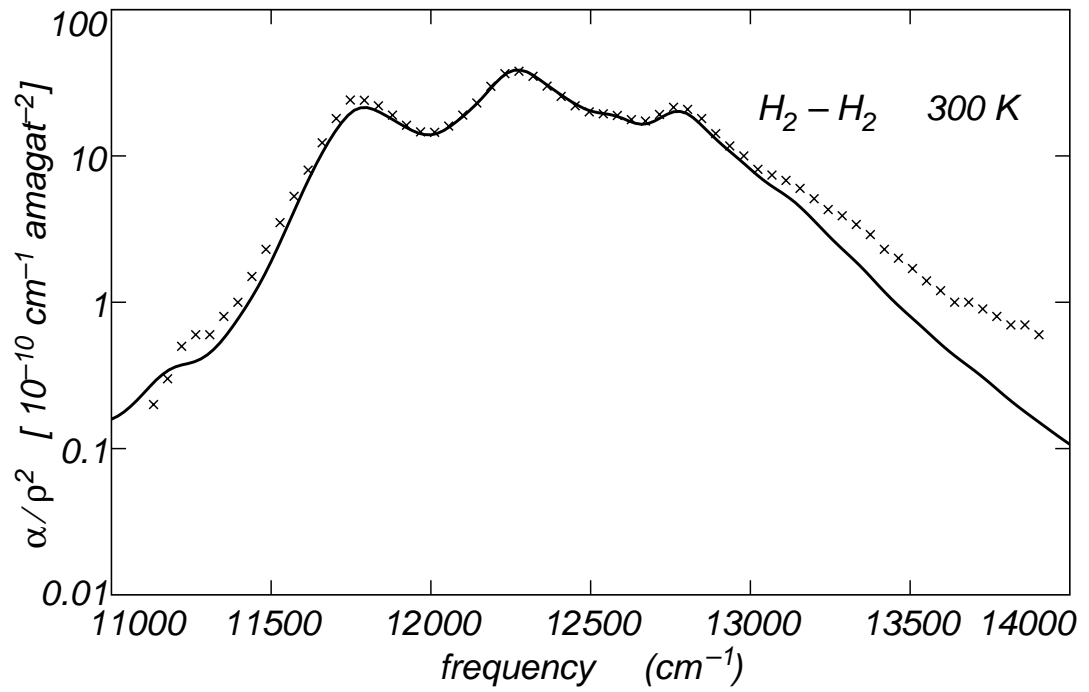
Figure 4.9: Comparison between the calculated (heavy solid curve) H$_2$ absorption spectrum at 300 K in the region of the second overtone and the measured spectrum (crosses: [17]).

photon of energy of 2.5 eV, the final rotovibrational state of an $H_2$ molecule of the collisional complex is even more highly excited, up to vibrational levels of $\nu = 7$ or 8. Under such conditions a potential energy surface $V(r_1,r_2,R)$ must be known as a function of the $H_2$ bond distances $r_1$ and $r_2$, so that suitable rotovibrational averaging of initial and final scattering state potentials is possible. For the recent most highly refined intermolecular potentials, the rotovibrational matrix elements are not available, but vibrational dependences for the lowest vibrational states ($\nu = 1$ and 2, but not for rotation) have been given previously [14, 15]. These vibrational corrections affect the calculations of the spectra significantly, but they are not sufficient for our present purposes. It was therefore necessary for this work to obtain a new *ab initio* PES [59, 61] that permits calculations of the $\nu$ and j dependences.

Figure 4.10 compares our intermolecular $H_2$–$H_2$ potential for $\nu_1 = j_1 = \nu_2 = j_2 = 0$ with an advanced model by Meyer [14] (also for the rotovibrational ground state). The agreement is a close one. We also show in figure 4.10 as an example a calculation for a vibrationally excited $H_2$ molecule, $\nu_1 = j_1 = j_2 = 0$, $\nu_2 = 5$ (dashed line).

Figure 4.11 compares CIA spectra at three temperatures, calculated with the Schaefer-Koehler potential [79, 85] (dotted line) and with our present one (solid line). The latter accounts for the exact rotovibrational excitations of the two $H_2$ molecules. The former model neglects all rotovibrational dependences of the intermolecular potentials of initial and final states. All other choices (the dipole functions) are the same for both runs. The spectra are
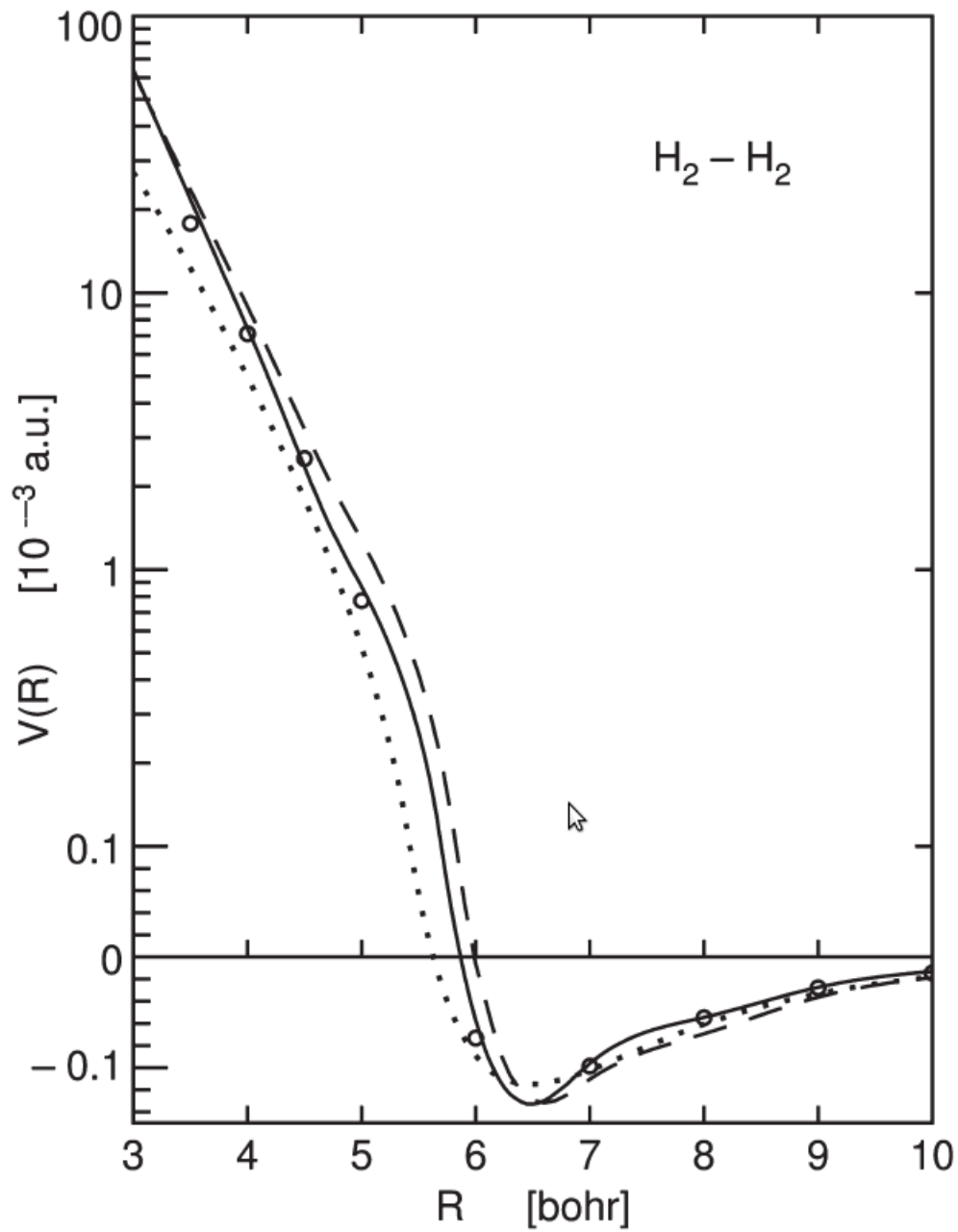
Figure 4.10: Intermolecular potential, for $\nu_1 = j_1 = \nu_2 = j_2 = 0$ (solid line) and $\nu_1 = j_1 = j_2 = 0$, $\nu_2 = 5$ (dashed line). Also shown is an "effective" potential [80] (dots) and an earlier calculation by Meyer [14] (circles).
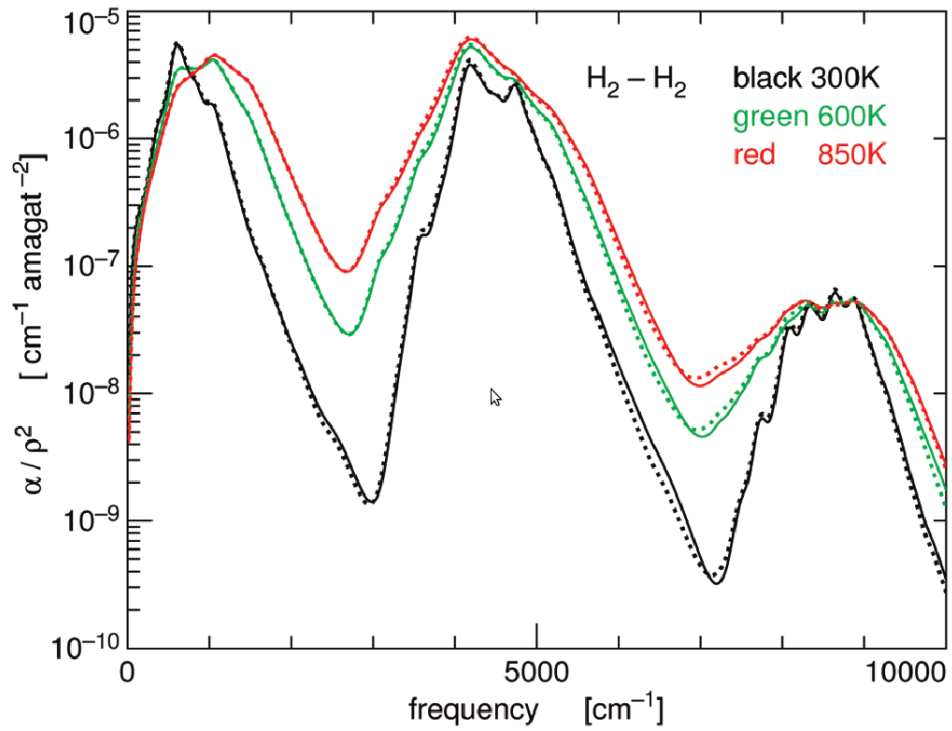
Figure 4.11: Comparison of CIA spectra calculated for three temperatures with different intermolecular potential models; solid line: present *ab initio* model with full accounting for the rotovibrational states involved; dotted line: from Ref. [85].

nearly indistinguishable at the temperatures and frequencies shown, an illustration of the near-equivalence of these intermolecular potential models under these conditions. We note, however, that (not surprisingly) at higher temperatures and frequencies substantial differences are seen.

## 4.2 Proceeding to higher temperatures

In figure 4.12 the complete collision-induced absorption spectrum of hydrogen at the temperature of 300 K from 0 to 20000 cm$^{-1}$ is shown. For better clarity of the plot the measurements are obmitted in this plot. As outlined above astrophysical applications require the knowledge of the collision-induced absorption by molecular hydrogen pairs up to temperatures of several thousand kelvin. Extensive comparison between the fundamental theory and existing measurements at temperatures of 300 K has yielded excellent agreement. With the new dipole and potential energy surfaces [61] it is now possible to proceed to higher temperatures where there are no measurements for comparison with the theory. These *ab initio* calculations of the absorption at higher temperatures have been undertaken, beginning at temperatures of 300 K and successively proceeding to higher temperatures [61]. As an example for such calculations that cannot be compared with measurements since there are no measurements available in this work the collision-induced absorption spectra of collisional hydrogen complexes at temperatures of 600 K, 1000 K, and 2000 K (see figure 4.13) are shown, again from 0 to 20000 cm$^{-1}$. Since there are no measurements one has to rely on the calculated absorption spectra, supported by excellent agreement between theory and measurements at lower temperatures. Data at these temperatures are useful for research of brown dwarf stars. Our opacity data have already been applied to models of the atmospheres of such objects [84].

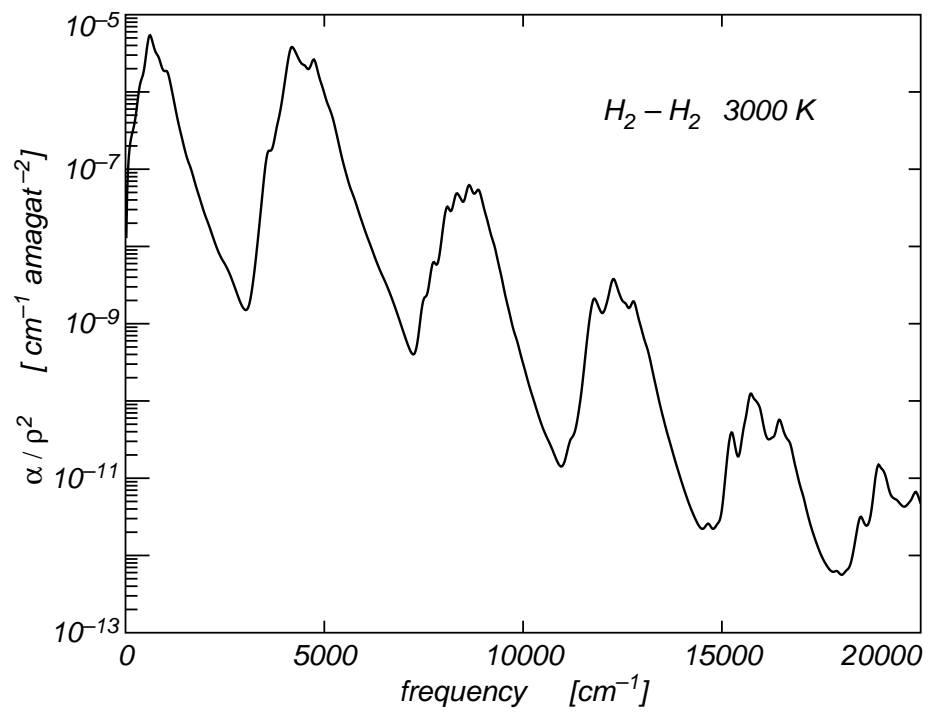In figure 4.14 we show as an example for calculations at even higher

110

Figure 4.12: The calculated collision-induced absorption spectrum of pairs of molecular hydrogen, from the far infrared to the visible, at the temperature of 300 K
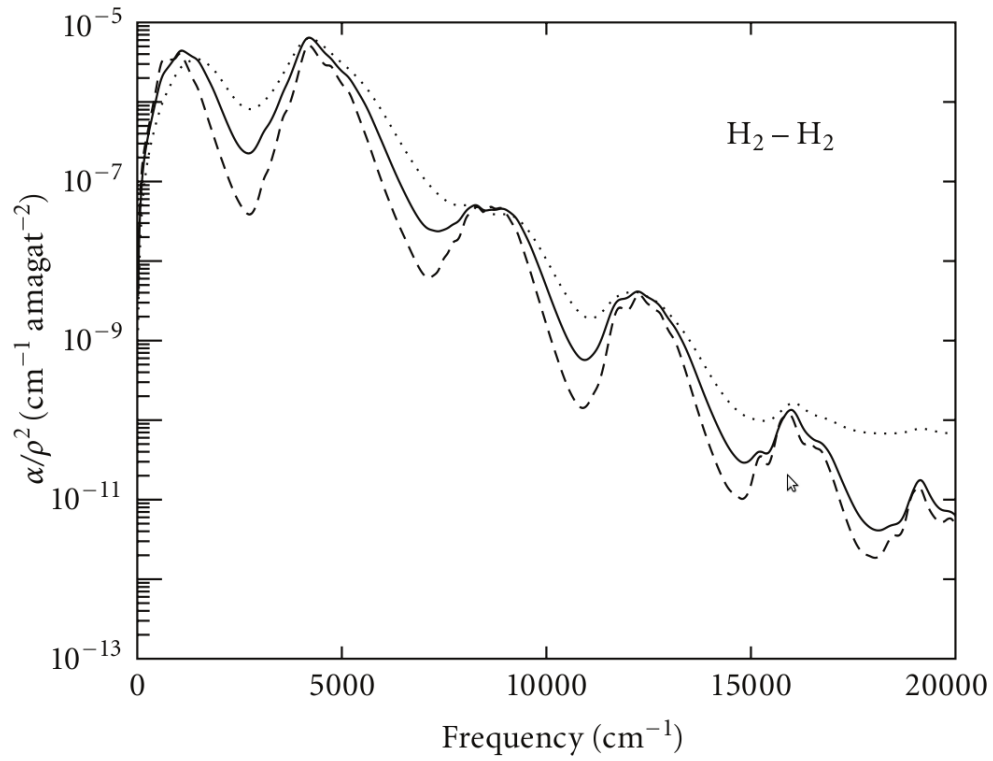
Figure 4.13: The calculated collision-induced absorption spectrum of pairs of molecular hydrogen, from the far infrared to the visible, at temperatures of 600 K, 1000 K, and 2000 K.
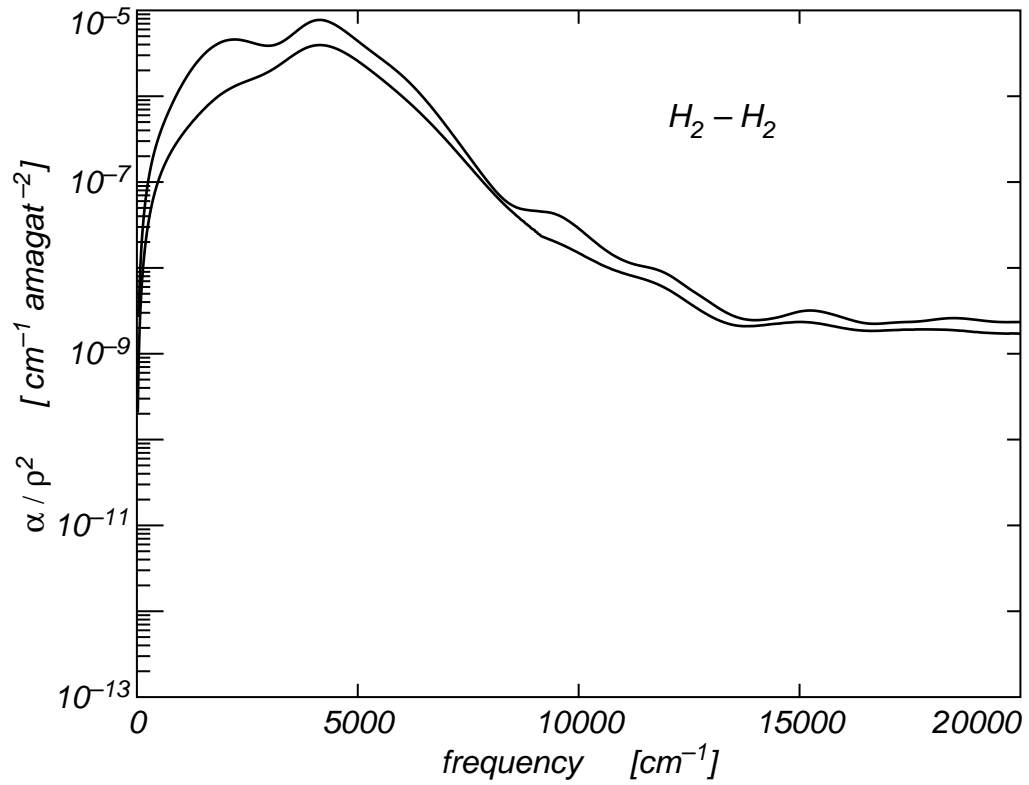
Figure 4.14: The calculated collision-induced absorption spectrum of pairs of molecular hydrogen, from the far infrared to the visible, at temperatures of 4000 K and 7000 K.

temperatures the calculated collision-induced absorption spectra of pairs of molecular hydrogen, normalized by the square of the gas density, at temperatures of 4000 K and 7000 K. These data are useful for hot and dense environments that are dominated by hydrogen, such as the upper atmospheres of cool white dwarf stars.

113

## 4.3  Results for $D_2$–$D_2$

The research described in this section has been published in [3, 4]. We have used the elaborate induced dipole surface (IDS) for pairs of $H_2$ molecules [35, 59, 61] to compute the CIA spectrum of pairs of $D_2$ molecules [3, 4]. The electronic structure of interacting $D_2$ pairs is virtually the same as that of $H_2$ pairs, but the collisional dynamics and the rotovibrational wave functions are different. In other words, the comparison of theoretical and measured CIA spectra of $D_2$–$D_2$ collisional complexes may be considered another test of the validity of the recent IDS [61]. The calculations are similar to the ones for the $H_2$–$H_2$ complex. A state-to-state quantum scattering calculation [35], which accounts for the interaction of the collisional complex with the radiation field, gives the absorption coefficient $\alpha(\omega, T)$, normalized by the square of density $\rho$. This quantity is shown in figure 4.15 for three temperatures: 200, 400, and 600 K. The magnitude of this quantity varies roughly over five orders of magnitude. The three preaks correspond approximately to the rotational band, fundamental band, and first overtone band of $D_2$. At the lowest temperature the minima that appear between the peaks are quite deep, but with increasing temperature the minima get shallower quickly.

Figure 4.16 compares the *ab initio* calculation (solid line) with a laboratory measurement [75] (dots) in the $D_2$ fundamental band. We note that the experimental points had to be read from a rather small figure of Ref. [75] and may not reflect the accuracy of the measurement; the error bars shown are our estimates (20%). Figures 4.17 and 4.18 similarly compare the theory
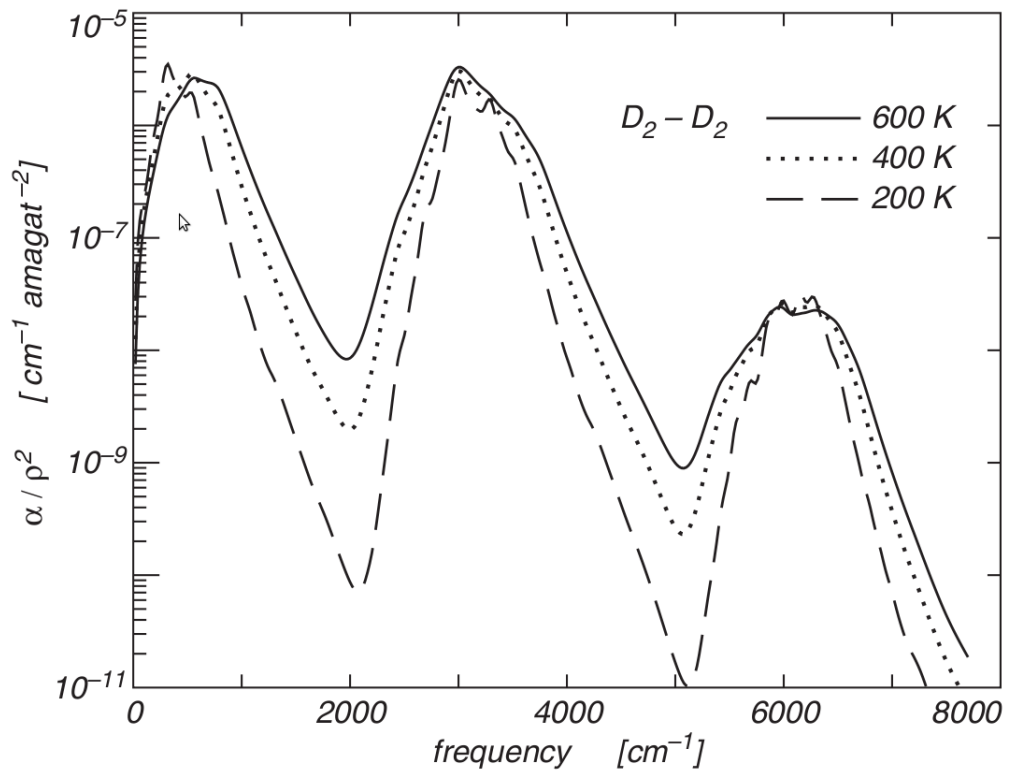
Figure 4.15: The collision-induced absorption spectrum of $D_2$ pairs at three temperatures: 200, 400, and 600 K.
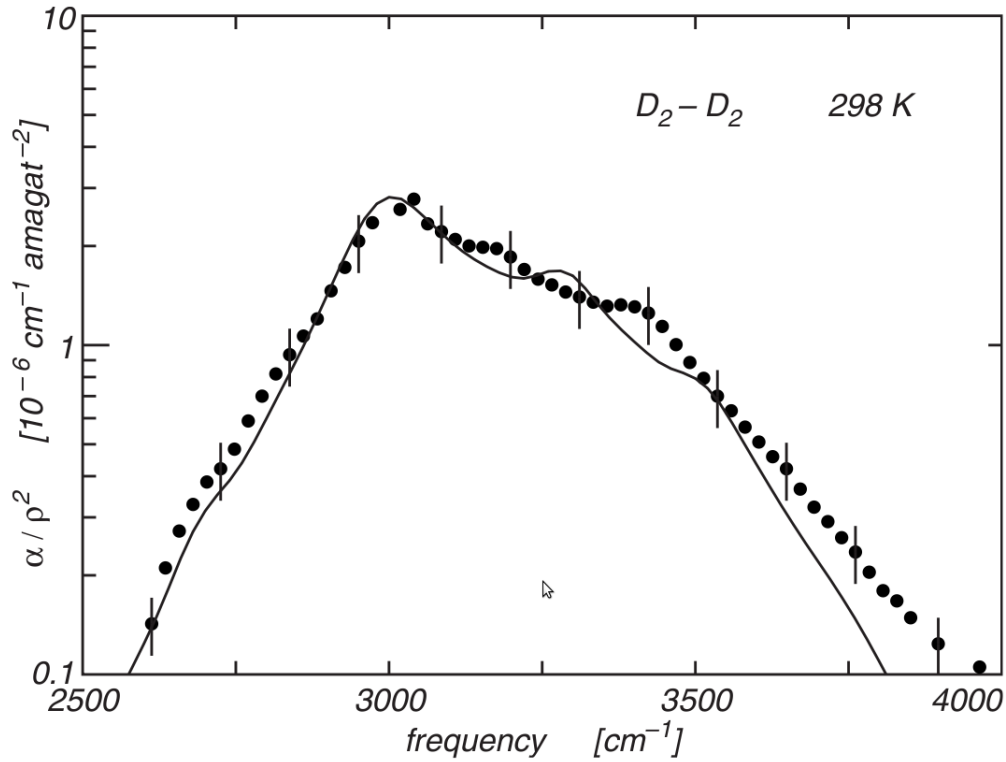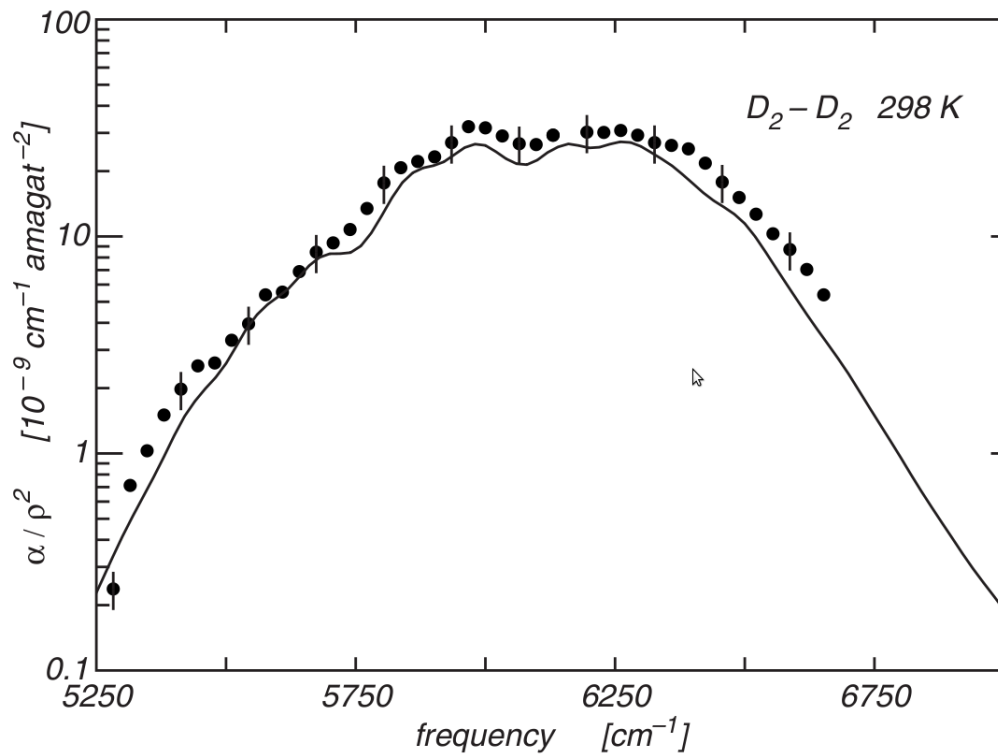
Figure 4.16: The collision-induced absorption spectrum, normalized by density squared, in the fundamental band of $D_2$ at room temperature; comparison of the calculation (solid line) with measurements (Ref. [75]) (dots).

and measurement [9] of the first overtone band of $D_2$ at the temperatures of 298 and 201 K, respectively. In all three cases, the agreement of theory and measurement is a close one, as much as this was seen in earlier comparisons of the common isotope, hydrogen.

Summarizing, we have seen that the new induced dipole surface [59, 61] permits the calculation of the collision-induced absorption spectra of dense deuterium gas in close agreement with the existing laboratory measurements.

116

Figure 4.17: The collision-induced absorption spectrum, normalized by density squared, in the first overtone band of $D_2$ at room temperature; comparison of the calculation (solid line) with measurements (Ref. [9]) (dots).
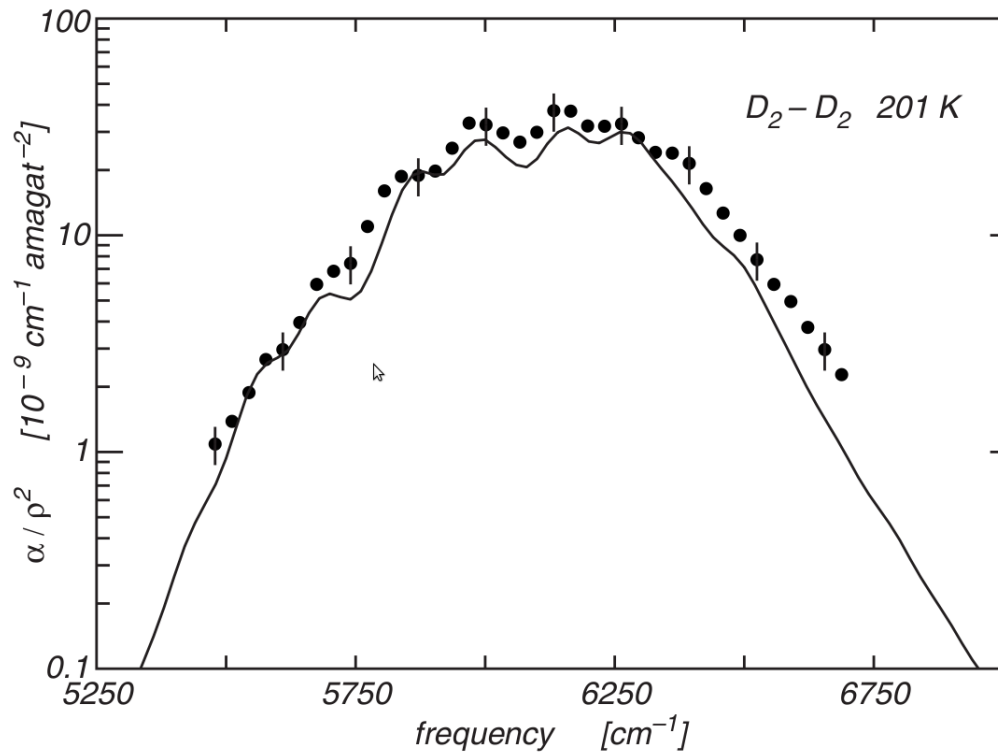
Figure 4.18: The collision-induced absorption spectrum normalized by density squared, in the first overtone band of $D_2$ at 201 K; comparison of the calculation (solid line) with measurements (Ref. [9]) (dots).

A close agreement was also seen for the CIA spectra of dense hydrogen gas. We feel therefore that the IDS and the computational techniques employed here are useful to predict reliable $H_2$–$H_2$ CIA spectra for higher temperatures and frequencies, which is necessary for the analyses of "cool" star atmospheres [35, 59, 61].

## 4.4  Results for $H_2$–He

The research described in this section is published in [8]. As pointed out above, the intermolecular potential V(R) of the $H_2$–He complex depends on the $H_2$ rotovibrational states. If high frequencies (photon energies up to 2.5 eV) are considered, along with high temperatures, this dependence is quite significant for the resulting spectra. It is also the reason why we need a two-dimensional PES $V_{00}$(r, R). Figure 4.19 compares the present potential with a well established theoretical model [69]. Overall agreement with this [69] and other recent potentials [13, 74] is excellent. As an illustration of the much stronger dependence of the intermolecular potential on the rotovibrational state of the $H_2$ molecule, the present potential is also shown for a rotovibrationally excited $H_2$ molecule in the $\nu = 5, j = 0$ state.

The calculations of collision-induced absorption spectra of the $H_2$–He complex are analogous to the ones for the $H_2$–$H_2$ complex. For temperatures of 300 K we have included initial $H_2$ rotovibrational states of $\nu = 0$ and $0 \leq j \leq 7$. Final states range up to $\nu' = 5$ and $j' = 11$. At 7000 K, we have included initial states up to $\nu = 5$ and $j = 27$.

Figure 4.20 shows the normalized absorption spectra of hydrogen-helium gas mixtures at eleven temperatures, from 300 to 9000 K, and for frequencies from the far infrared to the visible. At the lower temperatures several striking peaks are seen, which correspond, from left to right, roughly to the $H_2$ rotational band (far left), fundamental band, and first to fourth overtone bands (to the right). Peak intensities decrease strongly with increasing frequencies.
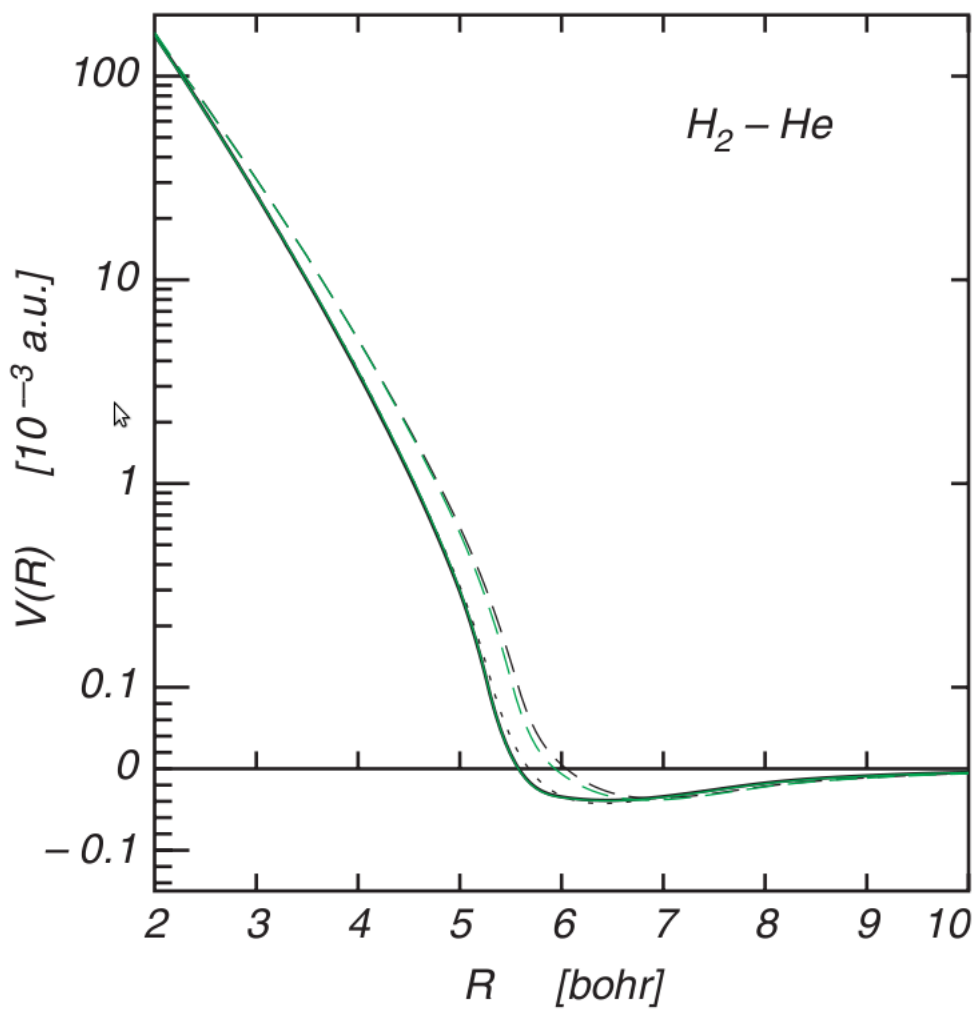
Figure 4.19: The isotropic intermolecular potential [60], for $\nu = j = 0$ (solid black line), $\nu = 5, j = 0$ (black dashes); an early, established potential [69] with $\nu = j = 0$ (dotted) and a recent potential (green line and dashes), Ref. [13], are shown for comparison.

At low temperatures there are deep minima between the peaks. However, these coarse structures become less striking with increasing temperature, to the point of near disappearance at the highest temperatures. Normalized absorption coefficients $\alpha/\rho_1\rho_2$ vary over a very wide range of intensities.

Figure 4.21 compares our calculation with laboratory measurements [11, 12] of the CIA spectrum in the $H_2$ rototranslational band at two temperatures.

Figure 4.22 compares similarly theory and measurement of a CIA spectrum in the $H_2$ fundamental band. In both cases close agreement of the measurements with the fundamental theory is observed.

It should be noted that the measurements shown in figure 4.22 exhibit sharp dips near the $H_2$ $Q_2(j)$ line positions, the so-called intercollisional dips, which are not reproduced by our calculations. These dips arise from interference of dipoles induced in subsequent collisions, an effect that cannot be described by a binary scattering theory [34].

An earlier exploratory study of CIA in unusual environments (sonoluminescence [46]) used the $H_2$–He collisional complex as an example of a simple, tractable system to obtain an idea of the high-temperature and high-frequency emission spectra to be expected under such conditions from supermolecular optical processes. The estimate used a small basis set for defining a PES and an IDS; accurate modeling of the specific $H_2$–He complex was not a concern. In the absence of better data, $H_2$–He opacity tables based on that work [46]
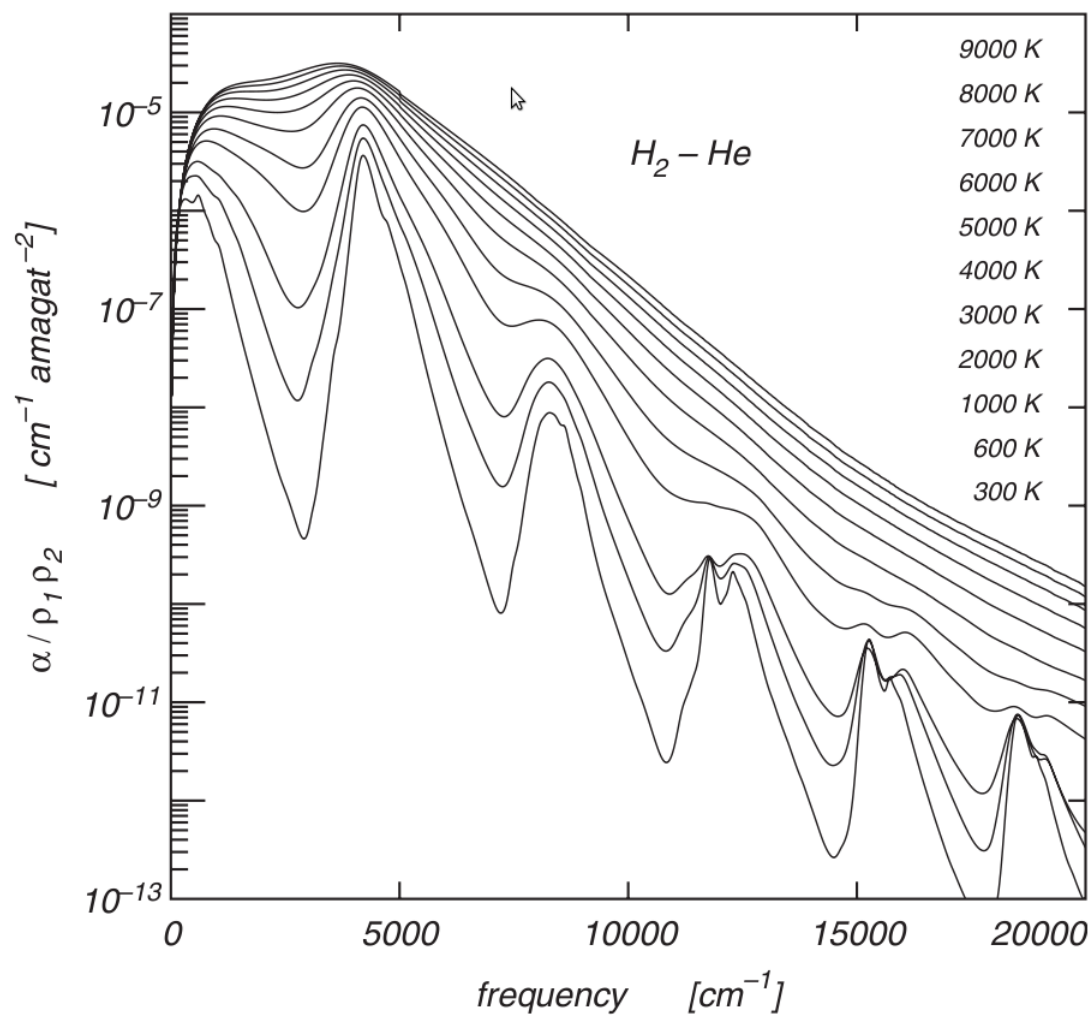
Figure 4.20: The normalized $H_2$–He collision-induced absorption spectrum at eleven temperatures, from 300 K (at the bottom) to 9000 K (at the top).
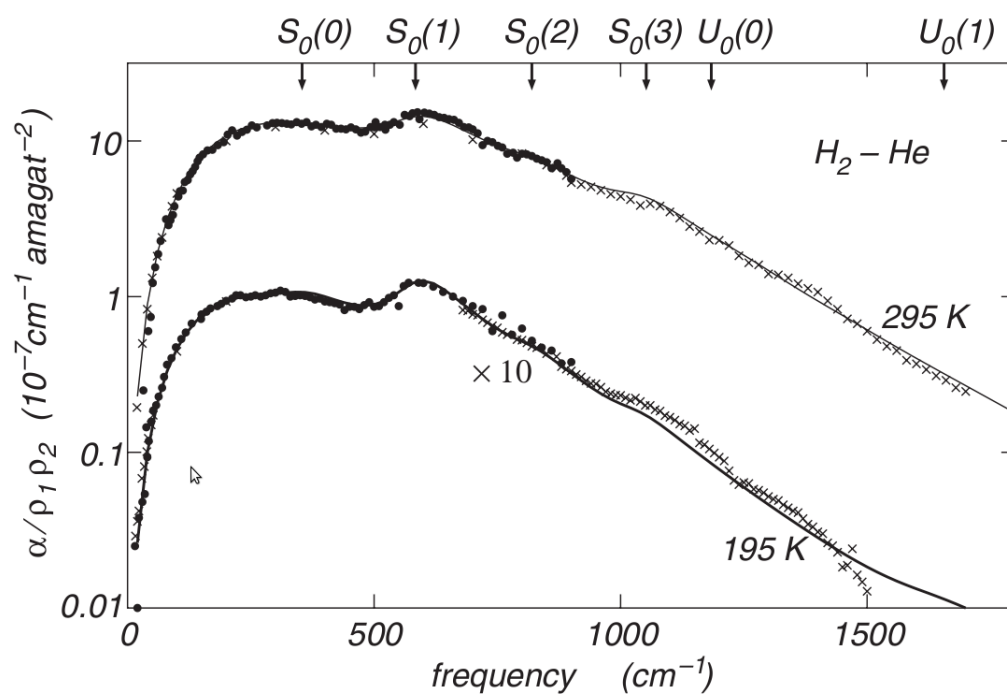
123

Figure 4.21: The rototranslational spectrum at 295 K (upper figure) and 195 K (lower figure): theory: solid line; laboratory measurements: dots: [11], crosses: [12]. Note that for better readibility of the figure the intensities at 195 K (lower set of data shown) are shown at one tenth of the actual intensities.
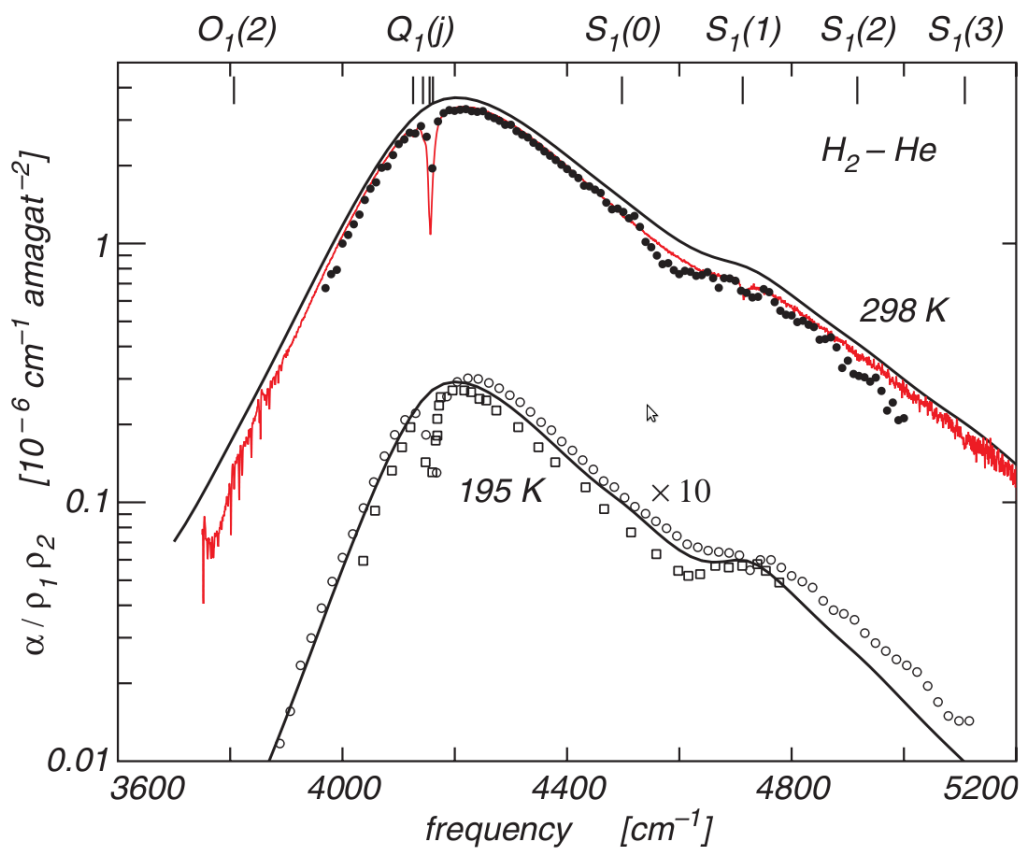
124

Figure 4.22: The collision-induced absorption spectra in the $H_2$ fundamental band, at temperatures of 298 K (top) and 195 K (bottom). Theory: smooth solid lines; laboratory measurements: dots: [52]; red trace: [16]; open circles: [77]; squares: [52]. Note that for better readability of the figure, the intensities at 195 K (lower set of data shown) are shown at one tenth of the actual intensities.
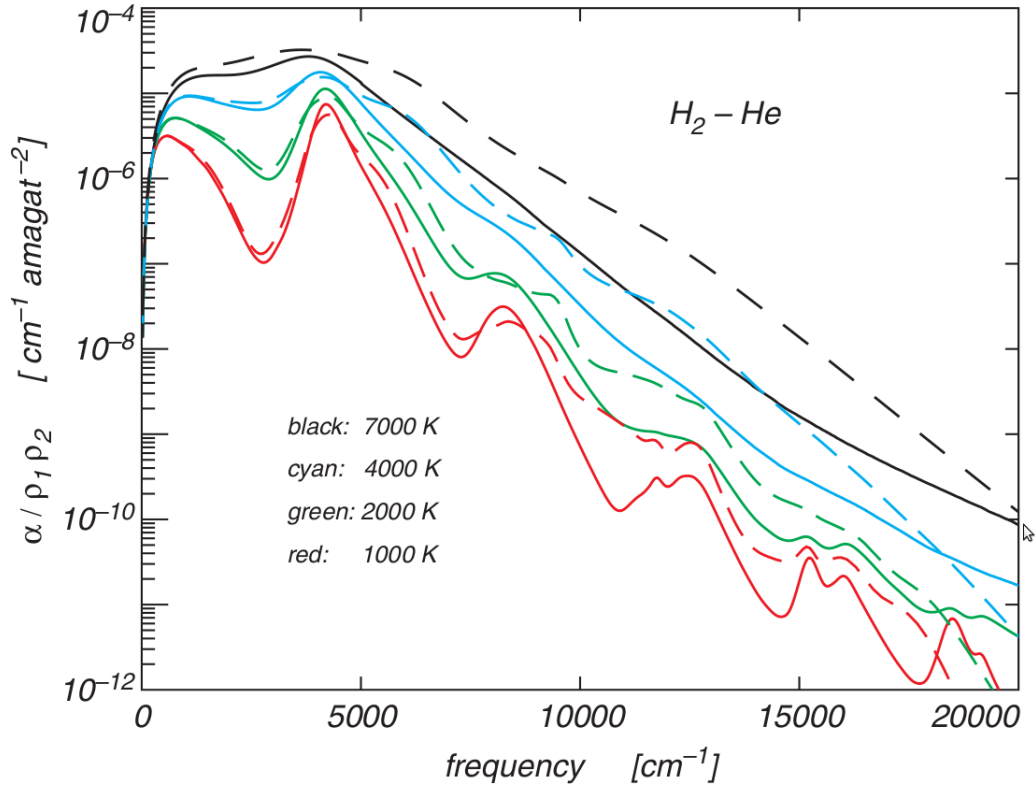
Figure 4.23: Comparison of present results (solid lines) with previous ones [55] (dashes).

were made available and used for the analysis of atmospheres of cool zero-metallicity stars [55]. These data are compared with present calculations in figure 4.23. Whereas at low frequencies reasonable consistency is observed, with increasing frequencies the previous data deviate more and more from the present data, up to a factor of $\approx 3$, as a consequence of the small basis set employed. Clearly, these previous $H_2$–He CIA data [46] are now obsolete and should no longer be used for any application.

## 4.5 Results for $D_2$–He

Recently, an elaborate IDS and PES were obtained for $H_2$ interacting with He [35]. We used the same surfaces to compute the CIA spectrum of $D_2$ interacting with He. The results described here have been published in [7]. The electronic structure of $D_2$ is virtually identical to that of $H_2$. However, the collisional dynamics and the molecular wave functions are different [4]. Whereas there are numerous laboratory measurements of collision-induced absorption spectra of $H_2$–$H_2$ and $H_2$–He, far fewer laboratory measurements of the CIA of $D_2$–He exist. Theoretical calculations provide the only knowledge of the collision-induced absorption of $D_2$–He in the rototranslational band and in the vibrational overtone bands. However, laboratory measurements [10, 81] are available for the CIA of $D_2$–He at room temperature in the fundamental vibrational band of $D_2$. It is, therefore, interesting to compare the theoretical calculations with these measurements.

The computational procedures are the same as the ones used for $H_2$–He. The absorption coefficient $\alpha(\omega, T)$, a function of frequency $\omega$ and temperature $T$, normalized by the gas densities $\rho_D$ of deuterium and $\rho_{He}$ of helium, is obtained by a state-to-state quantum scattering calculation, which accounts for the interaction of the collisional complex with the radiation field. This quantity is shown in figure 4.24 for the temperatures 150, 300, 600, 1000, 2000, 4000, 7000, and 9000 K for frequencies from 0 to 20 000 cm$^{-1}$. The normalized absorption intensity varies over several orders of magnitude. From the left to right, the peaks in figure 4.24 correspond roughly to the rotational band,

the fundamental band, and the first, second, third, fourth, fifth, and sixth overtone bands of $D_2$. The absorption minima that appear between the peaks are quite deep at the lowest temperatures but with increasing temperature the peaks merge more and more. For all calculations an isotropic potential has been employed, an approximation that has been found to be quite reasonable in previous studies [34]. Specifically, in [44] for collision-induced absorption by $H_2$–He mixtures, at frequencies in the fundamental band of $H_2$, the differences between calculations with isotropic and anisotropic potentials were found to amount to less than 10 % for $H_2$–He at $T = 298$ K, and even less at lower temperatures [44]. These results similarly apply to the case of $D_2$–He. This means that our binary collision-induced absorption calculation for $D_2$–He based on the isotropic potential approximation [44] should be able to reproduce the laboratory measurements, as long as ternary and higher order contributions to the absorption can be neglected.

In figure 4.25, we compare our *ab initio* calculations (the solid curve at 300 K and the dashed curve at 275 K) of the $D_2$ fundamental band with existing laboratory measurements [81] at 273 K (large dots) and [10] at 298 K (the three slightly noisy traces). It should be noted that the three traces at 298 K were kindly made available to us in the form of numerical tables of the absorption coefficient $\alpha$, which for the plotting in figure 4.25 were divided by us by the recorded deuterium and helium densities. Two of the four measurements, the green and red traces, agree closely with each other and with the theory at almost all frequencies, much as was observed in most other cases considered
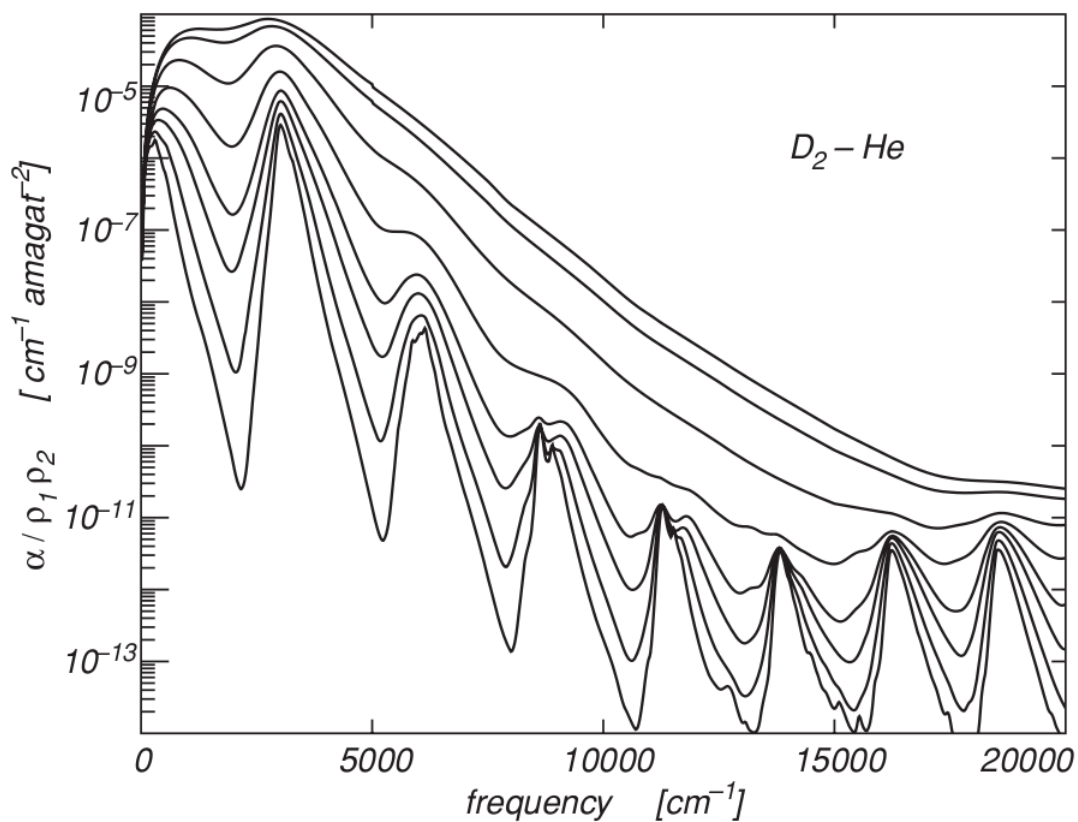
Figure 4.24: The collision-induced absorption spectrum of gaseous $D_2$–He, normalized by the deuterium and helium densities, at temperatures of 150, 300, 600, 1000, 2000, 4000, 7000, and 9000 K (from bottom to top) for frequencies from 0 to 20 000 cm$^{-1}$.

previously [6, 34]. The shapes of the remaining two spectral profiles resemble theory quite closely, but the intensities are substantially larger in one case and smaller in the other case [87].

We note that near a frequency of 3000 cm$^{-1}$, the "intercollisional dip" appears in the measurements. This is a true many-body feature involving dipole interferences in succesive molecular collisions [93], which is not present in a binary scattering theory as employed here.

It is well known that absorption intensities of gas mixtures are more difficult to determine than those of pure gases: the measurement of absorption by a deuterium-helium mixture yields the total absorption, that is, the sum of the $D_2$–$D_2$ and the $D_2$–He contributions. In order to obtain the absorption by $D_2$–He, one subtracts the absorption by $D_2$–$D_2$ complexes (assumed to be known from previous measurement) from the total absorption by the mixture. If the $D_2$–$D_2$ contributions subtracted from the total absorption were a little too strong at high frequencies within the fundamental band, this would explain the steep (unphysical) fall off of the three slightly noisy traces near 3800 cm$^{-1}$ (see figure 4.25).

Furthermore, fairly high helium densities were employed in the measurements shown, so that the measured spectra may well be affected by ternary and higher order contributions, whereas the theory strictly accounts for the binary collision-induced absorption. Three-body effects would be expected to reduce the observed intensities; this might account in part for the difference between the calculated spectra and the experimental spectrum at 273 K, which

was determined with relatively high densities, $\rho_D = 53$ amagat and $\rho_{He} = 380$ amagat [81]. The excellent agreement of theory and measurements, observed previously for the common isotope $H_2$, may be due to the generally much lower hydrogen and helium densities utilized in those measurements. Nonetheless, we do find strong agreement between the theory and the two experimental spectra for $D_2$–He at 298 K.
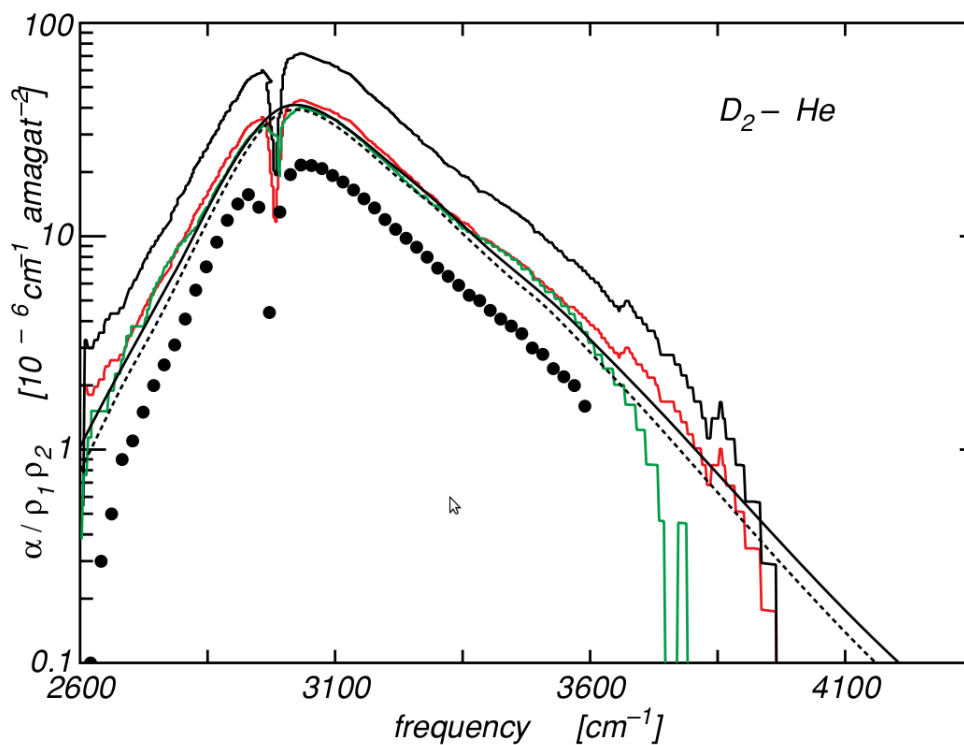
Figure 4.25: The collision-induced absorption spectrum of gaseous $D_2$–He, normalized by the deuterium and helium densities, in the fundamental band of $D_2$ at room temperature. Calculations are shown by the dashed curve (275 K) and the solid curve (300 K). Experimental spectra are shown by the large dots: $\rho_D = 53$ amagat, $\rho_{He} = 380$ amagat, at 273 K [81]; the red, slightly noisy trace: $\rho_D = 41.9$ amagat, $\rho_{He} = 125.7$ amagat, at 298 K; the green, slightly noisy trace: $\rho_D = 29.7$ amagat, $\rho_{He} = 76.2$ amagat, at 298 K; and the black slightly noisy trace: $\rho_D = 16.3$ amagat, $\rho_{He} = 195.1$ amagat, at 298 K [10].

## 4.6   Results for $T_2$–He

We have also used the induced dipole surface and potential energy surface of collisional $H_2$–He complexes to compute the binary collision-induced absorption spectra of $T_2$ molecules interacting with He atoms. The research described in this section has been published in [5]. Whereas the electronic structure of $T_2$–He is virtually the same as for $H_2$–He, the collisional dynamics and molecular scattering wave functions are different for the different collisional pairs. We have calculated spectra up to a temperature of 9000 K and frequencies up to 20,000 $\text{cm}^{-1}$. While we have observed reasonable agreement between our calculations and laboratory measurements for the collisional $H_2$–He and $D_2$–He complexes, there are no laboratory measurements for $T_2$–He collisional complexes, and one must rely on the fundamental theory, supported by agreement between theory and experiment for the other isotopes.

We have obtained the absorption coefficient $\alpha(\omega, T)$, normalized by the gas densities $\rho_T$ of tritium molecules and $\rho_{He}$ of helium, by a state-to-state quantum scattering calculation, which accounts for the interaction of the collisional complex with the radiation field. This quantity is shown in figure 4.26 for the temperatures 150 K, 600 K, 2000 K, and 9000 K, for frequencies from 0 to 20,000 $\text{cm}^{-1}$. It is remarkable that the normalized absorption intensity varies over several orders of magnitude. From left to right, the peaks in figure 4.26 correspond roughly to the rotational band, the fundamental band, and the first through eighth overtone bands of $T_2$. The absorption minima that appear between the peaks are quite deep at the lowest temperatures, but

133

with increasing temperature the peaks merge. For all calculations for $T_2$–He we have employed the isotropic potential approximation. Evidence of the applicability of the isotropic potential approximation in $H_2$–He comes from computational studies by Gianturco *et al.* [42] of a weakly bound "halo" state of He interacting with para $H_2$, observed by Kalin *et al.* [56], in molecular beams produced by cryogenic free-jet expansion. Gianturco *et al.* compared the binding energies, average $H_2$–He distances, and peak positions of the radial distribution functions computed with the potential of Boothroyd *et al.* [13] versus the values obtained with the isotropic component of that potential, averaged over the ground rotovibrational state. They concluded that "the isotropic approximation provides a very good description of the $H_2$ interaction with the helium partner." They also observed that the orientational anisotropy of the ground state probability density is very slight, for $H_2$–He [42]. We believe that the isotropic potential approximation is useful for the heavier species as well although we note that the separation of the zeroth-order vibration-rotation states is smaller for $D_2$–He and $T_2$–He than for $H_2$–He. Inclusion of the potential anisotropy in quantum close-coupled scattering calculations is impractical currently because the anisotropy causes coupling of a very large number of channels. We note that at the higher temperatures there is a significant population of tritium molecules in vibrational states with $\nu > 0$. We have included initial states up to $\nu = 11$ and $j = 32$. Final states range up to $\nu' = 14$ and $j' = 32$. An interesting feature of the $T_2$–He spectrum is the rise in peak intensities of the higher overtones; that is, the fifth, sixth, and seventh $T_2$ overtones are

134

more intense than the fourth $T_2$ overtones at the three lower temperatures, and, at the highest temperature shown, there is a high-frequency shoulder in the absorption spectrum. A similar effect is detectable in the $D_2$–He spectrum at intermediate temperatures. This effect might be due to an enhancement of the induced dipoles at larger bond lengths, for any given intermolecular separation, and the increased contributions of larger bond lengths to the transition matrix elements for the higher overtones. It also makes sense to see this for $T_2$–He because the lower vibrational frequency makes larger deviations from the equilibrium bond length more accessible thermally, at any given temperature.
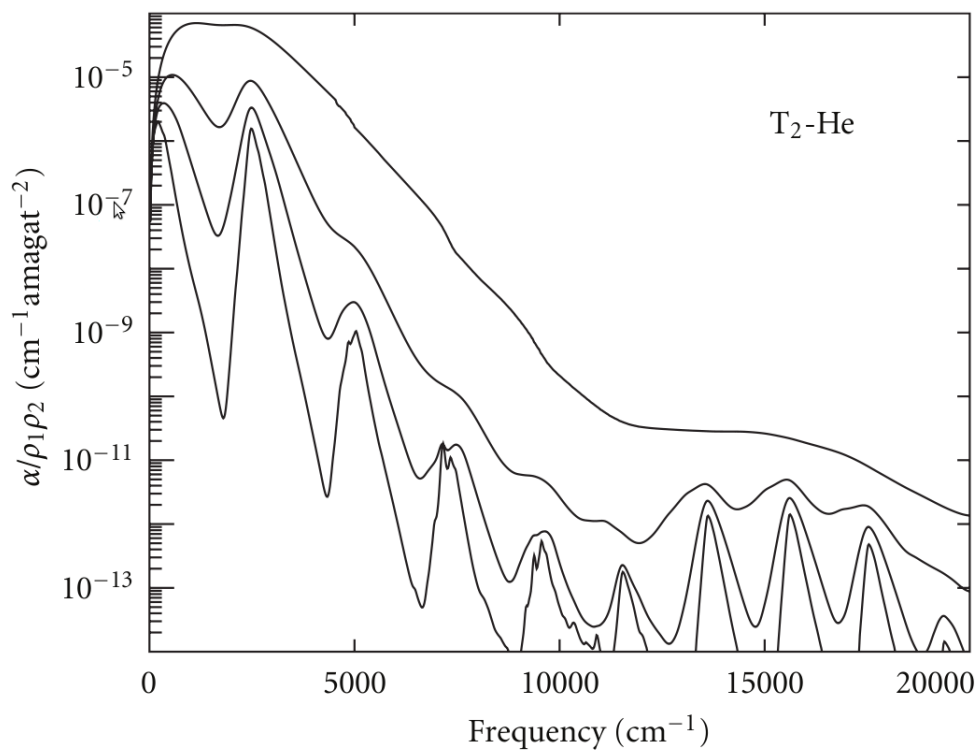
Figure 4.26: The collision-induced absorption spectrum of gaseous $T_2$–He, normalized by the tritium and helium densities, at temperatures of 150, 600, 2000, and 9000 K (from bottom to top) for frequencies from 0 to 20,000 cm$^{-1}$. From left to right, the peaks correspond roughly to the rotational band, the fundamental band, and the first through eighth overtone bands of $T_2$.

136

# Chapter 5

# Conclusion

In this work I have obtained the binary collision-induced opacity spectra of hydrogen helium gas mixtures from the fundamental theory. The emphasis was on the high temperatures (up to 9000 K) and frequencies from virtually zero to 20,000 cm$^{-1}$, for which no reliable previous data existed. The work was motivated by the needs of modern astronomical research on cool white dwarf stars, but it has already had some significant applications for other astronomical objects [84].

It was convenient in the course of the work to also consider isotopic opacities, arising from collisional complexes such as $D_2$–$D_2$, He-$D_2$, etc., for which no such data existed. At the lower temperatures, where laboratory measurements of the collision-induced absorption spectra exist, excellent agreement was observed of our theoretical/computational results with these measurements.

The new opacity data have already been included in the HITRAN data base [78]. HITRAN is an acronym for high-resolution transmission molecular absorption database. Now anybody in the scientific world will be able to use our opacity data.

# Appendix

In the following the physical constants and units which are important for this work are listed. Numbers in parantheses represent the uncertainties of the constants.

1 Debye $= 0.3934267$ atomic units of dipole strength $= 3.335611 \times 10^{-30}$ C m [34]

speed of light in vacuum:

$c = 299\ 792\ 458$ m s$^{-1}$ [50]

Planck constant:

$h = 6.626\ 068\ 96(33) \times 10^{-34}$ J s [50]

Planck constant, reduced:

$\hbar = h/2\pi = 1.054\ 571\ 628(53) \times 10^{-34}$ J s [50]

electron charge magnitude:

$e = 1.602\ 176\ 487(40) \times 10^{-19}$ C [50]

electron mass:

$m_e = 9.109\ 382\ 15(45) \times 10^{-31}$ kg [50]

proton mass:

$m_p = 1.672\ 621\ 637(83) \times 10^{-27}$ kg [50]

deuteron mass:

$m_d = 1875.612\ 793(47)$ MeV/c$^2$ [50]

unified atomic mass unit (u):

(mass $^{12}$C atom)/12 = (1 g) / ($N_A$ mol) = 1.660 538 782(83)$\times 10^{-27}$ kg

[50]

permittivity of free space:

$\epsilon_0$ = 8.854 187 817...$\times 10^{-12}$ F m$^{-1}$ [50]

Avogadro constant:

$N_A$ = 6.022 141 79(30)$\times 10^{23}$ mol$^{-1}$ [50]

Boltzmann constant:

$k_B$= 1.380 6504(24)$\times 10^{-23}$ J K$^{-1}$ [50]

the irrational number $\pi$:

$\pi \approx$ 3.141 592 653 589 793 238 [50]

conversion from inches to meters:

1 in = 0.0254 m [50]

conversion from electron volts to Joule:

1 eV = 1.602 176 487(40)$\times 10^{-19}$J [50]

$k_B$T at 300 K = [38.681 685(68)]$^{-1}$ eV [50]

# Bibliography

[1] Z. Phys. D. 13, 217, 1989.

[2] M. Abel, L. Frommhold, and M. Gustafsson. *Collision-induced absorption at wavelengths near 5μm by dense hydrogen gas.* J. Chem. Phys. 131, 181102, 2009.

[3] Martin Abel. *Collision-induced absorption by molecular deuterium (D_2) in the rototranslational band, the fundamental band, and the first overtone band of D_2.* Master of Science in Applied Physics, The University of Texas at Austin, 2010.

[4] Martin Abel and Lothar Frommhold. *Note: Collision-induced infrared absorption by gaseous deuterium.* Journal of Chemical Physics, 133, 146101, 2010.

[5] Martin Abel, Lothar Frommhold, Xiaoping Li, and Katharine L. C. Hunt. *Computation of the Calculated Collision-Induced Absorption Spectra by Dense Hydrogen-Helium, Deuterium-Helium, and Tritium-Helium Gas Mixtures.* Journal of Atomic, Molecular, and Optical Physics, Volume 2011, Article ID 470530.

[6] Martin Abel, Lothar Frommhold, Xiaoping Li, and Katharine L. C. Hunt. *Collision-Induced Absorption by H_2 Pairs: From Hundreds to*

*Thousands of Kelvin.* J. Phys. Chem. A 2011, 115, 6805-6812, 2011.

[7] Martin Abel, Lothar Frommhold, Xiaoping Li, and Katharine L. C. Hunt. *Note: Computation of collision-induced absorption by dense deuterium-helium gas mixtures.* Journal of Chemical Physics, 134, 076101, 2011.

[8] Martin Abel, Lothar Frommhold, Xiaoping Li, and Katharine L. C. Hunt. *Infrared absorption by collisional H_2–He complexes at temperatures up to 9000 K and frequencies from 0 to 20000 cm$^{-1}$.* Journal of Chemical Physics, 136, 044319, 2012.

[9] M. Abu-Kharma, P. Gillard, and S. Reddy. Eur. Phys. J.D 37, 59, 2006.

[10] M. Abu-Kharma, C. Stamp, S. Paddy Reddy, N. Shawagfeh, and H. Y. Omari. Journal of Physics B 43 135104 from [87].

[11] G. Birnbaum. J. Quant. Spectrosc. and Radiat. Transf. 19, 51, 1978.

[12] G. Birnbaum, G. Backet, and L. Frommhold. Phys. Rev. A 36, 3729, 1987.

[13] A. I. Boothroyd, P. G. Martin, and M. R. Peterson. J. Chem. Phys. 119, 3187, 2003.

[14] A. Borysow, W. Meyer, and L. Frommhold. *Absorption spectra of H_2–H_2 pairs in the fundamental band.* Phys. Review A, 40, 6931-6949, 1989.

[15] A. Borysow, W. Meyer, and L. Frommhold. *Collision-induced first overtone band of gaseous hydrogen from first principles.* Phys. Review A, 47, 4065-4077, 1993.

[16] J. P. Bouanich, C. Brodbeck, Nguyen van Thanh, and L. Frommhold. Phys. Rev. A 51, 1209, 1995.

[17] J.-P. Bouanich, Nguyen van Thanh, Y. Fu, A. Borysow, and C. Brodbeck. *Collision-induced absorption by $H_2$ pairs in the second overtone band at 298 and 77.5K: Comparison between experimental and theoretical results.* Journal of Chemical Physics, 10, 4750, 1999.

[18] Jean-Pierre Bouanich, Magnus Gustafsson, Lothar Frommhold, Denise Bailly, and Claude Brodbeck. *Collision-induced absorption in the roto-translational band of dense hydrogen gas.* Journal of Chemical Physics, 119, 23, 2003.

[19] J. N. Bradley. *Shock Waves in Chemistry and Physics.* (London: Mehtuesn), 1962.

[20] J. M. Branscomb. *Atomic and Molecular Processes.* edited by D. R. Bates (New York: Academic Press), pp. 100-140, 1962.

[21] F. R. Britton and M. F. Crawford. *Theory of collision-induced absorption in hydrogen and deuterium.* Can. J. Phys., 36:761, 1958.

[22] C. Brodbeck, P. Drossart, J. P. Bouanich, and E. Lellouch. J. Quant. Spectroscopy and Rad. Transfer 42, 141, 1989.

143

[23] C. Brodbeck, Nguyen van Thanh, A. Jean-Louis, J. P. Bouanich, and L. Frommhold. Phys. Rev. A, 50, 484-488, 1994.

[24] J. Camm, J. Keck, and B. Kivel. J. Chem. Phys., 28, 723, 1958.

[25] J. Camm, B. Kivel, J. Keck, and T. Wentin Jr. Ann. Phys. (New York), 7, 1, 1959.

[26] J. K. Cashion. J. Chem. Phys. 39, 1872-1877, 1963.

[27] E. R. Cohen, P. Dore, G. Bachet, and G. Birnbaum. Can. J. Phys. 61, 591, 1983.

[28] J. P. Colpa. *Induced absorption in the infrared.* In A. van Itterbeck, ed., Physics of High Pressure and the Condensed Phase, Ch. 12, p. 490, North Holland, Amsterdam, 1965.

[29] J. P. Colpa and J. A. A. Ketelaar. *The pressure-induced rotational absorption spectrum of hydrogen.* I. Molec. Phys., 1:14, 1958.

[30] B. Conrath, M. Flasar, V. Kunde, P. Lowman, W. McGuire, J. Pearl, J. Pirraglia, R. Samuelson, and D. Gautier *et al.* Science 204, 972, 1979.

[31] J. W. Cooley. J. Chem. Phys. 15, 363, 1961.

[32] M. F. Crawford, J. C. F. MacDonald, H. L. Welsh, and D. A. Chisholm. *Induced Infrared Absorptions of $H_2$, $N_2$, and $O_2$ in the First Overtone Regions.* McLennan Laboratory, University of Toronto, Toronto, Canada Phys. Rev. 83, 1264 - 1264 (1951), 1951.

[33] Y. B. Zel' Dovich and Y. P. Raizer. *Physics of Shock Waves and High Temperature Hydrodynamic Phenomena.* Vol. 1 (New York: Academic Press), 1966.

[34] L. Frommhold. *Collision-Induced Absorption in Gases.* Cambridge University Press, Cambridge, New York, 1993 and 2006.

[35] L. Frommhold, M. Abel, F. Wang, M. Gustafsson, X. Li, and K. L. C. Hunt. Molecular Physics 108, 2265, 2010.

[36] L. Frommhold and M. Gustafsson. *Spectra of two- and three- body van der Waals Complexes.* Physics Department, University of Texas.

[37] L. Frommhold, M. Gustafsson, and W. Meyer. J. Chem. Phys. 113, 3631, 2000.

[38] L. Frommhold, W. Meyer, and G. Birnbaum. *Rototranslational absorption spectra of $H_2$–$H_2$ pairs in the far infrared.* Phys. Review A, 39, 2434-2448, 1989.

[39] L. Frommhold, R. Samuelson, and G. Birnbaum. Astrophys. J. 283, L79, 1984.

[40] Lothar Frommhold. *Collision-Induced Spectroscopy.* University of Texas.

[41] R. Fuchs. Z. Phys., 130, 69, 1951.

145

[42] F. A. Gianturco, T. Gonzales-Lezana, G. Delagado-Barrio, and P. Villarreal. *The binding of $^4He$ and $^3He$ to a hydrogen molecule: a computational study for $pH_2$ and $oH_2$*. Journal of Chemical Physics, vol. 122, no. 8, Article ID 084308, 5 pages, 2005.

[43] H. Griem. *Principles of Plasma Spectroscopy*. New York: Cambridge University Press, 1977.

[44] M. Gustafsson, L. Frommhold, and W. Meyer. J. Chem. Phys. 113, 3641, 2000.

[45] Magnus Gustafsson. *Collision-induced absorption and the anisotropy of the intermolecular potential*. Dissertation, Supervisor: Lothar Frommhold, Physics Department, University of Texas at Austin, 2002.

[46] D. Hammer and L. Frommhold. J. Chem. Phys. 112, 654, 2000.

[47] Dominik Hammer and Lothar Frommhold. *Topical review Sonoluminescence: how bubbles glow*. Journal of Modern Optics, vol. 48, No. 2, 239-277, 2001.

[48] B. M. S. Hansen. *Old and blue white dwarf stars as a detectable source of microlensing events*. Nature, 394, 860-862, 1998.

[49] G. Herzberg. *Spectroscopic evidence of molecular hydrogen in the atmospheres of uranus and neptune*. Astrophys. J., 115:337, 1952.

146

[50] http://pdg.lbl.gov http://pdg.lbl.gov http://pdg.lbl.gov http://pdg.lbl.gov. 2009.

[51] J. L. Hunt. *Ph. D. thesis.* University of Toronto, 1959.

[52] J. L. Hunt. *The pressure-induced vibrational spectrum of hydrogen in the temperature range 300 to 40 K.* Ph.D. dissertation (University of Torronto), 1959.

[53] J. L. Hunt and H. L. Welsh. Can. J. Phys. 42, 873, 1964.

[54] U. G. Jorgensen, A. Borysow, and Y. Fu. *High Temperature (1000 - 7000 K) collision-induced absorption spectra of H_2 pairs from first principles with applications to dense stellar atmospheres.* J. Quant. Spectroscopy and Rad. Transfer, 68, 235-255, 2001.

[55] U. G. Jorgensen, D. Hammer, A. Borysow, and J. Falkesgard. Astron. Astrophys. 361, 283, 2000.

[56] A. Kalinin, O. Kornilov, L. Y. Rusin, and J. P. Toennies. *Evidence for a bound HeH_2 halo molecule by diffraction from a transmission grating.* Journal of Chemical Physics, vol. 121, no. 2, pp. 625-627, 2004.

[57] S. K. Leggett, P. Bergeron, and M. T. Ruiz. *Photometric and spectroscopic analysis of cool white dwarfs with trigonometric parallax.* Astrophys. J. Supp., 413-449, 2001.

[58] X. Li, C. Ahuja, J. F. Harrson, and K. L. C. Hunt. *The collision-induced polarizability of a pair of hydrogen molecules.* Journal of Chemical Physics, vol. 126, no. 21, Article ID 214302, 2007.

[59] X. Li, J. F. Harrison, M. Gustafsson, F. Wang, M. Abel, L. Frommhold, and K. L. C. Hunt. in Proceedings of the 7th ICCMSE, edited by G. Maroulis and T. Simos. AIP, New York, 2012.

[60] X. Li, A. Mandal, E. Miliordos, and K. L. C. Hunt. J. Chem. Phys. 136, 044320, 2012.

[61] Xiaoping Li, Katharine L. C. Hunt, Fei Wang, Martin Abel, and Lothar Frommhold. *Collision-Induced Infrared Absorption by Molecular Hydrogen Pairs at Thousands of Kelvin.* International Journal of Spectroscopy, vol. 2010, Article ID 371201, 11 pages, 2010. doi:10.1155/2010/371201.

[62] W. Lochte-Holtgreven and H. Maecker. Z. Phys., 38, 258, 1951.

[63] A. Marten, J. P. Baluteau, D. Gautier, and G. Bachet. Can. J. Phys. 61, 1455, 1983.

[64] G. T. McConville. *A consistent spherical potential function for para-hydrogen.* J. Chem. Phys., 74:2201, 1981.

[65] A.R.W. McKellar. Canadian Journal of Physics, 62, 760, 1984.

[66] A.R.W. McKellar. Journal of Chemical Physics, 92, 3261, 1990.

148

[67] W. Meyer and L. Frommhold. *in Collision- and Interaction-Induced Spectroscopy.* edited by G. C. Tabisz and M. N. Neumann (Kluwer, Dordrecht, 1995.

[68] W. Meyer and L. Frommhold. *Collision-induced rototranslational spectra of H_2–He from an accurate ab initio potential energy surface.* Phys. Review A, 34, 2771-2779, 1986.

[69] W. Meyer, P. C. Hariharan, and W. Kutzelnigg. J. Chem. Phys. 73, 1880, 1980.

[70] M. Mizushima. *A theory of pressure absorption.* Phys. Rev., 76:1268, Erratum: ibid. 77:149, 1950, 1949.

[71] M. Mizushima. *On the infrared absorption of the hydrogen molecule.* Phys. Rev., 77:150, 1950.

[72] M. Moraldi, M. Celli, and F. Barocchi. Phys. Review A 40, 1116, 1989.

[73] J. Mould and J. Liebert. *Infrared photometry and atmospheric composition of cool white dwarfs.* Astrophys. J., 226, L29-33, 1978.

[74] P. Muchnick and A. Russek. J. Chem. Phys. 100, 4336, 1994.

[75] R. J. Penney, R. D. G. Prasad, and S. P. Reddy. J. Chem. Phys. 77, 131, 1982.

[76] J. D. Poll and J. van Kranendonk. Can. J. Phys. 39, 189, 1961.

149

[77] S. P. Reddy and K. S. Chang. J. Mol. Spectrosc. 47, 22, 1973.

[78] C. Richard, I. E. Gordan, L. S. Rothman, M. Abel, L. Frommhold, J.-M. Hartmann, C. Hermans, W. J. Lafferty, G. Orton, K. M. Smith, and H. Tran. *New section of the HITRAN database: Collision-Induced Absorption (CIA).* Journal of Quantitative Spectroscopy & Radiative Transfer, 2012.

[79] M. Rigby, E. B. Smith, G. C. Maitland, and W. A. Wakeham. *in Collision- and Interaction-Induced Spectroscopy.* Intermolecular Forces (Clarendom Press, Oxford, 1981, 1989.

[80] M. Ross, H. Ree, and D. Young. J. Chem. Phys. 1983, 79, 1487-1494.

[81] W. E. Russel, S. Paddy Reddy, and C. W. Cho. Journal of Molecular Spectroscopy 52, 72, 1974.

[82] D. Saumon, P. Bergeron, and F. Wesemael. *New model of atmospheres for very cool white dwarfs with mixed H/ He and pure He compositions.* Astrophys. J., 443, 764-779, 1995.

[83] D. Saumon and S. B. Jacobson. *Pure hydrogen model atmospheres for very cool white dwarfs.* Astrophys. J., 511, L107-110, 1999.

[84] Didier Saumon, Mark S. Marley, Martin Abel, Lothar Frommhold, and Richard S. Freedman. *New $H_2$ collision-induced absorption and $NH_3$ opacity and the spectra of the coolest brown dwarfs.* The Astrophysical Journal, 750, 74, December 2011.

[85] J. Schaefer and W. E. Koehler. Z. Phys. D 1989, 13, 217-229.

[86] J. Schaefer and W. Meyer. Journal of Chemical Physics 70, 344-360, 1979.

[87] C. Stamp. Ph.D. dissertation, Memorial University of Newfoundland, 2006.

[88] A. J. Stone. *The Theory of Intermolecular Forces.* Oxford University Press, 1997.

[89] R. H. Tipping and J. D. Poll. *in Molecular Spectroscopy: Modern Research.* vol. 3, edited by K. N. Rao (Academic Press, New York, 1985), Chap. 7, pp. 421-446.

[90] L. M. Trafton. *The thermal opacity in the major planets.* Astrophys. J., 140, 1340, 1964.

[91] L. M. Trafton. *Planetary Atmospheres: The role of collision-induced absorption.* in [96], pages 177-193, 1998.

[92] A. Unsoeld. *Physik der Sternatmosphaeren.* Berlin: Springer, 1955.

[93] J. van Kranendonk. Can. J. Phys. 46,1173, 1968.

[94] J. van Kranendonk. *Intermolecular spectroscopy.* Physica, 73:156, 1974.

[95] G. Varghese, S. P. Reddy, and R. D. G. Prasad. Phys. Rev. A 15, 975, 1977.

[96] A. A. Vigasin and editors Z. Slanina. *Molecular Complexes in Earth's, Planetary, Cometary and Interstellar Atmospheres.* World Sci., Singapore, 1998.

[97] A. Watanabe. *Ph. D. thesis.* University of Toronto, 1964.

[98] A. Watanabe, J. L. Hunt, and H. L. Welsh. Can. J. Phys. 49, 860, 1971.

[99] H. L. Welsh. *Pressure induced absorption spectra of hydrogen.* A. D. Buckingham and D. A. Ramsay, editors, MTP Internat. Review of Science - Physical Chemistry, Series one, Vol. 3: Spectroscopy, chapter 3, pages 33-71, Butterworths, London, 1972.

[100] H. L. Welsh, M. F. Crawford, and J. L. Locke. *Infrared absorption of oxygen and nitrogen induced by intermolecular forces.* Phys. Rev., 75:1607, 1949.

[101] H.-J. Werner, P. J. Knowles, and J. Almlöf *et al. MOLPRO, Version 2000.1.* Universität Stuttgart, Stuttgart, Germany and Cardiff University, Cardiff, UK, 2000.

[102] R. N. Zare. *Angular Momentum, Understanding spatial aspects in chemistry and physics.* Wiley: New York, 1988.

# Index

153

154

# Vita

Martin Andreas Abel was born in Fulda, Germany, on August 28, 1985, the son of Roswitha Waltraud and Werner Gregor Abel. He graduated from the Wigbertgymnasium in Huenfeld, Germany, with the university-entrance diploma. In 2005 he started his higher education in the natural sciences and mathematics program at the University of Wuerzburg, Germany. He received his prediploma in physics in 2007 and the prediploma in mathematics in 2008 from the University of Wuerzburg, Germany. In August 2008 he entered the Graduate School of the University of Texas at Austin and since then he was a graduate student there. In August 2009 he earned the Master of Arts in physics and in August 2010 the Master of Science in Applied Physics.

Permanent address: Am Langen Garten 1
Eiterfeld/ Arzell, 36132, Germany

This dissertation was typeset with LaTeX$^{\dagger}$ by the author.

---

$^{\dagger}$LaTeX is a document preparation system developed by Leslie Lamport as a special version of Donald Knuth's TeX Program.